

Old Dominion University

ODU Digital Commons

Mechanical & Aerospace Engineering Theses & Dissertations

Mechanical & Aerospace Engineering

Spring 1991

Large-Amplitude Finite Element Flutter Analysis of Composite Panels in Hypersonic Flow

Carl E. Gray Jr.
Old Dominion University

Follow this and additional works at: https://digitalcommons.odu.edu/mae_etds



Part of the [Applied Mechanics Commons](#)

Recommended Citation

Gray, Carl E.. "Large-Amplitude Finite Element Flutter Analysis of Composite Panels in Hypersonic Flow" (1991). Doctor of Philosophy (PhD), Dissertation, Mechanical & Aerospace Engineering, Old Dominion University, DOI: 10.25777/8k69-3s53
https://digitalcommons.odu.edu/mae_etds/232

This Dissertation is brought to you for free and open access by the Mechanical & Aerospace Engineering at ODU Digital Commons. It has been accepted for inclusion in Mechanical & Aerospace Engineering Theses & Dissertations by an authorized administrator of ODU Digital Commons. For more information, please contact digitalcommons@odu.edu.

**LARGE-AMPLITUDE FINITE ELEMENT FLUTTER ANALYSIS OF COMPOSITE
PANELS IN HYPERSONIC FLOW**

by

Carl E. Gray, Jr.
B.S., December 1981, Old Dominion University
M.S., May 1987, Old Dominion University

A Dissertation Submitted to the Faculty of
Old Dominion University in Partial Fulfillment of the
Requirements for the Degree of

DOCTOR OF PHILOSOPHY

in

ENGINEERING MECHANICS

OLD DOMINION UNIVERSITY
May, 1991

Approved by:

Chuh Mei (Director)

Osama A. Kandil

Jean W. Hou

Duc T. Nguyen

Thomas L. Jackson

ABSTRACT

LARGE-AMPLITUDE FINITE ELEMENT FLUTTER ANALYSIS OF COMPOSITE PANELS IN HYPERSONIC FLOW

Carl E. Gray, Jr.
Old Dominion University
Director: Dr. Chuh Mei

A finite-element approach is presented for determining the nonlinear flutter characteristics of two-dimensional isotropic and three-dimensional composite laminated thin panels using the third-order-piston, transverse loading, aerodynamic theory. The unsteady, hypersonic, aerodynamic theory and the von Karman large deflection plate theory are used to formulate the aeroelastic problem. Nonlinear flutter analyses are performed to assess the influence of the higher-order aerodynamic theory on the structure's limit-cycle amplitude and the dynamic pressure of the flow velocity. A solution procedure is presented to solve the nonlinear panel flutter and large-amplitude free vibration finite element equations. This procedure is a linearized updated mode with a nonlinear time function approximation (LUM/NTF) method. Nonlinear flutter analyses are performed for different boundary support-conditions and for various system parameters: plate thickness-to-length ratio, h/a ; aspect ratio a/b ; material orthotropic ratio, lamination angle, and number of layers; Mach number, M ; flow mass-density-to-panel-mass-density ratio, μ/M ; dynamic pressure, λ ; and maximum-deflection-to-thickness ratio, c/h . For large amplitude free vibration, alternative classical analytical solutions are available for comparison. Linear finite element flutter for isotropic and composite panels and large-amplitude isotropic panel flutter results are compared with existing classical solutions. The large-amplitude panel flutter results using the full third-order piston aerodynamic theory are presented to assess the influence of the nonlinear aerodynamic theory.

ACKNOWLEDGEMENT

To Dr. Mei, my Committee Chairman and mentor, I would like to extend my deepest appreciation and gratitude for his willingness to share his time, knowledge, and enthusiasm for learning with me. I am especially appreciative of the encouragement and motivation that he has provided throughout my association with him.

To Dr. James R. Rooker, Head of the Structural Design Branch, I am grateful for the time and resources to complete this work. Also, I would like to extend a special thanks to Drs. Jiangning Qin and Duc T. Nguyen of the Civil Engineering Department for their tremendous and timely support in developing an outstanding eigensolver that substantially reduced the computational time to conduct this research. To Drs. Osama A. Kandil, Jean W. Hou, and Thomas L. Jackson, I thank them for their suggestions and support by serving on my Dissertation Committee. In addition, I would like to express my gratitude to the National Aeronautics and Space Administration for affording me the opportunity to advance my education. In particular, I thank Mrs. Cheryl W. Winstead and her staff for their assistance in the careful preparation of this document.

Most importantly, had it not been for the love and understanding of my wife, Belinda, who has constantly provided encouragement and understanding, this dissertation would have never been completed; to her I will be eternally grateful.

TABLE OF CONTENTS

	<u>Page</u>
ACKNOWLEDGEMENT	ii
LIST OF TABLES	v
LIST OF FIGURES	vii
LIST OF SYMBOLS	x
 <u>Chapter</u>	
1. INTRODUCTION	1
1.1 Preliminary Remarks	1
1.2 Review of Previous Work	2
1.3 Objectives and Scope	5
2. FINITE ELEMENT FORMULATION	11
2.1 Hamilton's Principle for a Continuum	11
2.2 Constitutive and Strain-Displacement Relationships	12
2.2.1 Two-Dimensional Isotropic Panel	12
2.2.2 Three-Dimensional Orthotropic Panel	12
2.3 Aerodynamic Pressure Function	13
2.4 Element Representation	14
2.4.1 Two-Dimensional Isotropic Panel	14
2.4.2 Three-Dimensional Rectangular Panel	18
3. SYSTEM FINITE ELEMENT FORMULATION AND SOLUTION PROCEDURE	31
3.1 System Finite Element Formulation	31
3.1.1 Two-Dimensional Isotropic Panel	32
3.1.2 Three-Dimensional Composite Rectangular Panel	33
3.2 Linearizing Procedure	35
3.2.1 Linearizing Method for Two-Dimensional Panel	38
3.2.2 Linearizing Method for Three-Dimensional Rectangular Panel	40
3.2.3 Linearizing Method for System Equations	42
3.3 Solution Procedure	43

4. VERIFICATION OF FINITE ELEMENT METHOD	46
4.1 Two-Dimensional Isotropic Panels	47
4.1.1 Large-Amplitude In-vacuo Vibration	47
4.1.2 Large-Amplitude Flutter with Linear Aerodynamics	48
4.2 Three-Dimensional Rectangular Panels	48
4.2.1 Large-Amplitude In-vacuo Vibration—Isotropic	49
4.2.2 Flutter with Linear Aerodynamics—Isotropic	49
4.2.3 Linear In-vacuo Vibration—Composite	50
4.2.4 Large-Amplitude In-vacuo Vibration—Composite	51
4.2.5 Flutter with Linear Aerodynamics—Composite	51
5. NONLINEAR PANEL FLUTTER NUMERICAL RESULTS	64
5.1 Two-Dimensional Isotropic Panel	64
5.1.1 System Parameter Effects	64
5.1.2 Boundary Support Effects	66
5.1.3 Nonlinear Aerodynamic Effects	66
5.2 Three-Dimensional Rectangular Panel	67
5.2.1 Limit-Cycle Oscillations	67
5.2.2 Laminated Panel Effects	70
5.2.3 Boundary Support and Aspect Ratio Effects	71
5.2.4 Influence of Orthotropic Materials	71
5.2.5 Nonlinear Aerodynamic Effects	72
6. SUMMARY AND CONCLUSIONS	97
6.1 Concluding Remarks	97
6.2 Future Work	98
REFERENCES	99
APPENDICES	105
A. DERIVATION OF THIRD-ORDER PISTON THEORY AERODYNAMICS	105
B. DERIVATION OF THREE-DIMENSIONAL PLATE ELEMENT MATRIX	109
C. TIME AND SPACE FUNCTIONS APPROXIMATIONS	112

LIST OF TABLES

<u>Table</u>	<u>Page</u>
4.1 Material Properties	52
4.2 Effects of Amplitude Ratios, c/h , on In-vacuo Frequency Ratios, ω_{nl}/ω_o , for Simply Supported In-plane Immovable 2-D Panel	53
4.3 Comparison of Amplitude Ratios, c/h , on In-vacuo Frequency Ratios, ω_{nl}/ω_o , for Clamped Supported In-plane Immovable 2-D Panel	53
4.4 Effects of μ/M on λ_ℓ vs. Amplitude Ratio for Simply Supported In-plane Immovable 2-D Panel [in-plane stiffness modified by $(1-\nu^2)$]	54
4.5 Flutter Amplitude, c/h , Critical Dynamic Pressure, λ_ℓ , Flutter Frequency, ω , for a Simply Supported In-plane Immovable 2-D Panel [in-plane stiffness modified by $(1-\nu^2)$]	54
4.6 Finite Element Mesh Convergence Study for an In-plane Immovable Simply Supported Isotropic 3-D Square Panel ($E = 30$ Msi, $\nu = .3$, $\rho = .00026$ lbs-sec/in ⁴ , $a = b = 12$ in, $h = .04$ in)	55
4.7 Finite Element Mesh Convergence Study for an In-plane Immovable Clamped Supported Isotropic 3-D Square Panel ($E = 30$ Msi, $\nu = .3$, $\rho = .00026$ lbs-sec ² /in ⁴ , $a = b = 12$ in, $h = .04$ in)	55
4.8 Free Vibration c/h Ratio vs. ω_{nl}/ω_o Ratio for In-plane Immovable Simply Supported Square Isotropic 3-D Square Panel (6×6: Quarter Plate)	56
4.9 Free Vibration c/h Ratio vs. ω_{nl}/ω_o Ratio for In-plane Immovable Clamped Supported Square Isotropic 3-D Square Panel (6×6: Quarter Plate)	56
4.10 Free Vibration c/h Ratio vs. ω_{nl}/ω_o Ratio for In-plane Movable Clamped Supported Square Isotropic 3-D Square Panel (6×6: Quarter Plate)	57
4.11 Linear Panel Flutter of 3-D Isotropic Square Panel ($E = 10$ Msi, $\nu = .3$, $\rho = .00026$ lbs-sec ² /in ⁴ , $a = b = 12$ in, $h = 0.04$ in)	57
4.12 Nonlinear Panel Flutter with Linear Aerodynamics, λ_ℓ , for 3-D Isotropic Square Panel ($E = 10$ Msi, $\nu = .3$, $\rho = .00026$ lbs-sec ² /in ⁴ , $a = b = 12$ in, $h = 0.04$ in)	58
4.13 Linear Free Vibration of Clamped Angle-Ply Laminated 3-D Square Panel ($E_{11} = 30$ Msi, $E_{22} = .75$ Msi, $G_{12} = .375$ Msi, $\nu_{12} = .25$, $\rho = .00026$ lbs-sec ² /in ⁴ , (30/−30), $a = b = 12$ in, $h = .12$ in)	58

4.14	Linear Free Vibration of Clamped Angle-Ply Laminated 3-D Square Panel ($E_{11} = 30$ Msi, $E_{22} = .75$ Msi, $G_{12} = .375$ Msi, $\nu_{12} = .25$, $\rho = .00026$ lbs-sec ² /in ⁴ , (30/-30/30), $a = b = 12$ in, $h = .12$ in)	59
4.15	Linear Free Vibration (ω_o rad/sec) of Simply Supported Angle-Ply Laminated 3-D Square Panel ($E_{11} = 30$ Msi, $E_{22} = 12.245$ Msi, $G_{12} = 5.9308$ Msi, $\nu_{12} = .23$, $\rho = .00026$ lb-sec ² /in ⁴ , $a = b = 12$ in, $h_{ply} = 0.04$ in)	59
4.16	Free Vibration c/h Ratio vs. ω_{nl}/ω_o Ratio Simply Supported In-plane Immovable Angle-Ply (45/-45) Laminated 3-D Square Panel ($E_{11} = 39.39$ Msi, $E_{22} = 4.788$ Msi, $G_{12} = 1.959$ Msi, $\nu_{12} = .3$, $r = .00026$ lbs-sec ² /in ⁴ , $a = b = 12$ in, $h = 0.04$ in)	60
4.17	Free Vibration c/h Ratio vs. ω_{nl}/ω_o Ratio Simply Supported In-plane Immovable Cross-Ply (0/90/90/0) Laminated 3-D Square Panel ($E_{11} = 40$ Msi, $E_{22} = 1$ Msi, $G_{12} = .5$ Msi, $\nu_{12} = .25$, $\rho = .00026$ lbs-sec ² /in ⁴ , $a = b = 12$ in, $h = 0.04$ in)	60
4.18	Free Vibration c/h Ratio vs. ω_{nl}/ω_o Ratio Clamped Supported In-plane Immovable Cross-Ply (0/90/90/0) Laminated 3-D Square Panel ($E_{11} = 40$ Msi, $E_{22} = 1$ Msi, $G_{12} = .5$ Msi, $\nu_{12} = .25$, $\rho = .00026$ lbs-sec ² /in ⁴ , $a = b = 12$ in, $h = 0.04$ in)	61
4.19	Linear Panel Flutter, λ_{cr} , for 3-D Anisotropic Cantilever Square Panel ($E_{11}/E_{22} = 2.$, $G_{12}/E_{22} = 0.364$, $\nu_{12} = .24$, $\rho = .00026$ lbs-sec ² /in ⁴ , $a = b = 12$ in, $h = 0.04$ in)	61
5.1	Effects on λ_ℓ by Neglecting Higher Order Terms in Aerodynamic Piston Theory (Eq. 2.8)	73
5.2	Effects on λ_ℓ by Neglecting Higher Order Terms in Aerodynamic Piston Theory (Eq. 2.8)	73
5.3	Effects on λ_ℓ by Neglecting Higher Order Terms in Aerodynamic Piston Theory (Eq. 2.8)	74
5.4	Effects on λ_ℓ by Neglecting Higher Order Terms in Aerodynamic Piston Theory (Eq. 2.8)	74
5.5	Effects on λ_ℓ by Including w_x^2 Higher Order Term with First-Order Aerodynamic Piston Theory (Eq. 2.8)	75
C.1	Linear Mode Shape Participation Factors	113

LIST OF FIGURES

<u>Figure</u>	<u>Page</u>
1.1 Aeroelastic Interaction	8
1.2 Panel Flutter: Schematic of Plate Response Using Piston Theory.	9
1.3 General Panel Flutter Theories	10
2.1 Two-Dimensional Panel Geometry	28
2.2 Three-Dimensional Panel Geometry	29
2.3 Nodal Displacement Quantities for a Two-Dimensional Panel	30
3.1 Nonlinear Panel Flutter Solution Procedure	45
4.1 Comparison of Large-Amplitude Vibration Solutions for a Simply-Supported Panel	62
4.2 Limit-cycle Amplitude Ratios vs. Non-Dimensional Dynamic Pressure, λ_ℓ	63
5.1 Variation of Eigenvalue With Nondimensional Dynamic Pressure for a Simply-Supported Panel. ($\mu/M = .01$, $Mh/a = .05$)	76
5.2 Variation of Eigenvalue With Nondimensional Dynamic Pressure for a Simply-Supported Panel Using First- and Third-Order Piston Theory Aerodynamics. ($\mu/M = 0.1$, $Mh/a = 0.1$)	77
5.3 Simply-Supported Panel Deflection Shapes for $c/h = +1.0$, $c/h = -1.0$, and $c/h = -.909$. ($\mu/M = .01$, $Mh/a = .05$)	78
5.4 Comparison of Nonlinear and Linear Piston Theory Aerodynamics on Large-Amplitude Panel Flutter. ($\mu/M = .01$, $Mh/a = .05$)	79
5.5 Limit-Cycle Amplitude at $x/a = .75$ vs. Nondimensional Dynamic Pressure for a Simply-Supported Panel for Several Flow Parameters	80
5.6 Limit-Cycle Amplitude at $x/a = .75$ vs. Nondimensional Dynamic Pressure for Various Support Conditions	81
5.7 Eigenvalue Variation for First Four Linear Modes of a Simply-Supported, Square Panel for Material 3. ($\mu/M = .10$, $Mh/a = .05$)	82

5.8	Nonlinear Panel Flutter Eigenvalue Variation vs. Dynamic Pressure Using Third-Order Piston Theory Aerodynamics of a Simply-Supported, Square Panel for Material 3. ($\mu/M = .10$, $Mh/a = .05$)	83
5.9	Variation of Limit-Cycle Amplitude vs. Limit-Cycle Dynamic Pressure of a Simply-Supported, Square Panel for Material 3. ($\mu/M = .10$, $Mh/a = .05$)	84
5.10	Variation of Limit-Cycle Frequency Ratio vs. Limit-Cycle Amplitude of a Simply-Supported, Square Panel for Material 3. ($\mu/M = .10$, $Mh/a = .05$)	85
5.11	Limit-Cycle Deflection Shape of a Simply-Supported, Single Layer Square Panel for Material 3. ($\mu/M = .10$, $Mh/a = .05$, $\lambda = 67.71$, $c/h = +1.0$, 12×8 Full Panel)	86
5.12	Panel Limit-Cycle Deflection of a Simply-Supported, Single Layer Square Panel for Material 3. ($\mu/M = .10$, $Mh/a = .05$, $\lambda = 67.71$, $c/h = +1.0$, 12×8 Full Panel)	87
5.13	Longitudinal Surface Stresses Along a Simply-Supported, Single Layer Square Panel at $y/b = 0.5$ for Material 3. ($\mu/M = .10$, $Mh/a = .05$, $\lambda = 67.71$, $c/h = +1.0$, 12×8 Full Panel)	88
5.14	Longitudinal Surface Stresses Along a Simply-Supported, Single Layer Square Panel at $x/a = .88$ for Material 3. ($\mu/M = .10$, $Mh/a = .05$, $\lambda = 67.71$, $c/h = +1.0$, 12×8 Full Panel)	89
5.15	Effects of Number of Plies on Limit-Cycle Amplitude and Dynamic Pressure for a Simply-Supported, Square Panel for Material 3. ($\mu/M = .10$, $Mh/a = .05$)	90
5.16	Effects of Number of Plies on Limit-Cycle Frequency and Dynamic Pressure for a Simply-Supported, Square Panel for Material 3. ($\mu/M = .10$, $Mh/a = .05$)	91
5.17	Effects of Lamination Angle Variation on Limit-Cycle Dynamic Pressure for a Simply-Supported, Single Layer Square Panel for Material 3. ($\mu/M = .10$, $Mh/a = .05$, $c/h = 0.6$)	92
5.18	Limit-Cycle Amplitude at $x/a = .75$ and $y/b = .50$ vs. Dynamic Pressure for Various Support Conditions for a Single Layer Square Panel of Material 3. ($\mu/M = .10$, $Mh/a = .05$)	93
5.19	Limit-Cycle Amplitude at $x/a = .75$ and $y/b = .50$ vs. Dynamic Pressure for a Simply-Supported Single Layer Square Panel of Material 3 with In-Plane Movable and Immovable Support Conditions ($\mu/M = .10$, $Mh/a = .05$)	94
5.20	Limit-Cycle Amplitude at $x/a = .75$ and $y/b = .50$ vs. Dynamic Pressure for a Simply-Supported Single Layer Panel for Several Aspect Ratios for Material 3. ($\mu/M = .10$, $Mh/a = .05$)	95
5.21	Limit-Cycle Parameter vs. Orthotropic Material Parameter for Limit-Cycle Amplitudes and a Simply-Supported Single Layer Square Panel of Material 3. ($\mu/M = .10$, $Mh/a = .05$)	96

A.1	Piston Theory Aerodynamics	108
B.1	3-D Laminated Plate Finite Element	111
C.1	Time Function Approximation	114
C.2	Panel Flutter Deformation Shape	115

LIST OF SYMBOLS

a, b	panel length and width
a_e	two-dimensional panel finite element length
$[a]$	element aerodynamic matrix
$[A]$	panel aerodynamic matrix
$[A], [B], [D]$	laminate stiffness matrices
c	maximum panel deflection
$[C_\theta]$	matrix relating element displacements to membrane bending strains
D	plate bending rigidity
D_c	composite panel rigidity parameter
$\{e\}$	membrane strains
E, E_{11}, E_{22}	isotropic and lamina elastic modulus
$[g]$	element aerodynamic damping matrix
$[G]$	panel aerodynamic damping matrix
G, G_{12}	isotropic and lamina shear modulus
h	panel thickness
$[k]$	element stiffness matrix
$[K]$	panel stiffness matrix
M	Mach number
$[m]$	element mass matrix
$[M]$	panel mass matrix
$\{N_A\}, \{\mathcal{N}_A\}$	nonlinear and linearized midsurface force associated with $[A]$
$\{N_B\}, \{\mathcal{N}_B\}$	nonlinear and linearized midsurface force associated with $[B]$
p, p_∞	aerodynamic pressure
$[Pw]$	matrix relating element displacements to curvature
$[Pu]$	matrix relating element displacements to membrane strains

q	dynamic pressure
$[Q], [\bar{Q}]$	reduced and transformed reduced lamina stiffness matrices
r	h/a
U	internal strain energy
u, v, w	in-plane and transverse panel displacements
V	flow velocity
$\{w\}$	two-dimensional element displacement
$\{\Delta u\}, \{\Delta v\}, \{\Delta w\}$	three-dimensional element displacements
$\{U\}, \{V\}, \{W\}$	global finite element displacements
x, y, z	Cartesian coordinates
<u>Greek symbols</u>	
α	real part of eigenvalue
β	eigenvalue phase angle
γ	ratio of specific heats, $\gamma = 1.4$
δ	variational operator
$\epsilon, \{\epsilon\}$	two- and three-dimensional strain
θ	lamination angle
ϑ	two-dimensional element rotation
$[\theta], [\Theta]$	nonlinear and linearized displacement matrix
$\{\kappa\}$	laminate bending curvatures
λ	non-dimensional dynamic pressure
μ	$\rho_a a / \rho h$
ν	Poisson's ratio, $\nu = .3$ for isotropic
ξ	non-dimensional length, x/a
ρ, ρ_a	panel mass density and flow mass density
$\sigma, \{\sigma\}$	two- and three-dimensional stress
τ	non-dimensional time, $t\omega_o$
φ, ϕ	interpolation functions
$\{\Phi\}$	complex eigenvector

ω	imaginary part of eigenvalue
Ω	complex eigenvalue, $\alpha + i\omega$
<u>Subscripts</u>	
b	bending
cr	critical
f	flexural
ℓ	limit-cycle
m	membrane
nl	non-linear
o	linear
u, v, w	membrane and bending properties

Chapter 1

INTRODUCTION

1.1 Preliminary Remarks

The interaction study between structures and aerodynamics identified a new field of engineering known as aeroelasticity, see Fig. 1.1. As a result of the need for high speed aircraft, aeroelasticity has become a dominant consideration in the design of high-speed flight vehicles. During the late 1950's through the mid-to-late 1970's, the panel flutter phenomena, pertaining to aircraft structures, received a great deal of attention from a large number of investigators. The aeroelastic panel flutter is the self-excited or self-sustained oscillations of an external panel of a flight vehicle when exposed to supersonic or hypersonic air flow. Panel flutter differs from aeroelastic wing flutter in that the aerodynamic forces resulting from the air flow act only on one side of the panel.

The dawning of flight into the supersonic regime, during the 1950's, stressed the conflicting conditions of fabricating a structure strong enough to withstand large aerodynamic forces during supersonic flight, yet light enough to be economically efficient to allow for an increase in the flight vehicle's payload capability. Because of the resurgent interest in flight vehicles such as the High-Speed Civil Transport (HSCT), the National Aero-Space Plane (NASP), and the Advanced Tactical Fighter (ATF) that will operate not only at high-supersonic Mach numbers but well into the hypersonic regime, the additional requirement for energy-efficient, high-strength and minimum-weight vehicles has become apparent. These requirements have generated an interest in the advanced composite materials to meet the high-strength minimum-weight requirements. In addition to the structural material concerns, the issue of the range of applicability of the most used first-order piston aerodynamic theory into the hypersonic regime has been questioned. These questions have been generated in response to neglecting the higher-order terms in the derivation of the first-order theory. It has been hypothesized that the higher-order terms in the

piston aerodynamic theory, at the large Mach numbers of interest, may be significant. Coupling these concerns with the realistic need for analytical tools to evaluate complex structures, the finite element method presents itself as the most appropriate means that can conveniently and efficiently incorporate all of the known complexities of the physical problem.

1.2 Review of Previous Work

In the previous section, a synopsis to the subject was presented. The panel flutter phenomenon has been studied in detail to comprehend the physics associated with the problem. Again, panel flutter is the self-excited or self-sustained (limit-cycle) oscillations of an external panel of a flight vehicle when exposed to supersonic or hypersonic air flow only on one side of the panel. In the framework of small deflection (linear) structural theory, there is a critical value, λ_{cr} , of the dynamic pressure (or flow velocity) above which the panel motion becomes unstable and grows exponentially with time, and below which any disturbance to the panel results in a decaying motion.

Theoretical considerations of panel flutter using linear theory, as well as an early survey on the subject up to 1966, was given by Dugundji [1]¹. A thorough summary on both linear and nonlinear panel flutter through 1970 was given by Dowell [2]. Most recently, 1987, Reed, Hanson, and Alford [3], conducted a survey in the area of hypersonic panel flutter in support of the NASP program. As disclosed by all of these survey papers, a great quantity of literature exists on linear panel flutter using different aerodynamic theories, for example references [1,4,5] and many others. The aerodynamic theory employed for the most part for panel flutter at high supersonic Mach numbers ($M > 1.7$ [5]) is the quasi-steady first-order piston aerodynamic theory [6]. Because of the recent renewed interest [3] in flight vehicles that will operate not only at high-supersonic Mach numbers but well into the hypersonic regime, there is an interest in approaches that can employ unsteady nonlinear aerodynamic theories. The piston aerodynamic theories, although several decades old, have generally been employed to approximate the aerodynamic loads on the panel from local pressures generated by the body's motion as related to the local normal component of the fluid velocity. This theory, thus, defines a point-function relationship between the normal component of the fluid velocity and the local panel pressure. For supersonic

¹Numbers in brackets indicate reference.

Mach numbers, these theories reasonably estimate the aerodynamic pressures and are the most widely used in the literature, see Fig. 1.2. Figure 1.2 was taken from Dowell [7] where he demonstrated remarkable correlation between conventional flutter analysis and experimental data to predict the panel's response. An outstanding presentation of the fundamental theories and the physical understanding of panel flutter can be found in the book on the subject by Dowell [7].

In actuality, it is well known [8] that the panel not only bends but also stretches due to large-amplitude vibrations. Such membrane tensile forces in the panel, due to the induced stretching, provides a limited stabilizing effect of the "hard spring" type that restrains the panel motion to be of bounded amplitude for limit-cycle oscillations that increases with amplitude as the dynamic pressure, λ_ℓ , increases. The external skin of a flight vehicle can, thus, withstand velocities beyond the linear critical value. However, McIntosh [9] has investigated the effects of hypersonic nonlinear aerodynamic loadings on panel flutter, and his findings indicate that the higher-order aerodynamic theory may, for some system parameters, produce a "soft spring" effect that will predict lower limit-cycle flutter velocities than those predicted by the first-order piston theory even including the effect of membrane tensile forces in the panel. In reference [2], Dowell identifies four panel flutter theories, types 1–4 shown in Fig. 1.3, and with the theories in reference [9] these theories increase to five.

The first partial nonlinear behavior of a fluttering panel was studied by several investigators: Bolotin [10], Fung [11], Houbolt [12], and Eisely [13]. They were primarily concerned with determining stability boundaries of two-dimensional plates. Using a two-mode Galerkin approach, the three-dimensional plate buckling effects on flutter boundaries using the von Karman deflection theory and Ackert's aerodynamic theory (also known as a static strip theory [5,14]) was studied by Fralich [15].

For the full structural nonlinear limit-cycle approach, a variety of analyses methods have been employed to assess the panel flutter problem. The direct numerical integration approach in conjunction with Galerkin's method was first used by Dowell [16,17] to study the nonlinear oscillations of simply supported, in-plane elastically restrained, fluttering plates. Dowell determined that the direct numerical integration (classical) approaches required as a minimum six linear normal modes to achieve a converged solution for displacements and possibly more if

stresses are required [9,18]. For the clamped plates, Ventres [19] also used the direct numerical integration method by employing both the quasi-steady aerodynamic theory and the generalized aerodynamic theory, type 2 analysis. Both Dowell and Ventres used the Galerkin's method to reduce the governing partial differential equations in time and space to a set of coupled ordinary differential equations in time which were numerically integrated for arbitrary initial conditions. The integration was continued until a limit-cycle oscillation of constant amplitude, that was independent of the initial conditions, was encountered. But because of the highly nonlinear nature of the aerodynamic theory, there exists just a few references that have investigated the limit-cycle oscillations of panels for hypersonic flow. McIntosh [9], using a nonlinear, partial-third-order piston aerodynamic theory, also integrated the nonlinear equations of motion for given initial conditions and observed the resultant panel motion versus time until a limit-cycle of constant amplitude that was independent of initial conditions was reached. As noted earlier, McIntosh's findings indicate that the higher-order aerodynamic theory, for some system parameters, produces a "soft spring" effect that predicted lower limit-cycle flutter velocities.

A number of other classical analytical methods exist for the investigation of limit-cycle oscillations of panels in supersonic flow. In general, for the supersonic case, Galerkin's method is used in the spatial domain, and the panel deflection is then expressed in terms of one to six linear normal modes. Various techniques in the temporal domain such as harmonic balance [10, 20–23] have been used successfully to study the subject of panel flutter. This method requires less computational time than the method of direct integration and is mathematically comprehensible and systematic, but extremely tedious to implement. Another popular method to study panel flutter is the perturbation method. Correlation between perturbation techniques and the harmonic balance method has been shown to be quite good [21,24,25].

Most of the early research in panel flutter using classical analytical methods [26–30] has been limited to orthotropic materials. Recently, a considerable focus has turned to the application of anisotropic materials. However, most of this work has been limited to the area of linear structural theory using classical laminated plate theory. Librescu [31], retaining only the linear aerodynamic damping terms, derived the governing equations for an arbitrary number of modes using Galerkin's method and the Lyapunov stability criterion. He investigated the aeroelastic stability of orthotropic panels in the vicinity of the critical dynamic pressure. The geometric

nonlinear flutter of orthotropic panels was recently studied by Eslami [32,33] using harmonic balance. All of the analytical investigations have been limited to two-dimensional or three-dimensional rectangular plates with all four edges simply supported or clamped.

Extension of the finite element method to study the linear panel flutter problem was due to Olson [34,35]. Because of its versatile applicability, effects of aerodynamic damping, complex panel configurations, flow angularities, in-plane prestress, and laminated anisotropic panel properties can be easily and conveniently included in the finite element formulation. A review of the linear panel flutter using finite element methods was given by Yang and Sung [36].

Application of the finite element method to study the supersonic limit-cycle oscillations of two-dimensional panels was given by Mei and Rogers [37] and Mei [38]. Rao and Rao [39] also investigated the large-amplitude supersonic flutter of two-dimensional panels with ends elastically restrained against rotation. Mei and Weidman [40], Han and Yang [41], and Mei and Wang [42] further extended the finite element method to treat supersonic limit-cycle oscillations of three-dimensional rectangular and triangular isotropic plates, respectively.

Recently, Sarma and Varadan [43] studied the nonlinear behavior of two-dimensional isotropic panels using the linear aerodynamic theory. They presented two solution methods using a seventh-order displacement based finite element; the first method uses the nonlinear free vibration mode shape as an approximation to the nonlinear panel flutter problem, and the second method uses the linear panel flutter mode shape as an initial estimate for an iterative solution process similar to those given in Refs. [37–42]. Because of the recent renewed interest in panel flutter at the high-supersonic/hypersonic speeds [3], Gray, et al. [44] extend the finite element method to investigate the hypersonic limit-cycle oscillations of two-dimensional panels which constitutes part of this dissertation. A treatment of the aeroelastic concepts and principles is covered at the fundamental level in Refs. 45–47.

1.3 Objectives and Scope

The overall goal of the present study is to develop an effective computational strategy for predicting the nonlinear flutter response of thin anisotropic panels in hypersonic flow. To this end, there are three global objectives. Since the panel flutter solution using the finite element formulation is performed in the frequency domain, the first objective is to develop and validate

a large-amplitude free vibration linearizing method. To assess the effects of the full nonlinear third-order piston theory aerodynamics, the second objective is to develop and implement a solution method to solve the nonstandard, nonlinear eigenvalue problem. This objective will also allow for the solution of large-amplitude, nonlinear, damped, free vibration of panels. The final objective is to combine the first two objectives and extend the finite element formulation to include the anisotropic laminated plate theory to study the large-amplitude fluttering composite panel in hypersonic flow.

Under the influence of large-amplitude displacements, the mid-plane forces and aerodynamic damping restrain the motion of the panel to a bounded limit-cycle. Consequently, the von Karman nonlinear strain-displacement relationships are used in the present formulation. The aerodynamic loading used in this study is the unsteady full third-order piston aerodynamic theory. This is the complete expansion up to order three that the most widely used, linear, first-order theory is derived. The first-order theory has been shown to be valid and yields reasonable results for supersonic Mach numbers ($M > 1.7$). The effects of hypersonic nonlinear aerodynamic loadings on panel flutter will be studied to assess the higher-order aerodynamic theory to determine the extent to which it produces a “soft spring” effect that will predict lower limit-cycle flutter velocities than those predicted by the first-order piston theory. The proposed solution method develops the nonlinear stiffness and nonlinear aerodynamic influence matrices, linearizes the nonlinear matrices, transforms the problem formulation from the configuration space to the state space, then solves, in an iterative manner, the general eigenvalue problem.

The finite element formulation for a type 5 flutter analysis is developed in Chapter 2. In this Chapter, the governing variational principles for the two-dimensional and three-dimensional fluttering panel are presented and discussed. The nonlinear homogeneous equations of motion for the nonlinear finite element formulation are developed to include the displacement dependent aerodynamic influence and the aerodynamic damping matrices. Large deflection terms are included in the first- and second-order nonlinear stiffness, aerodynamic influence, and aerodynamic damping matrices.

The computational solution procedure is developed in Chapter 3. This procedure introduces a linearization technique for the nonlinear, displacement dependent stiffness, aerodynamic influence, and aerodynamic damping matrices. The constrained system matrices are linearized

and an iterative solution procedure similar to that first introduced by Mei [48–50] is implemented to solve the nonlinear eigenvalue problem by using a single, linearized updated mode shape. The iterative method is extended to include the generalized velocities so that nonlinear velocity-dependent aerodynamic effect can be included.

The solution of the large deflection panel flutter problem, including anisotropic material behavior and unsteady displacement and velocity dependent aerodynamics, is the ultimate objective of the present research. The present study is the first finite element solution technique for the large-amplitude composite panel flutter using unsteady displacement and velocity dependent aerodynamics.

The methodology developed in the present study can be used to obtain large-amplitude free, damped or undamped, vibration solution, as well as panel flutter results, for two- and three-dimensional anisotropic panels with arbitrary boundary conditions. Using the finite element principles to derive these nonlinear solutions is considered to be a significant contribution, since for complex boundary conditions and unsymmetrical laminates, classical solutions are laborious, and in some cases, impossible to apply.

Numerical verification results are presented in Chapter 4. The purpose of this chapter is to provide complete confidence in the numerical procedure and method. This is accomplished by presenting numerical comparisons with alternate solutions starting from the simplest, large-amplitude free vibration of a two-dimensional simply-supported panel to the flutter results for a three-dimensional composite panel. Chapter 5 presents flutter results for two- and three-dimensional isotropic/composite panels. In addition, studies are presented to illustrate the effect of each of the nonlinear aerodynamic terms. Concluding remarks and recommendations for future work are presented in Chapter 6.

PANEL FLUTTER
AEROELASTICITY

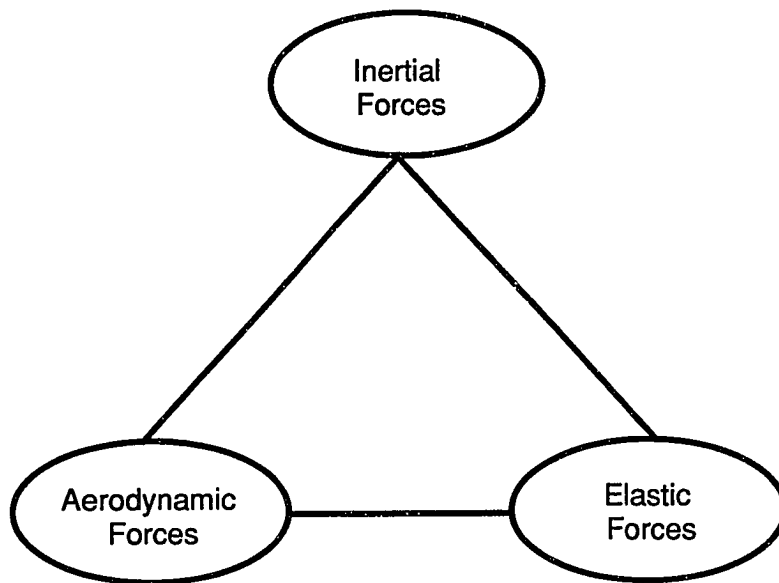


Fig. 1.1 Aeroelastic Interaction.

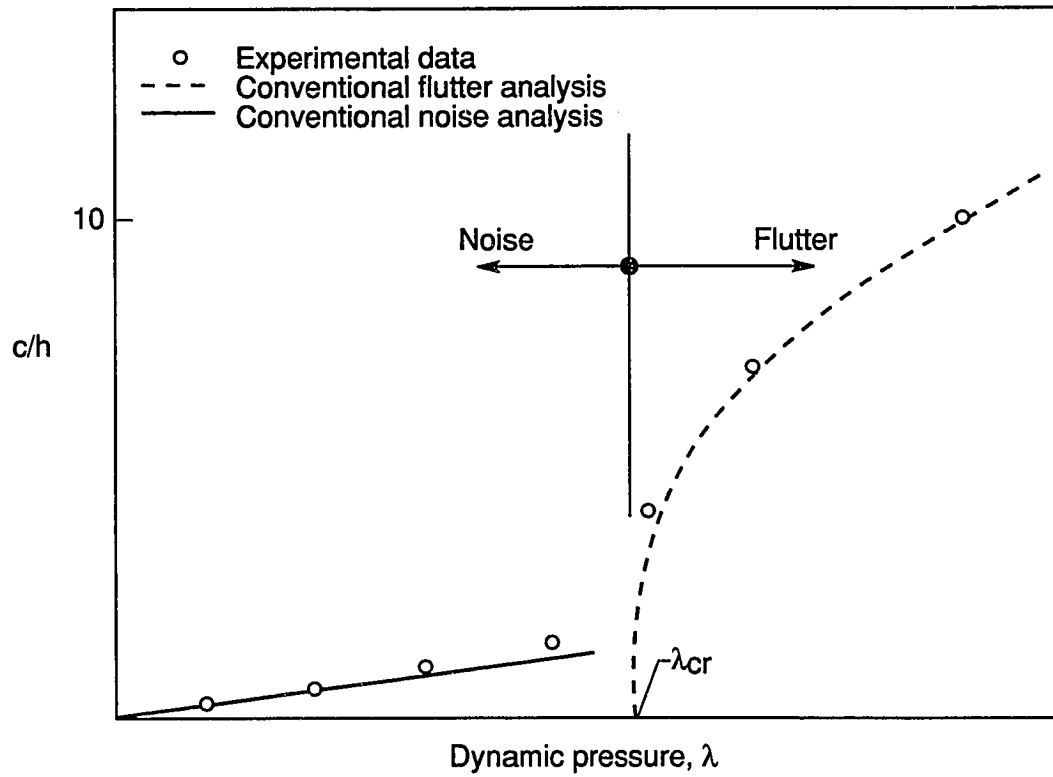


Fig. 1.2 Panel Flutter: Schematic of Plate Response using Piston Theory.
(from Dowell [7])

PANEL FLUTTER THEORIES

TYPE

- 1. Linear structural theory; linear piston theory aerodynamics.**
- Defines flutter boundary, $\sqrt{2} < M < 5$.
- 2. Linear structural theory; linearized potential flow aerodynamics.**
- Defines flutter boundary, $1 < M < 5$.
- 3. Nonlinear structural theory; linear piston theory aerodynamics.**
- Defines limit-cycle frequency and amplitude, $\sqrt{2} < M < 5$.
- 4. Nonlinear structural theory; linearized potential flow aerodynamics.**
- Defines limit-cycle frequency and amplitude, $1 < M < 5$.
- 5. Nonlinear structural theory; nonlinear piston theory aerodynamics.**
- Defines limit-cycle frequency and amplitude, $M > 5$.
(TYPE 3 is a special case of type 5)

Fig. 1.3 General Panel Flutter Theories.

Chapter 2

FINITE ELEMENT FORMULATION

In this chapter, the governing element equations are derived for both two- and three-dimensional thin panels subjected to aerodynamic loads using the third-order piston aerodynamic theory.

Consider the two-dimensional flat panel as shown in Fig. 2.1 or the three-dimensional laminated panel as shown in Fig. 2.2 of length a , width b for a three-dimensional panel, thickness h , and mass density ρ with a fluid flow above the panel at Mach number M . It is assumed that fluid flow above the panel is in the positive x coordinate direction and that the effects of the cavity on the back side of the panel can be neglected. The sign convention to be followed is that positive flow is in the direction of increasing x and a positive deflection is into the cavity. Since this study addresses thin panels ($a/h > 50$), the effect of transverse shear deformations, normally associated with thick plates (laminates) is neglected (see Jones [51] for example). This assumption is justified due to the minimum weight constraint that generally drives the panel's design parameters such that a/h is greater than 100.

2.1 Hamilton's Principle for a Continuum

The most general form of Hamilton's principle for a nonconservative elastic continuous medium is

$$\int_{t_1}^{t_2} \left[\int_V (\rho \ddot{\mathbf{u}}_{,tt} \cdot \delta \mathbf{u}) dV - \left(\int_V (\vec{f} \cdot \delta \mathbf{u}) dV + \int_S (\vec{p} \cdot \delta \mathbf{u}) dS - \int_V (\sigma : \delta \epsilon) dV \right) \right] dt = 0 \quad (2.1)$$

where S and V are the surface area and volume of the element, respectively. The terms under the time integral represent the work done on the body at any time t by the resultant force in moving through the virtual displacement $\delta \mathbf{u}$; \vec{f} is the body force, and is neglected in this formulation; \vec{p} is the specified surface stress vector; and $(\sigma : \delta \epsilon)$ is a stress-virtual strain-tensor product.

2.2 Constitutive and Strain-Displacement Relationships

For the two-dimensional panel, the basic material properties are associated with a single direction. Thus, only an isotropic material will be considered. However, since for the three-dimensional panel, there are two primary material directions, the formulation will be for the most general anisotropic laminated material of which an isotropic material is a special case.

2.2.1 Two-Dimensional Isotropic Panel

For the two-dimensional isotropic panel, the stress-strain relationship becomes

$$\sigma = \frac{E}{(1 - \nu^2)} \epsilon \quad (2.2)$$

where E is the isotropic Young's modulus and ν is Poisson's ratio.

The form of the strain-displacement relationship for an arbitrary point through the thickness, h , is as follows:

$$\epsilon = u_{,x} + \frac{1}{2} w_{,x}^2 - zw_{,xx} \quad (2.3)$$

2.2.2 Three-Dimensional Orthotropic Panel

For the orthotropic lamina [51], the stress-strain relationship in x - y coordinates are

$$\{\sigma\} = \begin{Bmatrix} \sigma_x \\ \sigma_y \\ \tau_{xy} \end{Bmatrix} = [\bar{Q}] \begin{Bmatrix} \epsilon_x \\ \epsilon_y \\ \gamma_{xy} \end{Bmatrix} = [\bar{Q}]\{\epsilon\} \quad (2.4)$$

in which

$$\begin{aligned} \bar{Q}_{11} &= Q_{11} \cos^4 \theta + 2(Q_{12} + 2Q_{66}) \sin^2 \theta \cos^2 \theta + Q_{22} \sin^4 \theta \\ \bar{Q}_{22} &= Q_{11} \sin^4 \theta + 2(Q_{12} + 2Q_{66}) \sin^2 \theta \cos^2 \theta + Q_{22} \cos^4 \theta \\ \bar{Q}_{12} &= (Q_{11} + Q_{22} - 4Q_{66}) \sin^2 \theta \cos^2 \theta + Q_{12}(\sin^4 \theta + \cos^4 \theta) \\ \bar{Q}_{16} &= (Q_{11} - Q_{12} - 2Q_{66}) \sin \theta \cos^3 \theta + (Q_{12} - Q_{22} + 2Q_{66}) \sin^3 \theta \cos \theta \\ \bar{Q}_{26} &= (Q_{11} - Q_{12} - 2Q_{66}) \sin^3 \theta \cos \theta + (Q_{12} - Q_{22} + 2Q_{66}) \sin \theta \cos^3 \theta \\ \bar{Q}_{66} &= (Q_{11} + Q_{22} - 2Q_{12} - 2Q_{66}) \sin^2 \theta \cos^2 \theta + Q_{66}(\sin^4 \theta + \cos^4 \theta) \end{aligned} \quad (2.5)$$

The bar over the \bar{Q}_{ij} denotes the transformed reduced stiffnesses relative to the x - y - z coordinate system noted in Fig. 2.2. The Q_{ij} 's are the reduced stiffnesses in the material coordinate systems, also shown in Fig. 2.2.

For the orthotropic lamina the reduce stiffnesses, Q_{ij} 's, are

$$\begin{aligned} Q_{11} &= \frac{E_{11}}{(1 - \nu_{12}\nu_{21})} \\ Q_{12} &= \frac{\nu_{12}E_{22}}{(1 - \nu_{12}\nu_{21})} \\ Q_{22} &= \frac{E_{22}}{(1 - \nu_{12}\nu_{21})} \\ Q_{66} &= G_{12} \end{aligned} \tag{2.6}$$

where the i and j subscripts denote the material coordinate axes. The constitutive relationship for an isotropic material is a special case where $E_{11} = E$, $E_{22} = E$, $G_{12} = G = \frac{E}{2(1 + \nu)}$, and $\nu_{12} = \nu$.

Similarly, the form of the strain-displacement relationships for an arbitrary point through the thickness, h , are as follows:

$$\begin{aligned} \epsilon_x &= u_{,x} + \frac{1}{2}w_{,x}^2 - zw_{,xx} \\ \epsilon_y &= v_{,y} + \frac{1}{2}w_{,y}^2 - zw_{,yy} \\ \gamma_{xy} &= u_{,y} + v_{,x} + w_{,x}w_{,y} - zw_{,xy} \end{aligned} \tag{2.7}$$

where u and v are the in-plane (midsurface) displacements measured along the x and y coordinate axes, respectively, and w is the transverse displacement measured along the z -axis normal to the plane of the panel. The nonlinear terms in Eqs. (2.3) and (2.7) are commonly referred to as the von Karman nonlinear (finite) strains.

2.3 Aerodynamic Pressure Function

The virtual work integral involving the surface stress vector is evaluated using the unsteady full third-order piston theory aerodynamics [6] to develop the aerodynamic loads on the upper surface of the panel. Again, this relates the local point function pressure generated by the panel's motion to the local normal component of the flow velocity. Thus, the aerodynamic pressure loading as given by this theory is

$$\begin{aligned} p - p_\infty &= \frac{2q}{M} \left[\frac{1}{V}w_{,t} + w_{,x} + \frac{(\gamma + 1)}{4}M \left(\frac{1}{V}w_{,t} + w_{,x} \right)^2 \right. \\ &\quad \left. + \frac{(\gamma + 1)}{12}M^2 \left(\frac{1}{V}w_{,t} + w_{,x} \right)^3 \right] \end{aligned} \tag{2.8}$$

The first two terms in the bracket in Eq. (2.8) constitutes what is commonly referred to as the first-order piston theory aerodynamics and Eq. (2.8) without the cubic term represents the second-order piston theory aerodynamics.

In reference [9], McIntosh uses a modified form of Eq. (2.8). In his work, the $w_{,t}$ in the cubed bracket is neglected. Since a complete derivation (see Appendix A) of the third-order piston aerodynamic theory would include this term, and since the additional complications to include this term in the finite element formulation is minimal, this term is retained in this study. Retaining this term will allow for a full evaluation of it's influence on the panel's response.

Piston, Ackeret, and other quasi-steady aerodynamic theories have been shown [14] to give good estimates of the panel thickness required to prevent panel flutter. However, all of the references in the literature do strongly suggest that these theories are only valid for Mach number ranges greater than 1.6–2.0. Generally, this is taken to be greater than $\sqrt{2}$. Since this study is concerned with the panel flutter phenomena at high supersonic ($M = 3 \dots 5$) to hypersonic ($M > 5$) speeds, piston theory is adequate for computational purposes.

2.4 Element Representation

2.4.1 Two-Dimensional Isotropic Panel

Using Eqs. (2.2), (2.3), and (2.8) in (2.1) results in the following expression for Hamilton's principle for an element of length a_e :

$$\begin{aligned}
& \int_0^{a_e} \rho h (u_{,tt} \delta u + w_{,tt} \delta w) dx \\
& + \frac{2q}{M} \int_0^{a_e} \left(\frac{1}{V} w_{,t} + w_{,x} + \frac{(\gamma+1)}{4} M \left(\frac{1}{V} w_{,t} + w_{,x} \right)^2 + \frac{(\gamma+1)}{12} M^2 \left(\frac{1}{V} w_{,t} + w_{,x} \right)^3 \right) \delta w dx \\
& + \int_0^{a_e} \frac{Eh}{(1-\nu^2)} \left(u_{,x} \delta u_{,x} + \frac{1}{2} w_{,x}^2 \delta u_{,x} + u_{,x} w_{,x} \delta w_{,x} \right. \\
& \left. + \frac{1}{2} w_{,x}^3 \delta w_{,x} + \frac{h^2}{12} w_{,xx} \delta w_{,xx} \right) dx
\end{aligned} \tag{2.9}$$

The displacement functions for the two-dimensional plate are chosen as

$$\begin{aligned}
w(x, t) &= [\phi_1 \ \phi_2 \ \phi_3 \ \phi_4] \{w_f\} \\
u(x, t) &= [\varphi_1 \ \varphi_2 \ \varphi_3 \ \varphi_4] \{w_m\}
\end{aligned} \tag{2.10}$$

where $\{w_f\}$ and $\{w_m\}$ are the element nodal displacement quantities at the two ends of the plate, see Fig. 2.3,

$$\{w_f\} = \begin{Bmatrix} w_1 \\ \vartheta_1 \\ w_2 \\ \vartheta_2 \end{Bmatrix}, \quad \{w_m\} = \begin{Bmatrix} u_1 \\ \epsilon_1 \\ u_2 \\ \epsilon_2 \end{Bmatrix} \quad (2.11)$$

The subscripts 1 and 2 refer to the two end nodes of the element and ϕ_j and φ_j , where $j = 1$ to 4, are the cubic interpolation functions defined as

$$\begin{aligned} \phi_1 = \varphi_1 &= 1 - 3(x/a_e)^2 + 2(x/a_e)^3 \\ \phi_2 = \varphi_2 &= x \left[1 - 2(x/a_e) + (x/a_e)^2 \right] \\ \phi_3 = \varphi_3 &= 3(x/a_e)^2 - 2(x/a_e)^3 \\ \phi_4 = \varphi_4 &= x \left[(x/a_e) - (x/a_e)^3 \right] \end{aligned} \quad (2.12)$$

Using Eq. (2.10) in Eq. (2.9), dividing by a^3/D , letting $t = \tau/\omega_o$ and $x = a\xi$ (τ and ξ are nondimensional time and position, respectively), $\lambda = 2qa^3/MD$ (nondimensional dynamic pressure), $\mu = \rho_a a/\rho h$ (nondimensional mass parameter); $r = h/a$, $M = \text{Mach number}$, $D = Eh^3/12(1 - \nu^2)$ and assuming constant properties over an element, the nondimensional element mass, stiffness, and aerodynamic influence matrices can be developed and written in terms of the interpolation functions and nodal quantities. Assembling the mass, stiffness, and aerodynamic influence matrices, the equations of motion for an element become

$$\begin{aligned} & \begin{bmatrix} [m_f] & [0] \\ [0] & [m_m] \end{bmatrix} \begin{Bmatrix} \ddot{w}_f \\ \ddot{w}_m \end{Bmatrix} + \begin{bmatrix} ([g] + [g1_t] + [g2_{ft}] + [g2_t]) & [0] \\ [0] & [0] \end{bmatrix} \begin{Bmatrix} \dot{w}_f \\ \dot{w}_m \end{Bmatrix} \\ & + \begin{bmatrix} ([a] + [a1_t] + [a1_f] + [a2_{ft}] + [a2_f]) & [0] \\ [0] & [0] \end{bmatrix} \begin{Bmatrix} w_f \\ w_m \end{Bmatrix} + \begin{bmatrix} [k_{ff}] & [0] \\ [0] & [k_{mm}] \end{bmatrix} \begin{Bmatrix} w_f \\ w_m \end{Bmatrix} \\ & + \begin{bmatrix} [k1_{ff}] & [k1_{fm}] \\ [k1_{mf}] & [0] \end{bmatrix} \begin{Bmatrix} w_f \\ w_m \end{Bmatrix} + \begin{bmatrix} [k2_{ff}] & [0] \\ [0] & [0] \end{bmatrix} \begin{Bmatrix} w_f \\ w_m \end{Bmatrix} = \begin{Bmatrix} f_f \\ f_m \end{Bmatrix} \end{aligned} \quad (2.13)$$

where $\{f\}$ is the internal element equilibrium forces, $[k]$ is the linear elastic stiffness matrix, $[k1]$ and $[k2]$ are nonlinear stiffness matrices which depend linearly and quadratically upon displacements, respectively, and are defined as follows.

$$\underline{\text{mass}} \quad (2.14)$$

$$[m_f] = \int_0^{a_e/a} \{\phi\}[\phi] d\xi \quad (2.14a)$$

$$[m_m] = \int_0^{a_e/a} \{\varphi\}[\varphi] d\xi \quad (2.14b)$$

$$\underline{\text{stiffness}} \quad (2.15)$$

$$[k_{ff}] = \int_0^{a_e/a} \{\phi''\}[\phi''] d\xi \quad (2.15a)$$

$$[k_{mm}] = 12/r^2 \int_0^{a_e/a} \{\varphi'\}[\varphi'] d\xi \quad (2.15b)$$

$$[k1_{mf}] = 6/r \int_0^{a_e/a} \left(\frac{w_{,\xi}}{h}\right) \{\varphi'\}[\phi'] d\xi \quad (2.15c)$$

$$[k1_{fm}] = 6/r \int_0^{a_e/a} \left(\frac{w_{,\xi}}{h}\right) \{\phi'\}[\varphi'] d\xi \quad (2.15d)$$

$$[k1_{ff}] = 6/r \int_0^{a_e/a} \left(\frac{u_{,\xi}}{h}\right) \{\phi'\}[\phi'] d\xi \quad (2.15e)$$

$$[k2_{ff}] = 6 \int_0^{a_e/a} \left(\frac{w_{,\xi}}{h}\right)^2 \{\phi'\}[\phi'] d\xi \quad (2.15f)$$

$$\underline{\text{aerodynamic influence}} \quad (2.16)$$

$$[a] = \lambda \int_0^{a_e/a} \{\phi\}[\phi'] d\xi \quad (2.16a)$$

$$[g] = \sqrt{\lambda\mu/M} \int_0^{a_e/a} \{\phi\}[\phi] d\xi \quad (2.16b)$$

$$[g1_t] = \frac{\gamma+1}{4} \left(M \frac{h}{a}\right) \left(\frac{\mu}{M}\right) \int_0^{a_e/a} \left(\frac{w_{,\tau}}{h}\right) \{\phi\}[\phi] d\xi \quad (2.16c)$$

$$[g2_t] = \frac{\gamma+1}{12} \left(M \frac{h}{a}\right)^2 \sqrt{\frac{1}{\lambda} \left(\frac{\mu}{M}\right)^3} \int_0^{a_e/a} \left(\frac{w_{,\tau}}{h}\right)^2 \{\phi\}[\phi] d\xi \quad (2.16d)$$

$$[g2_{ft}] = \frac{\gamma+1}{4} \left(M \frac{h}{a}\right)^2 \left(\frac{\mu}{M}\right) \int_0^{a_e/a} \left(\frac{w_{,\xi} w_{,\tau}}{h^2}\right) \{\phi\}[\phi] d\xi \quad (2.16e)$$

$$[a1_t] = \frac{\gamma+1}{2} \left(M \frac{h}{a}\right) \sqrt{\lambda \left(\frac{\mu}{M}\right)} \int_0^{a_e/a} \left(\frac{w_{,\tau}}{h}\right) \{\phi\}[\phi'] d\xi \quad (2.16f)$$

$$[a1_f] = \frac{\gamma+1}{4} \lambda \left(M \frac{h}{a}\right) \int_0^{a_e/a} \left(\frac{w_{,\xi}}{h}\right) \{\phi\}[\phi'] d\xi \quad (2.16g)$$

$$[a2_{ft}] = \frac{\gamma+1}{4} \left(M \frac{h}{a}\right)^2 \sqrt{\lambda \left(\frac{\mu}{M}\right)} \int_0^{a_e/a} \left(\frac{w_{,\xi} w_{,\tau}}{h^2}\right) \{\phi\}[\phi'] d\xi \quad (2.16h)$$

$$[a2_f] = \frac{\gamma+1}{12} \lambda \left(M \frac{h}{a}\right)^2 \int_0^{a_e/a} \left(\frac{w_{,\xi}}{h}\right)^2 \{\phi\}[\phi'] d\xi \quad (2.16i)$$

where $\{\phi\} = [\phi]^T$, $\{\varphi\} = [\varphi]^T$, and $(\cdot)' = \frac{d(\cdot)}{d\xi}$, $(\cdot) = \frac{d(\cdot)}{d\tau}$, $(\cdot)_{,\xi} = \frac{\partial(\cdot)}{\partial\xi}$, $(\cdot)_{,\tau} = \frac{\partial(\cdot)}{\partial\tau}$.

The variational principle in Eq. (2.1) represents a finite element approach to study the limit-cycle oscillations of a two-dimensional panel at hypersonic speeds. Unlike first-order piston theory aerodynamics which will produce two linear aerodynamic influence matrices, $[g]$ and $[a]$, the third-order piston theory aerodynamics yields, in addition to the same two linear matrices, seven nonlinear aerodynamic influence matrices, $[g1_t]$, $[g2_t]$, $[g2_{ft}]$, $[a1_t]$, $[a1_f]$, $[a2_{ft}]$, and $[a2_f]$, where the aerodynamic matrices are functions of the system aerodynamic parameters, in particular the dynamic pressure, λ . The aerodynamic influence matrices $[g]$ and $[a]$ are linear, whereas $[g1_t]$, $[a1_t]$, and $[a1_f]$ depend linearly, denoted with 1, upon the displacements, denoted with subscript f , or the time derivative of the displacements (generalized velocities), denoted with subscript t . The other four matrices, $[g2_{ft}]$, $[g2_t]$, $[a2_{ft}]$, and $[a2_f]$ are quadratic, denoted with 2, in displacement, subscript f , and/or generalized velocities, subscript t . The symmetry in the first-order nonlinear stiffness matrix, $[k1]$, has been preserved at the expense of transferring the nonlinearity on $w_{,\xi}$ to $u_{,\xi}$ by splitting $u_{,x} w_{,x} \delta w_{,x}$ into two equal parts and producing the $[k1_{ff}]$ term. Since the element matrices associated with the aerodynamic damping, $[g]$, are similar in form to $[m]$ they are symmetrical; however, since the aerodynamic influence $[a]$ involves a spatial derivative, the resulting element matrices are skew-symmetric.

2.4.2 Three-Dimensional Rectangular Panel

Since a typical four-node plate element has considerable more degrees of freedom per node, the derivation for a general rectangular plate finite element is easier to conduct using matrix notation. The derivation starts by considering the terms in Eq. (2.1) separately.

The first term to consider is the variation of the internal strain energy, δU , (fourth term in Eq. (2.1)). This term, in matrix notation, has the following form:

$$\delta U = \int_V \{\delta \epsilon\}^T \{\sigma\} dV \quad (2.17)$$

where $\{\epsilon\}$ and $\{\sigma\}$ are defined in Eq. (2.4) and V represents the volume of the element. Using Eq. (2.4) for $\{\sigma\}$ in Eq. (2.17), then Eq. (2.17) can be written as

$$\delta U = \int_V \{\delta \epsilon\}^T [\bar{Q}] \{\epsilon\} dV \quad (2.18)$$

For a general plate element undergoing both bending and extension, the complete strain, for any point through the thickness located at coordinate z , is composed of two parts. The first part is due to stretching the midsurface, and the second part is due to the change in curvature, $\{\kappa\}$, during bending. Thus, using Kirchhoff hypothesis, the total strain can be written as

$$\{\epsilon\} = \{e\} + z\{\kappa\} = \begin{Bmatrix} e_x \\ e_y \\ e_{xy} \end{Bmatrix} + z \begin{Bmatrix} \kappa_x \\ \kappa_y \\ \kappa_{xy} \end{Bmatrix} \quad (2.19)$$

If the relationships between the strain-displacement in Eq. (2.7) are written as a vector, then the membrane strain, $\{e\}$, takes on the form

$$\{e\} = \begin{Bmatrix} u_{,x} + \frac{1}{2}x_{,x}^2 \\ v_{,y} + \frac{1}{2}w_{,y}^2 \\ u_{,y} + v_{,x} + w_{,x}w_{,y} \end{Bmatrix} \quad (2.20)$$

The membrane strains in Eq. (2.20) can also be written as

$$\{e\} = \{e_m\} + \{e_{mb}\} \quad (2.21)$$

where $\{e_m\}$ is the linear portion of the membrane strain and $\{e_{mb}\}$ is the nonlinear, von Karman, membrane-bending coupling strains. The curvatures written in terms of the transverse

displacement, w , become

$$\{\kappa\} = \begin{Bmatrix} -w,_{xx} \\ -w,_{yy} \\ -2w,_{xy} \end{Bmatrix} \quad (2.22)$$

Using Eq. (2.19) in Eq. (2.18) and expanding, then the internal strain energy can be written as

$$\delta U = \int_V \left[\{\delta e\}^T [\bar{Q}] \{e\} + z \{\delta e\}^T [\bar{Q}] \{\kappa\} + z \{\delta \kappa\}^T [\bar{Q}] \{e\} + z^2 \{\delta \kappa\}^T [\bar{Q}] \{\kappa\} \right] dV \quad (2.23)$$

Integrating Eq. (2.23) through the thickness, h , and using the definition for the classical laminated stiffnesses of

$$[A] = \int_{-\frac{h}{2}}^{+\frac{h}{2}} [\bar{Q}] dz \quad (2.24)$$

$$[B] = \int_{-\frac{h}{2}}^{+\frac{h}{2}} z [\bar{Q}] dz \quad (2.25)$$

$$[D] = \int_{-\frac{h}{2}}^{+\frac{h}{2}} z^2 [\bar{Q}] dz \quad (2.26)$$

yields,

$$\delta U = \int_S \left[\{\delta e\}^T [A] \{e\} + \{\delta e\}^T [B] \{\kappa\} + \{\delta \kappa\}^T [B] \{e\} + \{\delta \kappa\}^T [D] \{\kappa\} \right] dS \quad (2.27)$$

The $[A]$, $[B]$, and $[D]$ matrices are the classical laminate extensional, bending-extensional, and bending stiffnesses, respectively.

Proceeding from this point, the displacements in Eqs. (2.20) and (2.22) are approximated over a typical element using interpolation functions, see Appendix B for derivation and definitions, and nodal displacement quantities as follows:

$$\begin{aligned} w &= [\phi_w] \{\Delta w\} \\ u &= [\phi_u] \{\Delta u\} \\ v &= [\phi_v] \{\Delta v\} \end{aligned} \quad (2.28)$$

Using the Eqs. (2.2) and (2.22), the curvatures and midsurface strains, in the von Karman sense, are related to the nodal displacements as

$$\{\kappa\} = \begin{Bmatrix} -w,_{xx} \\ -w,_{yy} \\ -2w,_{xy} \end{Bmatrix} = \begin{bmatrix} -[\phi_w]_{,xx} \\ -[\phi_w]_{,yy} \\ -2[\phi_w]_{,xy} \end{bmatrix} \{\Delta w\} \quad (2.29)$$

and for $\{e\} = \{e_m\} + \{e_{mb}\}$

$$\begin{aligned} \{e_m\} &= \begin{bmatrix} [\phi_u]_{,x} & 0 \\ 0 & [\phi_v]_{,y} \\ [\phi_u]_{,y} & [\phi_v]_{,x} \end{bmatrix} \begin{Bmatrix} \{\Delta u\} \\ \{\Delta v\} \end{Bmatrix} \\ \{e_{mb}\} &= \frac{1}{2} \begin{bmatrix} w,_{x} & 0 \\ 0 & w,_{y} \\ w,_{y} & w,_{x} \end{bmatrix} \begin{bmatrix} [\phi_w]_{,x} \\ [\phi_w]_{,y} \end{bmatrix} \{\Delta w\} \end{aligned} \quad (2.30)$$

Similarly, the variation of the curvatures and midsurface strains are related to the nodal displacements as

$$\{\delta\kappa\} = \begin{bmatrix} -[\phi_w]_{,xx} \\ -[\phi_w]_{,yy} \\ -2[\phi_w]_{,xy} \end{bmatrix} \{\delta\Delta w\} \quad (2.31)$$

and for $\{\delta e\} = \{\delta e_m\} + \{\delta e_{mb}\}$

$$\begin{aligned} \{\delta e_m\} &= \begin{bmatrix} [\phi_u]_{,x} & 0 \\ 0 & [\phi_v]_{,y} \\ [\phi_u]_{,y} & [\phi_v]_{,x} \end{bmatrix} \begin{Bmatrix} \{\delta\Delta u\} \\ \{\delta\Delta v\} \end{Bmatrix} \\ \{\delta e_{mb}\} &= \begin{bmatrix} w,_{x} & 0 \\ 0 & w,_{y} \\ w,_{y} & w,_{x} \end{bmatrix} \begin{bmatrix} [\phi_w]_{,x} \\ [\phi_w]_{,y} \end{bmatrix} \{\delta\Delta w\} \end{aligned} \quad (2.32)$$

The following notation is adopted to further simplify the matrix equations:

$$[P_w] = \begin{bmatrix} -[\phi_w]_{,xx} \\ -[\phi_w]_{,yy} \\ -2[\phi_w]_{,xy} \end{bmatrix} \quad (2.33)$$

$$[P_u] = \begin{bmatrix} [\phi_u]_{,x} & 0 \\ 0 & [\phi_v]_{,y} \\ [\phi_u]_{,y} & [\phi_v]_{,x} \end{bmatrix} \quad (2.34)$$

$$[C_\theta] = \begin{bmatrix} [\phi_w]_{,x} \\ [\phi_w]_{,y} \end{bmatrix} \quad (2.35)$$

$$[\theta] = \begin{bmatrix} w_{,x} & 0 \\ 0 & w_{,y} \\ w_{,y} & w_{,x} \end{bmatrix} \quad (2.36)$$

Using the definitions, Eqs. (2.33)–(2.36) in Eqs. (2.29)–(2.32), then the results can be used in the variation of the internal strain energy, δU . Since there are four parts to Eq. (2.27), each term will be expanded separately. The first term, $\{\delta e\}^T[A]\{e\}$, when expanded out consists of the following four parts:

$$\{\delta e_m\}^T[A]\{e_m\} = [\delta \Delta u \ \delta \Delta v][P_u]^T[A][P_u] \begin{Bmatrix} \Delta u \\ \Delta v \end{Bmatrix} \quad (2.37)$$

$$\{\delta e_m\}^T[A]\{e_{mb}\} = \frac{1}{2}[\delta \Delta u \ \delta \Delta v][P_u]^T[A][\theta][C_\theta]\{\Delta w\} \quad (2.38)$$

$$\{\delta e_{mb}\}^T[A]\{e_m\} = [\delta \Delta w][C_\theta]^T[\theta]^T[A][P_u] \begin{Bmatrix} \Delta u \\ \Delta v \end{Bmatrix} \quad (2.39)$$

$$\{\delta e_{mb}\}^T[A]\{e_{mb}\} = \frac{1}{2}[\delta \Delta w][C_\theta]^T[\theta]^T[A][C_\theta]\{\Delta w\} \quad (2.40)$$

The second term in Eq. (2.27), $\{\delta e\}^T[B]\{\kappa\}$, when expanded out generates two additional terms due to the unsymmetrical nature of the laminate. These terms are

$$\{\delta e_m\}^T[B]\{\kappa\} = [\delta \Delta u \ \delta \Delta v][P_u]^T[B][P_w]\{\Delta w\} \quad (2.41)$$

$$\{\delta e_{mb}\}^T[B]\{\kappa\} = [\delta \Delta w][C_\theta]^T[\theta]^T[B][P_w]\{\Delta w\} \quad (2.42)$$

The third term, like the second, yields two more terms as a result of the unsymmetrical nature of the laminate. These terms are

$$\{\delta \kappa\}^T[B]\{e_m\} = [\delta \Delta w][P_w]^T[B][P_u] \begin{Bmatrix} \Delta u \\ \Delta v \end{Bmatrix} \quad (2.43)$$

$$\{\delta \kappa\}^T[B]\{e_{mb}\} = \frac{1}{2}[\delta \Delta w][P_w]^T[B][\theta][C_\theta]\{\Delta w\} \quad (2.44)$$

The final term in Eq. (2.27) is the standard, symmetric, pure bending expression,

$$\{\delta \kappa\}^T[D]\{\kappa\} = [\delta \Delta w][P_w]^T[D][P_w]\{\Delta w\} \quad (2.45)$$

Equations (2.37)–(2.45) represent the full nonlinear, in the von Karman sense, internal strain energy for the most general composite (anisotropic) panel. A closer inspection of Eqs. (2.37)–(2.45) reveals that the nine terms will not yield a symmetrical system. However, the system can be made symmetric (although not a requirement since the aerodynamic system is skewed

symmetric) by using a procedure similar to that given in reference [52] where it is noted that the mid-plane force is $\{N\} = [A](\{e_m\} + \{e_{mb}\}) + [B]\{\kappa\}$.

Rewriting Eq. (2.39) as the sum of two equal parts as follows

$$\{\delta e_{mb}\}^T [A] \{e_m\} = \frac{1}{2} [\delta \Delta w] [C_\theta]^T [\theta]^T [A] [P_u] \begin{Bmatrix} \Delta u \\ \Delta v \end{Bmatrix} + \frac{1}{2} [\delta \Delta w] [C_\theta]^T [\theta]^T [A] [P_u] \begin{Bmatrix} \Delta u \\ \Delta v \end{Bmatrix} \quad (2.46)$$

is equivalent to Eq. (2.39).

Next, working with the last term in Eq. (2.46)

$$\frac{1}{2} [\delta \Delta w] [C_\theta]^T [\theta]^T [A] [P_u] \begin{Bmatrix} \Delta u \\ \Delta v \end{Bmatrix} \quad (2.47)$$

then Eq. (2.47) can be rewritten as

$$\frac{1}{2} [\delta \Delta w] [C_\theta]^T [\theta]^T \{N_A\} \quad (2.48)$$

where

$$\{N_A\} = [A] \{e_m\} = [A] [P_u] \begin{Bmatrix} \Delta u \\ \Delta v \end{Bmatrix} \quad (2.49)$$

which represents a portion of the midsurface force.

Using the transpose of Eq. (2.36),

$$[\theta]^T = \begin{bmatrix} w_{,x} & 0 & w_{,y} \\ 0 & w_{,y} & w_{,x} \end{bmatrix} \quad (2.50)$$

and noting that

$$\{N_A\} = \begin{Bmatrix} N_{Ax} \\ N_{Ay} \\ N_{Axy} \end{Bmatrix} \quad (2.51)$$

The product of the two terms, Eqs. (2.50) and (2.51),

$$[\theta]^T \{N_A\} = \begin{bmatrix} N_{Ax} w_{,x} + N_{Axy} w_{,y} \\ N_{Ay} w_{,y} + N_{Axy} w_{,x} \end{bmatrix} \quad (2.52)$$

is the last two terms in Eq. (2.48). Equation (2.52) can also be factored and written as the product of two new matrices as

$$\begin{bmatrix} N_{Ax} N_{Axy} \\ N_{Axy} N_{Ay} \end{bmatrix} \begin{Bmatrix} w_{,x} \\ w_{,y} \end{Bmatrix} \quad (2.53)$$

Thus, transforming the $\{N_A\}$ vector, Eq. (2.51), to a nonlinear stiffness denoted as

$$[\theta]^T \{N_A\} = [N_A] \begin{Bmatrix} w_{,x} \\ w_{,y} \end{Bmatrix} \quad (2.54)$$

Equation (2.54) can also be written as

$$[N_A][C_\theta]\{\Delta w\} \quad (2.55)$$

To summarize,

$$[\theta]^T[A][P_u]\left\{\begin{matrix}\Delta u \\ \Delta v\end{matrix}\right\} = [N_A][C_\theta]\{\Delta w\} \quad (2.56)$$

Thus, transforming the nonlinearity from w to u and v . Using Eq. (2.55), then Eq. (2.48) becomes

$$\frac{1}{2}[\delta\Delta w][C_\theta]^T[N_A][C_\theta]\{\Delta w\} \quad (2.57)$$

which is now symmetric.

Similarly, Eq. (2.42) and Eq. (2.44) can be summed and factored to produce a symmetric form as follows:

$$[\delta\Delta w]\left(\frac{1}{2}[C_\theta]^T[\theta]^T[B][P_w] + \frac{1}{2}[C_\theta]^T[\theta]^T[B][P_w] + \frac{1}{2}[P_w]^T[B][\theta][C_\theta]\right)\{\Delta w\} \quad (2.58)$$

Eq. (2.58) can be rewritten using the following transformation:

$$\{N_B\} = [B][P_w]\{\Delta w\} \quad (2.59)$$

which represents the force resulting from the bending-extension coupling of the laminate.

Using Eq. (2.50) and noting that

$$\{N_B\} = \begin{Bmatrix} N_{Bx} \\ N_{By} \\ N_{Bxy} \end{Bmatrix} \quad (2.60)$$

The product of these two terms, $[\theta]^T[B]$, is as follows:

$$\begin{bmatrix} N_{Bx}w_{,x} + N_{Bxy}w_{,y} \\ N_{By}w_{,y} + N_{Bxy}w_{,x} \end{bmatrix} = \begin{bmatrix} N_{Bx} & N_{Bxy} \\ N_{Bxy} & N_{By} \end{bmatrix} \begin{Bmatrix} w_{,x} \\ w_{,y} \end{Bmatrix} = [N_B] \begin{Bmatrix} w_{,x} \\ w_{,y} \end{Bmatrix} \quad (2.61)$$

Equation (2.61) can also be written as

$$[N_B][C_\theta]\{\Delta w\} \quad (2.62)$$

To summarize, using Eq. (2.62), then Eq. (2.58) becomes

$$\frac{1}{2}[\delta\Delta w]\left([C_\theta]^T[N_B][C_\theta] + [C_\theta]^T[\theta]^T[B][P_w] + [P_w]^T[B][\theta][C_\theta]\right)\{\Delta w\} \quad (2.63)$$

Thus, transforming the nonlinearity in w to a symmetric form.

Integrating Eqs. (2.37), (2.38), (2.40), (2.41), (2.43), (2.45), (2.46), (2.63), and (2.57) for the second half of (2.46) over the area of the element, S , and making the usual arguments about the variation being arbitrary leads to the following definition for the element stiffness matrices.

$$\text{stiffness} \tag{2.64}$$

$$[k_{mm}] = \int_S [P_u]^T [A] [P_u] dS \tag{2.64a}$$

$$[k_{1mf}] = \frac{1}{2} \int_S [P_u]^T [A] [\theta] [C_\theta] dS \tag{2.64b}$$

$$[k_{2ff}] = \frac{1}{2} \int_S [C_\theta]^T [\theta]^T [A] [\theta] [C_\theta] dS \tag{2.64c}$$

$$[k_{Bmf}] = \int_S [P_u]^T [B] [P_w] dS \tag{2.64d}$$

$$[k_{Bfm}] = \int_S [P_w]^T [B] [P_u] dS \tag{2.64e}$$

$$[k_{ff}] = \int_S [P_w]^T [D] [P_w] dS \tag{2.64f}$$

$$[k_{1Bff}] = \frac{1}{2} \int_S \left([C_\theta]^T [N_B] [C_\theta] + [C_\theta]^T [\theta]^T [B] [P_w] + [P_w]^T [B] [\theta] [C_\theta] \right) dS \tag{2.64g}$$

$$[k_{1fm}] = \frac{1}{2} \int_S [C_\theta]^T [\theta]^T [A] [P_u] dS \tag{2.64h}$$

$$[k_{1ff}] = \frac{1}{2} \int_S [C_\theta]^T [N_A] [C_\theta] dS \tag{2.64i}$$

The standard linear stiffnesses are given by Eqs. (2.64a) and (2.64f) while the linear stiffnesses given in Eqs. (2.64d) and (2.64e) are a result of the unsymmetrically laminated plate considerations. First-order nonlinear stiffnesses, dependent on element displacements to the first power, are accounted for in Eqs. (2.64b), (2.64g), (2.64h), and (2.64i). Equation (2.64g) is due to the unsymmetrical laminate and large-amplitude deflections. The second-order element stiffness term is given by Eq. (2.64c). The subscript “B” is used to denote those terms that depend upon or are a result of the bending-extension coupling. The number denotes the order of

the nonlinearity while the “ f ” or “ m ” denotes the type, e.g., “ 1_{fm} ” implies first-order nonlinear bending-membrane.

Using the notation,

$$\begin{Bmatrix} \Delta w \\ \Delta u \\ \Delta u \end{Bmatrix} = \begin{Bmatrix} w_f \\ w_m \end{Bmatrix} \quad (2.65)$$

and Eqs. (2.64) results in the following matrix equation for the rectangular plate element:

$$\left(\begin{bmatrix} [k_{ff}] & [k_{Bfm}] \\ [k_{Bmf}] & [k_{mm}] \end{bmatrix} + \begin{bmatrix} [k1_{Bff}] & [0] \\ [0] & [0] \end{bmatrix} + \begin{bmatrix} [k1_{ff}] & [k1_{fm}] \\ [k1_{mf}] & [0] \end{bmatrix} + \begin{bmatrix} [k2_{ff}] & [0] \\ [0] & [0] \end{bmatrix} \right) \begin{Bmatrix} w_f \\ w_m \end{Bmatrix} \quad (2.66)$$

Since the virtual work of the aerodynamic forces are independent of the midsurface displacements, the aerodynamic influence matrices are of the same form as was presented for the two-dimensional panel. Thus, the aerodynamic influence matrices for a rectangular plate element with the flow in the direction of the positive x coordinate axis are

$$\underline{\text{aerodynamic influence}} \quad (2.67)$$

$$[a] = \frac{2q}{M} \int_S \{\phi_w\} [\phi_w]_{,x} dS \quad (2.67a)$$

$$[g] = \frac{2q}{MV} \int_S \{\phi_w\} [\phi_w] dS \quad (2.67b)$$

$$[g1_t] = \frac{q(\gamma+1)}{2V^2} \int_S (w) \{\phi_w\} [\phi_w] dS \quad (2.67c)$$

$$[g2_t] = \frac{q(\gamma+1)M}{6V^3} \int_S (w_{,t})^2 \{\phi_w\} [\phi_w] dS \quad (2.67d)$$

$$[g2_{ft}] = \frac{q(\gamma+1)M}{2V^2} \int_S (w_{,x} w_{,t}) \{\phi_w\} [\phi_w] dS \quad (2.67e)$$

$$[a1_t] = \frac{q(\gamma+1)}{V} \int_S (w_{,t}) \{\phi_w\} [\phi_w]_{,x} dS \quad (2.67f)$$

$$[a1_f] = \frac{q(\gamma+1)}{2} \int_S (w_{,x}) \{\phi_w\} [\phi_w]_{,x} dS \quad (2.67g)$$

$$[a2_{ft}] = \frac{q(\gamma+1)M}{2V} \int_S (w_{,x} w_{,t}) \{\phi_w\} [\phi_w]_{,x} dS \quad (2.67h)$$

$$[a2_f] = \frac{q(\gamma+1)M}{6} \int_S (w_{,x})^2 \{\phi_w\} [\phi_w]_{,x} dS \quad (2.67i)$$

where $(\cdot)_{,x} = \frac{\partial(\cdot)}{\partial x}$, $(\cdot)_{,t} = \frac{\partial(\cdot)}{\partial t}$, $\{\phi_w\} = [\phi_w]^T$, and $[\phi_w]$ is defined in Eq. (2.28).

The notation used in Eqs. (2.67) is similar to that used for the two-dimensional panel, Eqs. (2.16). These three-dimensional panel equations are the dimensional counter parts to the nondimensional equations for a two-dimensional panel. The three-dimensional equations are presented in the dimensional form to provide a direct correlation between the physical parameters and the nondimensional parameters with their associated term in the governing equation. Since the influence of the aerodynamic terms are the same for either two-dimensional or three-dimensional panels and only the elementary structure, 2-D or 3-D, is different, the same notation should be clear from the application and should not present any confusion.

The last term in Eq. (2.1) to be evaluated is the virtual work of the inertial forces. Integrating the virtual work due to the inertial forces, including both transverse and midsurface accelerations, results in the following expression:

$$\rho h \int_S (w_{,tt} \delta w + u_{,tt} \delta u + v_{,tt} \delta v) dS \quad (2.68)$$

Next, using Eqs. (2.28) in Eq. (2.68) results in the following mass matrix for a rectangular plate element.

$$\underline{\text{mass}} \\ [m] = \begin{bmatrix} [m_f] & [0] & [0] \\ [0] & [m_u] & [0] \\ [0] & [0] & [m_v] \end{bmatrix} = \begin{bmatrix} [m_f] & [0] \\ [0] & [m_m] \end{bmatrix} \quad (2.69)$$

where

$$\begin{aligned} [m_f] &= \rho h \int_S \{\phi_w\} [\phi_w] dS \\ [m_u] &= \rho h \int_S \{\phi_u\} [\phi_u] dS \\ [m_v] &= \rho h \int_S \{\phi_v\} [\phi_v] dS \end{aligned} \quad (2.70)$$

Assembling the mass Eq. (2.69), stiffness Eq. (2.64), and aerodynamic influence Eq. (2.67) matrices, the equation of motion for an anisotropic plate element becomes

$$\begin{aligned}
& \begin{bmatrix} [m_f] & [0] \\ [0] & [m_m] \end{bmatrix} \begin{Bmatrix} \ddot{w}_f \\ \ddot{w}_m \end{Bmatrix} + \begin{bmatrix} ([g] + [g1_t] + [g2_{ft}] + [g2_t]) & [0] \\ [0] & [0] \end{bmatrix} \begin{Bmatrix} \dot{w}_f \\ \dot{w}_m \end{Bmatrix} \\
& + \begin{bmatrix} ([a] + [a1_t] + [a1_f] + [a2_{ft}] + [a2_f]) & [0] \\ [0] & [0] \end{bmatrix} \begin{Bmatrix} w_f \\ w_m \end{Bmatrix} + \begin{bmatrix} [k_{ff}] & [k_{Bfm}] \\ [k_{Bmf}] & [k_{mm}] \end{bmatrix} \begin{Bmatrix} w_f \\ w_m \end{Bmatrix} \\
& + \begin{bmatrix} [k1_{ff}] & [k1_{fm}] \\ [k1_{mf}] & [0] \end{bmatrix} \begin{Bmatrix} w_f \\ w_m \end{Bmatrix} + \begin{bmatrix} [k1_{Bff}] & [0] \\ [0] & [0] \end{bmatrix} \begin{Bmatrix} w_f \\ w_m \end{Bmatrix} \\
& + \begin{bmatrix} [k2_{ff}] & [0] \\ [0] & [0] \end{bmatrix} \begin{Bmatrix} w_f \\ w_m \end{Bmatrix} = \begin{Bmatrix} f_f \\ f_m \end{Bmatrix} \tag{2.71}
\end{aligned}$$

where $\{f\}$ is the internal element equilibrium forces, $[k]$ is the linear elastic stiffness matrix, and $[k1]$ and $[k2]$ are nonlinear stiffness matrices which depend linearly and quadratically upon displacements, respectively.

The variation principle in Eq. (2.1) represents a finite element approach to study the limit-cycle oscillations of three-dimensional panels at hypersonic speeds.† As was the case for the two-dimensional panel, the third-order piston theory aerodynamics for the three-dimensional case will produce two linear aerodynamic influence matrices, $[g]$ and $[a]$, and seven nonlinear aerodynamic influence matrices, $[g1_t]$, $[g2_t]$, $[g2_{ft}]$, $[a1_t]$, $[a1_f]$, $[a2_{ft}]$, and $[a2_f]$, where the aerodynamic matrices are functions of the system aerodynamic parameters, in particular the dynamic pressure, λ . The aerodynamic influence matrices $[g]$ and $[a]$ are linear, whereas $[g1_t]$, $[a1_t]$, and $[a1_f]$ depend linearly, denoted with 1, upon the displacements, denoted with subscript f , and/or the time derivative of the displacements (generalized velocities), denoted with subscript, t . The other four matrices, $[g2_{ft}]$, $[g2_t]$, $[a2_{ft}]$, and $[a2_f]$, are quadratic, denoted with 2, in displacement and/or generalized velocities. The symmetry in the first-order nonlinear stiffness matrix has been preserved at the expense of transferring the nonlinearity $[k1_{fm}]$ into two equal parts and producing the $[k1_{ff}]$ term. A similar transformation was used in developing the $[k1_{Bff}]$ term. As was the case with the two-dimensional aerodynamic matrices, the aerodynamic damping matrices, $[g]$, are symmetrical while the aerodynamic influence matrices, $[a]$, are skew-symmetric.

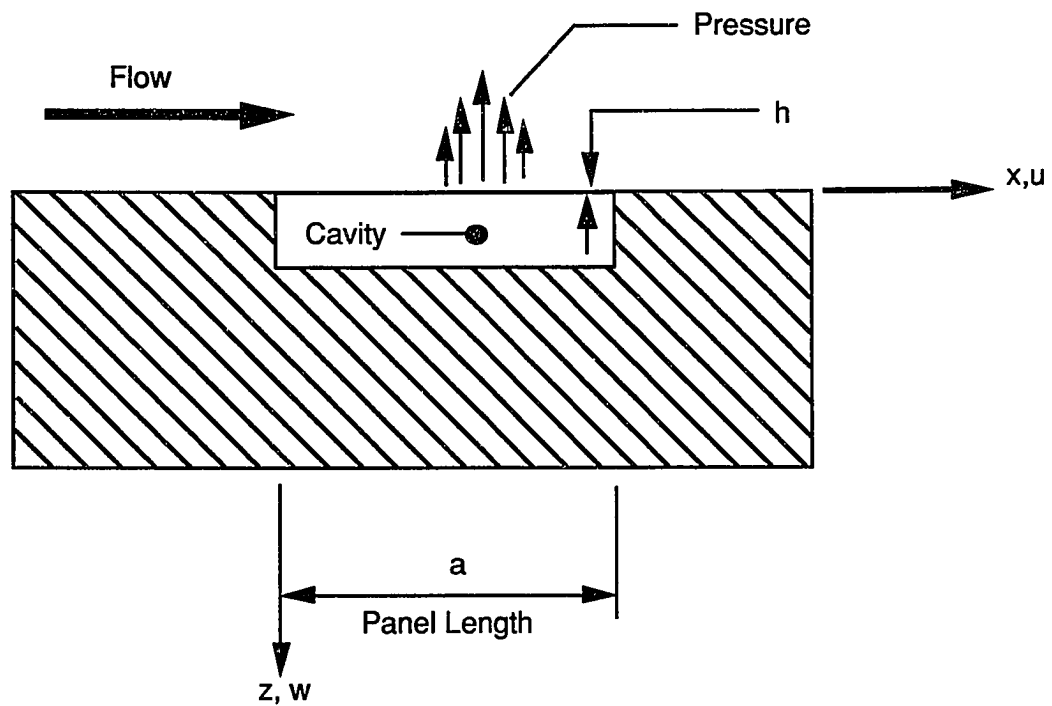


Fig. 2.1 Two-Dimensional Panel Geometry.

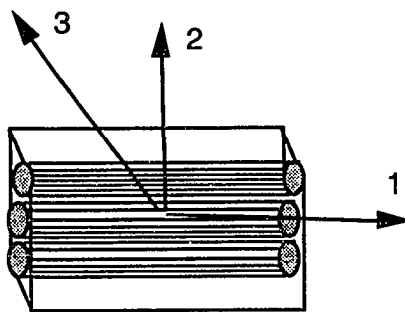
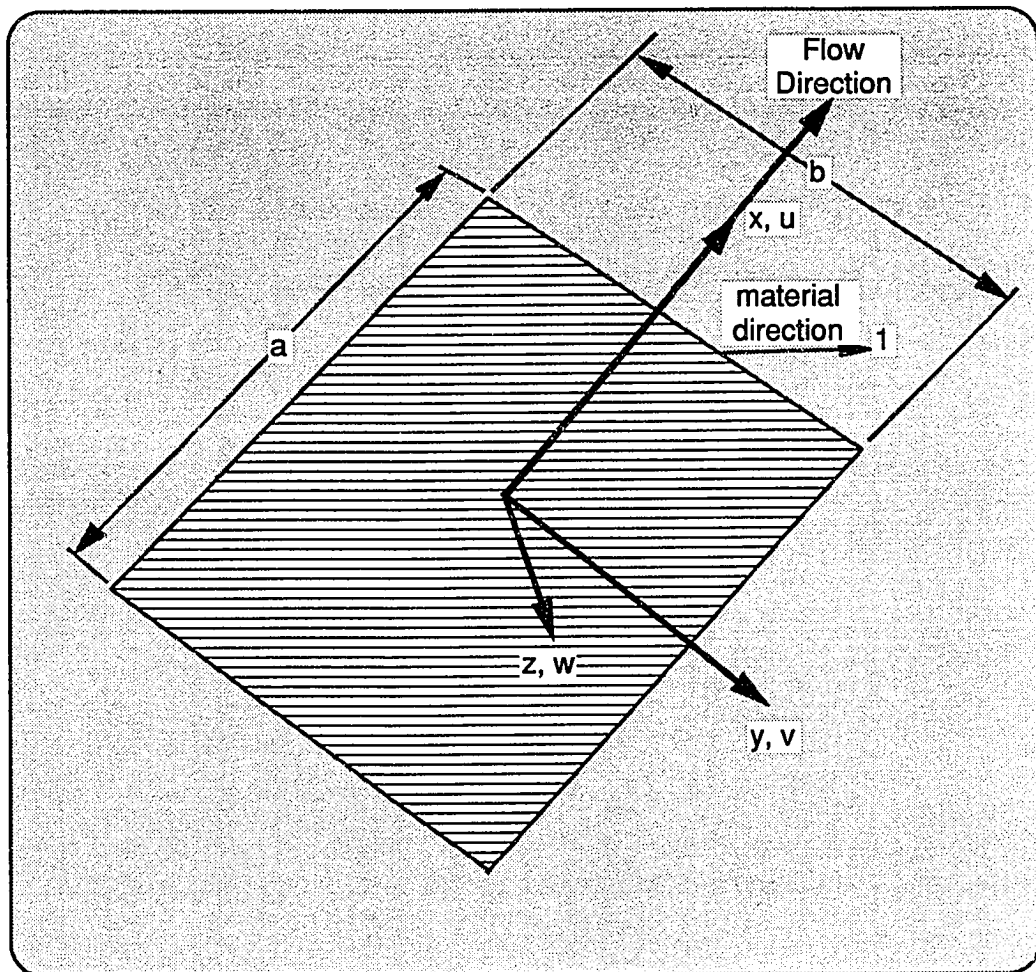


Fig. 2.2 Three-Dimensional Panel Geometry.

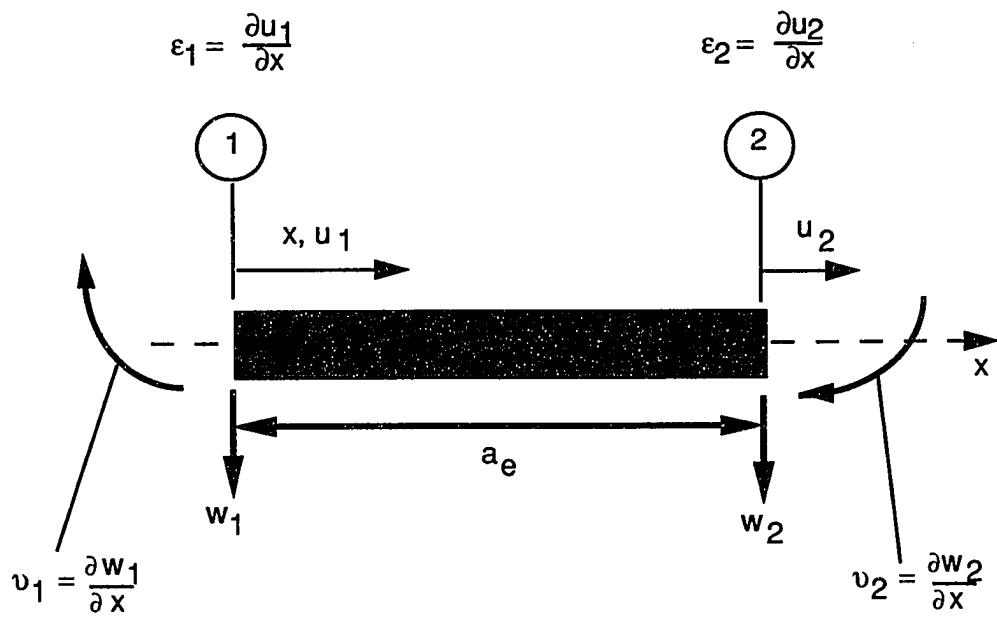


Fig. 2.3 Nodal Displacement Quantities for a Two-Dimensional Panel.

Chapter 3

SYSTEM FINITE ELEMENT FORMULATION AND SOLUTION PROCEDURE

In this chapter, a detailed description, for both two- and three-dimensional panels, of the assembly procedure, solution procedure and computational methods that were developed to solve the large-amplitude free vibration and large-amplitude panel flutter, using third-order piston aerodynamic theory, equations is presented. Each of the problems is nonlinear, and therefore, must be solved using an iterative solution procedure that is terminated when the appropriated convergence criteria are satisfied.

3.1 System Finite Element Formulation

By sub-dividing the problem domain into a finite number of discrete elements, a subsystem of elements for the two-dimensional panel Eq. (2.13) or Eq. (2.71) for the three-dimensional panel can be assembled. After assembly of the elements, using the methods of references [53] and [54], the boundary conditions are imposed on the assembled system equation using the method outlined by Reddy [55]. The constrained system finite element equation for both two- and three-dimensional panels are then available for an iterative solution.

After assembling the individual finite elements for the entire system and applying the kinematic boundary conditions (e.g., for simple, in-plane immovable supports; $u(0) = u(a) = w(0) = w(a) = 0$ for the two-dimensional panel and $u(0,y) = u(a,y) = v(x,0) = v(x,b) = w(0,y) = w(a,y) = w(x,0) = w(x,b) = 0$ for the three-dimensional panel), the nonlinear equation of motion for the coupled (bending/membrane) system represents a finite element approach for solving the two- or three-dimensional panel flutter problem. The convention that upper case matrix notation pertains to the assembled structure is used in this study to parallel the system and element formulations.

3.1.1 Two-Dimensional Isotropic Panel

The constrained system equations for a two-dimensional panel have the following form:

$$\begin{aligned}
& \begin{bmatrix} [M_f] & [0] \\ [0] & [M_m] \end{bmatrix} \begin{Bmatrix} \ddot{W}_f \\ \ddot{W}_m \end{Bmatrix} + \begin{bmatrix} ([G] + [G1_t] + [G2_t] + [G2_{ft}]) & [0] \\ & [0] \end{bmatrix} \begin{Bmatrix} \dot{W}_f \\ \dot{W}_m \end{Bmatrix} \\
& + \begin{bmatrix} ([A] + [A1_t] + [A1_f] + [A2_{ft}] + [A2_f]) & [0] \\ & [0] \end{bmatrix} \begin{Bmatrix} W_f \\ W_m \end{Bmatrix} + \begin{bmatrix} [K_{ff}] & [0] \\ [0] & [K_{mm}] \end{bmatrix} \begin{Bmatrix} W_f \\ W_m \end{Bmatrix} \\
& + \begin{bmatrix} [K1_{ff}] & [K1_{fm}] \\ [K1_{mf}] & [0] \end{bmatrix} \begin{Bmatrix} W_f \\ W_m \end{Bmatrix} + \begin{bmatrix} [K2_{ff}] & [0] \\ [0] & [0] \end{bmatrix} \begin{Bmatrix} W_f \\ W_m \end{Bmatrix} = \begin{Bmatrix} 0 \\ 0 \end{Bmatrix} \quad (3.1)
\end{aligned}$$

where

$$\begin{Bmatrix} W_f \\ W_m \end{Bmatrix} \quad (3.2)$$

are the constrained nodal displacements of the assembled system. By neglecting the in-plane mass for the lower frequencies, Eq. (3.1) can be partitioned and written as two separate equations. Solving the partitioned equations for $\{W_m\}$ leads to the following reduced system equation in terms of the transverse displacement quantities $\{W_f\}$

$$\begin{aligned}
& [M_f]\{\ddot{W}_f\} + ([G] + [G1_t] + [G2_t] + [G2_{ft}]) \{\dot{W}_f\} \\
& + ([K_{ff}] + [K1_{ff}] - [K1_{fm}][K_{mm}]^{-1}[K1_{mf}] + [K2_{ff}]) \{W_f\} \\
& ([A] + [A1_t] + [A1_f][A2_{ft}] + [A2_f]) \{W\} = \{0\} \quad (3.3)
\end{aligned}$$

where the relationship

$$\{W_m\} = -[K_{mm}]^{-1}[K1_{mf}]\{W_f\} \quad (3.4)$$

was used in deriving Eq. (3.3) by neglecting the midplane mass, $[M_m]$, in Eq. (3.1). This equation, as written, is a damped vibration problem in the configuration space; and as such, does not lend itself to standard eigenvalue solution algorithms. Thus, the approach to be adopted transforms the problem from the configuration space to a state space, which results in a more standard form of the eigenvalue problem. By making the transformation to the state space, the governing matrix equation, Eq. (3.3), becomes

$$\begin{bmatrix} [M] & [0] \\ [0] & [I] \end{bmatrix} \begin{Bmatrix} \dot{W} \\ W \end{Bmatrix} + \begin{bmatrix} [G] & [K] \\ [-I] & [0] \end{bmatrix} \begin{Bmatrix} \dot{W} \\ W \end{Bmatrix} = \{0\} \quad (3.5)$$

where $\{W\} = \{W_f\}$, $[I]$ is an identity matrix, and

$$[M] = [M_f] \quad (3.6)$$

$$[G] = [G] + [G1_t] + [G2_t] + [G2_{ft}] \quad (3.7)$$

$$\begin{aligned} [K] = & [K_{ff}] + [K1_{ff}] - [K1_{fm}][K_{mm}]^{-1}[K1_{mf}] + [K2_{ff}] \\ & + [A] + [A1_t] + [A1_f] + [A2_{ft}] + [A2_f] \end{aligned} \quad (3.8)$$

3.1.2 Three-Dimensional Composite Rectangular Panel

The constrained system equation for the three-dimensional rectangular panels has the following form:

$$\begin{aligned} & \begin{bmatrix} [M_f] & [0] \\ [0] & [M_m] \end{bmatrix} \begin{Bmatrix} \ddot{W}_f \\ \ddot{W}_m \end{Bmatrix} + \begin{bmatrix} ([G] + [G1_t] + [G2_t] + [G2_{ft}]) & [0] \\ & [0] \end{bmatrix} \begin{Bmatrix} \dot{W}_f \\ \dot{W}_m \end{Bmatrix} \\ & + \begin{bmatrix} ([A] + [A1_t] + [A1_f] + [A2_{ft}] + [A2_f]) & [0] \\ & [0] \end{bmatrix} \begin{Bmatrix} W_f \\ W_m \end{Bmatrix} \\ & + \begin{bmatrix} [K_{ff}] & [K_{Bfm}] \\ [K_{Bmf}] & [K_{mm}] \end{bmatrix} \begin{Bmatrix} W_f \\ W_m \end{Bmatrix} + \begin{bmatrix} [K1_{ff}] & [K1_{fm}] \\ [K1_{mf}] & [0] \end{bmatrix} \begin{Bmatrix} W_f \\ W_m \end{Bmatrix} \\ & + \begin{bmatrix} [K1_{Bff}] & [0] \\ [0] & [0] \end{bmatrix} \begin{Bmatrix} W_f \\ W_m \end{Bmatrix} + \begin{bmatrix} [K2_{ff}] & [0] \\ [0] & [0] \end{bmatrix} \begin{Bmatrix} W_f \\ W_m \end{Bmatrix} = \begin{Bmatrix} 0 \\ 0 \end{Bmatrix} \end{aligned} \quad (3.9)$$

where

$$\begin{Bmatrix} W_f \\ W_m \end{Bmatrix} \quad (3.10)$$

are the constrained nodal displacements of the assembled three-dimensional system.

The approach for the three-dimensional panel differs slightly at this point. For the two-dimensional panel, the number of degrees-of-freedom associated with the midplane inertia were few and only associated with one direction. Thus, assembling Eq. (3.4) with a matrix inversion at each iteration did not consume an appreciable amount of computational time as compared with that for solving a larger eigenvalue problem. However, the computational time needed to solve a similar three-dimensional equation, Eq. (3.4), at each iteration did present a severe computational penalty when compared to solving a larger eigensystem. Therefore, it was

opted to solve the larger eigensystem and not to condense out the midplane degrees-of-freedom. This approach is considered more complete than the previous assumption—that the midplane mass is negligible. This approach also provides the results necessary to validate the previous assumption. For all of the cases considered in this study, the eigenvalues associated with the midplane degrees-of-freedom were at least two orders of magnitude higher than the lowest full system eigenvalue (i.e., 10^2 versus 10^4). The lowest full system eigenvalue was always associated with the transverse degrees-of-freedom.

Similar to the two-dimensional case, Eq. (3.9), as written, is a damped vibration problem in the configuration space; and as such, does not conform to standard eigenvalue solution algorithms. Thus, the same approach of transforming the problem from the configuration space to a state space is used. By making the transformation to the state space, the governing matrix equation, Eq. (3.9), becomes

$$\begin{bmatrix} [M] & [0] \\ [0] & [I] \end{bmatrix} \begin{Bmatrix} \dot{W} \\ W \end{Bmatrix} + \begin{bmatrix} [G] & [K] \\ [-I] & [0] \end{bmatrix} \begin{Bmatrix} \dot{W} \\ W \end{Bmatrix} = \{0\} \quad (3.11)$$

where

$$[M] = \begin{bmatrix} [M_f] & [0] \\ [0] & [M_m] \end{bmatrix} \quad (3.12)$$

$$[G] = \begin{bmatrix} ([G] + [G1_t] + [G2_t] + [G2_{ft}]) & [0] \\ [0] & [0] \end{bmatrix} \quad (3.13)$$

where

$$\begin{aligned} [K] = & \begin{bmatrix} ([A] + [A1_t] + [A1_f] + [A2_{ff}] + [A2_f]) & [0] \\ [0] & [0] \end{bmatrix} + \begin{bmatrix} [K_{ff}] & [K_{Bfm}] \\ [K_{Bmf}] & [K_{mm}] \end{bmatrix} \\ & + \begin{bmatrix} [K1_{ff}] & [K1_{fm}] \\ [K1_{mf}] & [0] \end{bmatrix} + \begin{bmatrix} [K1_{Bff}] & [0] \\ [0] & [0] \end{bmatrix} + \begin{bmatrix} [K2_{ff}] & [0] \\ [0] & [0] \end{bmatrix} \end{aligned} \quad (3.14)$$

where

$$\{W\} = \begin{Bmatrix} W_f \\ W_m \end{Bmatrix} \quad (3.15)$$

$$\{\dot{W}\} = \begin{Bmatrix} \dot{W}_f \\ \dot{W}_m \end{Bmatrix} \quad (3.16)$$

and $[I]$ is again the identity matrix.

3.2 Linearizing Procedure

The solution procedure for both the two- and three-dimensional panel is basically the same. This is readily seen by comparing the homogeneous Eqs. (3.5) and (3.11). Thus, for this reason the solution procedure is developed for a problem of the form of either Eq. (3.5) or Eq. (3.11), and where there are specific differences, these differences are pointed out.

The solution to the homogeneous problem is sought in the form of

$$\begin{Bmatrix} \dot{W} \\ W \end{Bmatrix} = \tilde{c} \begin{Bmatrix} \Phi_1 \\ \Phi_2 \end{Bmatrix} e^{\Omega t} \quad (3.17)$$

where $\{\Phi_1\}$ and $\{\Phi_2\}$ are complex eigenvectors that are arranged as a single column vector, $\Omega = (\alpha + i\omega)$ is the complex eigenvalue, and \tilde{c} is a nonzero (scalar) constant displacement amplitude. Substituting the assumed response into Eq. (3.5) or Eq. (3.11) results in the following eigenvalue problem:

$$\tilde{c} \left(\Omega \begin{bmatrix} [M] & [0] \\ [0] & [I] \end{bmatrix} + \begin{bmatrix} [G] & [K] \\ [-I] & [0] \end{bmatrix} \right) \begin{Bmatrix} \Phi_1 \\ \Phi_2 \end{Bmatrix} e^{\Omega t} = \{0\} \quad (3.18)$$

By expressing $e^{\Omega t}$ as a complex quantity in the Euler form and requiring both coefficients of $\sin(\omega t)$ and $\cos(\omega t)$ to vanish, then Eq. (3.18) can be written as two separate equations

$$\tilde{c} e^{\alpha t} \left(\Omega \begin{bmatrix} [M] & [0] \\ [0] & [I] \end{bmatrix} + \begin{bmatrix} [G] & [K] \\ [-I] & [0] \end{bmatrix} \right) \begin{Bmatrix} \Phi_1 \\ \Phi_2 \end{Bmatrix} \cos(\omega t) = \{0\} \quad (3.19)$$

$$i \tilde{c} e^{\alpha t} \left(\Omega \begin{bmatrix} [M] & [0] \\ [0] & [I] \end{bmatrix} + \begin{bmatrix} [G] & [K] \\ [-I] & [0] \end{bmatrix} \right) \begin{Bmatrix} \Phi_1 \\ \Phi_2 \end{Bmatrix} \sin(\omega t) = \{0\} \quad (3.20)$$

Since \tilde{c} is nonzero, Eq. (3.5) or Eq. (3.11) is for the constrained system, and the solution sought is for all times greater than zero, both Eqs. (3.19) and (3.20) represent the same eigenvalue problem. To solve Eq. (3.19) or (3.20), the nonlinear matrices in Eq. (3.1) or Eq. (3.9) need to be evaluated. Also, since all of the system quantities used in developing these equations are real, it must be concluded that the nodal response quantities must also be real [1]. As is generally the case with most nonlinear problems, numerous methodologies are available to obtain linearized solutions. One focus of this study has been centered around linearizing the resulting nonlinear eigenvalues problem of Eq. (3.19) or (3.20) for synchronous motions. This can be accomplished by linearizing either equation and employing an iterative solution

procedure. The field expressions for the transverse panel displacement, velocity, and slope are given in Eqs. (2.10) or (2.28). All of these quantities can be approximated from Eq. (3.17) by normalizing the eigenvector as follows and recognizing that $\{W\}$ is a real quantity, and as such take only the real part of the normalized Eq. (3.17).

$$\begin{Bmatrix} \dot{W} \\ W \end{Bmatrix} = \frac{\bar{c} e^{\alpha t}}{|(\Phi_2)_k|} \begin{Bmatrix} |\Phi_1| \cos(\beta - \beta_k) \\ |\Phi_2| \cos(\beta - \beta_k) \end{Bmatrix} \cos(\omega t) \quad (3.21)$$

The quantity $|(\Phi_2)_k|$ is the magnitude of the largest transverse displacement component of the eigenvector that corresponds to $\{W\}$, and β_k is the corresponding phase angle. Next, denote $c = \bar{c} e^{\alpha t}$ as the damped amplitude. Thus, it is clear from Eq. (3.21) that the sign of the real part of the eigenvalue controls the stability of the solution. The solution is stable for all α that are less than zero. For α equal to zero, then c equals \bar{c} and the resulting solution corresponds to that of a limit-cycle oscillation. By letting

$$\begin{Bmatrix} \bar{\Phi}_1 \\ \bar{\Phi}_2 \end{Bmatrix} = \frac{1}{|(\Phi_2)_k|} \begin{Bmatrix} |\Phi_1| \cos(\beta - \beta_k) \\ |\Phi_2| \cos(\beta - \beta_k) \end{Bmatrix} \quad (3.22)$$

then Eq. (3.21) becomes,

$$\begin{Bmatrix} \dot{W} \\ W \end{Bmatrix} = c \begin{Bmatrix} \bar{\Phi}_1 \\ \bar{\Phi}_2 \end{Bmatrix} \cos(\omega t) \quad (3.23)$$

Using Eqs. (3.22), (2.10), and (2.28) the (scalar magnitude) transverse velocities and slopes become

two-dimensional panel

$$\begin{aligned} w(x, t)_{,\tau} &= [\phi] \{ \bar{\Phi}_1 \}_j \cos(\omega t) \\ w(x, t)_{,\xi} &= [\phi'] \{ \bar{\Phi}_2 \}_j \cos(\omega t) \\ u(x, t)_{,\xi} &= [\varphi'] \{ (\bar{\Phi}_2)_m \}_j \cos(\omega t) \end{aligned} \quad (3.24)$$

three-dimensional panel

$$\begin{aligned}
w(x, y, t)_{,t} &= [\phi_w] \{ \bar{\Phi}_{1f} \}_j \cos(\omega t) \\
w(x, y, t)_{,x} &= [\phi_w]_{,x} \{ \bar{\Phi}_{2f} \}_j \cos(\omega t) \\
w(x, y, t)_{,y} &= [\phi_w]_{,y} \{ \bar{\Phi}_{2f} \}_j \cos(\omega t) \\
u(x, y, t)_{,x} &= [\phi_u]_{,x} \{ \bar{\Phi}_{2m} \}_j \cos(\omega t) \\
u(x, y, t)_{,y} &= [\phi_u]_{,y} \{ \bar{\Phi}_{2m} \}_j \cos(\omega t) \\
v(x, y, t)_{,x} &= [\phi_v]_{,x} \{ \bar{\Phi}_{2m} \}_j \cos(\omega t) \\
v(x, y, t)_{,y} &= [\phi_v]_{,y} \{ \bar{\Phi}_{2m} \}_j \cos(\omega t)
\end{aligned} \tag{3.25}$$

In Eqs. (3.24) and Eqs. (3.25), the column vectors $\{ \bar{\Phi}_1 \}_j$ and $\{ \bar{\Phi}_2 \}_j$ contain the appropriate global eigenvector quantities that correspond to the particular j -th finite element, and for the two-dimensional case, the column vector $\{ (\bar{\Phi}_2)_m \}_j$ contains the appropriate membrane global eigenvector using Eq. (3.4). The three-dimensional vector $\{ \bar{\Phi}_{1f} \}_j$ uses the subscript “ f ” or “ m ” to denote the appropriate bending or membrane quantity that correspond to the particular j -th finite element, respectively. Thus, with Eqs. (3.24) or (3.25), the nonlinear terms in Eq. (3.19) can be evaluated. By making use of the following identities

$$\begin{aligned}
\cos^2(\omega t) &= \left(\frac{1}{2} + \frac{1}{2} \cos(2\omega t) \right)^{\frac{1}{2}} \cos(\omega t) \\
\cos^3(\omega t) &= \frac{1}{4} (3 \cos(\omega t) + \cos(3\omega t))
\end{aligned} \tag{3.26}$$

Neglecting the second and third harmonics (see Appendix C), the following approximations may be used to linearize Eq. (3.19):

$$\begin{aligned}
\cos^2(\omega t) &\approx \frac{\sqrt{2}}{2} \cos(\omega t) \\
\cos^3(\omega t) &\approx \frac{3}{4} \cos(\omega t)
\end{aligned} \tag{3.27}$$

The various linearizing methods, [36]–[43], that have been used in the past have bounded these values. From Eq. (3.26), the time functions have an absolute value range from zero to one. The lower value of zero will reduce the nonlinear problem to a linear one while the upper limit of one would calculate the nonlinear stiffness based on the maximum deflected configuration. The lower (linear) limit as discussed in the introduction merely defines the flutter boundary as an instability. The upper limit defines an over-stiff system by assuming the maximum value

of the developed midsurface force to occur over the entire cycle. Physically, the actual value starts at zero then progresses to the maximum value of one then back to zero over a half-cycle and then repeated through negative values. Thus, neglecting the second and third harmonics in Eq. (3.27) will predict a solution that is clearly bounded between the physical extremes. In fact, the value, $\frac{\sqrt{2}}{2}$, is exactly the root-mean-square value of a harmonic function over its period, and $\frac{3}{4}$ is in the same range. A similar approach may be used to linearize Eq. (3.20) and will result in the same eigenvalue problem.

3.2.1 Linearizing Method for Two-Dimensional Panel

Using Eq. (3.27) and the nonlinear Eqs. (2.15) and (2.16) for the two-dimensional panel, results in the following element equations:

$$\underline{\text{stiffness}} \quad (3.28)$$

$$[k1_{fm}] = \frac{c}{h} [k1_{fm}] \cos(\omega t) \quad (3.28a)$$

$$[k1_{mf}] = \frac{c}{h} [k1_{mf}] \cos(\omega t) \quad (3.28b)$$

$$[k1_{ff}] = \frac{c}{h} [k1_{ff}] \cos(\omega t) \quad (3.28c)$$

$$[k2_{ff}] = \left(\frac{c}{h}\right)^2 [k2_{ff}] \cos^2(\omega t) \quad (3.28d)$$

$$\underline{\text{aerodynamic influence}} \quad (3.29)$$

$$[g1_t] = \frac{c}{h} [g1_t] \cos(\omega t) \quad (3.29a)$$

$$[g2_t] = \left(\frac{c}{h}\right)^2 [g2_t] \cos^2(\omega t) \quad (3.29b)$$

$$[g2_{ft}] = \left(\frac{c}{h}\right)^2 [g2_{ft}] \cos^2(\omega t) \quad (3.29c)$$

$$[a1_t] = \frac{c}{h} [a1_t] \cos(\omega t) \quad (3.29d)$$

$$[a1_f] = \frac{c}{h} [a1_f] \cos(\omega t) \quad (3.29e)$$

$$[a2_{ft}] = \left(\frac{c}{h}\right)^2 [a2_{ft}] \cos^2(\omega t) \quad (3.29f)$$

$$[a2_f] = \left(\frac{c}{h}\right)^2 [a2_f] \cos^2(\omega t) \quad (3.29g)$$

where the linearized element stiffness and aerodynamic influence matrices are defined to be

$$\underline{\text{linearized stiffness}} \quad (3.30)$$

$$[k_{1mf}] = 6/r \int_0^{a_e/a} ([\phi'] \{\bar{\Phi}_2\}_j) \{\phi'\} [\phi'] d\xi \quad (3.30a)$$

$$[k_{1fm}] = 6/r \int_0^{a_e/a} ([\phi'] \{\bar{\Phi}_2\}_j) \{\phi'\} [\phi'] d\xi \quad (3.30b)$$

$$[k_{1ff}] = 6/r \int_0^{a_e/a} ([\phi'] \{\bar{\Phi}_2\}_j) \{\phi'\} [\phi'] d\xi \quad (3.30c)$$

$$[k_{2ff}] = 6 \int_0^{a_e/a} ([\phi'] \{\bar{\Phi}_2\}_j)^2 \{\phi'\} [\phi'] d\xi \quad (3.30d)$$

$$\underline{\text{linearized aerodynamic influence}} \quad (3.31)$$

$$[g_{1t}] = \frac{\gamma+1}{4} \left(M \frac{h}{a}\right) \left(\frac{\mu}{M}\right) \int_0^{a_e/a} ([\phi] \{\bar{\Phi}_1\}_j) \{\phi\} [\phi] d\xi \quad (3.31a)$$

$$[g_{2ft}] = \frac{\gamma+1}{4} \left(M \frac{h}{a}\right)^2 \left(\frac{\mu}{M}\right) \int_0^{a_e/a} ([\phi'] \{\bar{\Phi}_2\}_j) ([\phi] \{\bar{\Phi}_1\}_j) \{\phi\} [\phi] d\xi \quad (3.31b)$$

$$[g_{2t}] = \frac{\gamma+1}{12} \left(M \frac{h}{a}\right)^2 \sqrt{\frac{1}{\lambda} \left(\frac{\mu}{M}\right)^3} \int_0^{a_e/a} ([\phi] \{\bar{\Phi}_1\}_j)^2 \{\phi\} [\phi] d\xi \quad (3.31c)$$

$$[a_{1t}] = \frac{\gamma+1}{2} \left(M \frac{h}{a}\right) \sqrt{\lambda \left(\frac{\mu}{M}\right)} \int_0^{a_e/a} ([\phi] \{\bar{\Phi}_1\}_j) \{\phi\} [\phi'] d\xi \quad (3.31d)$$

$$[a_{1f}] = \frac{\gamma+1}{4} \lambda \left(M \frac{h}{a}\right) \int_0^{a_e/a} ([\phi'] \{\bar{\Phi}_2\}_j) \{\phi\} [\phi'] d\xi \quad (3.31e)$$

$$[a_{2ft}] = \frac{\gamma+1}{4} \left(M \frac{h}{a}\right)^2 \sqrt{\lambda \left(\frac{\mu}{M}\right)} \int_0^{a_e/a} ([\phi'] \{\bar{\Phi}_2\}_j) ([\phi] \{\bar{\Phi}_1\}_j) \{\phi\} [\phi'] d\xi \quad (3.31f)$$

$$[a_{2f}] = \frac{\gamma+1}{12} \lambda \left(M \frac{h}{a}\right)^2 \int_0^{a_e/a} ([\phi'] \{\bar{\Phi}_1\}_j)^2 \{\phi\} [\phi'] d\xi \quad (3.31g)$$

where $(\cdot)' = \frac{d(\cdot)}{d\xi}$.

3.2.2 Linearizing Method for Three-Dimensional Rectangular Panel

Using Eq. (3.27) and the nonlinear Eqs. (2.64) and (2.67) for the three-dimensional panel results in the following element equations:

$$\underline{\text{stiffness}} \quad (3.32)$$

$$[k1_{fm}] = c[k1_{fm}] \cos(\omega t) \quad (3.32a)$$

$$[k1_{mf}] = c[k1_{mf}] \cos(\omega t) \quad (3.32b)$$

$$[k1_{ff}] = c[k1_{ff}] \cos(\omega t) \quad (3.32c)$$

$$[k2_{ff}] = c^2[k2_{ff}] \cos^2(\omega t) \quad (3.32d)$$

$$\underline{\text{aerodynamic influence}} \quad (3.33)$$

$$[g1_t] = c[g1_t] \cos(\omega t) \quad (3.33a)$$

$$[g2_t] = c^2[g2_t] \cos^2(\omega t) \quad (3.33b)$$

$$[g2_{ft}] = c^2[g2_{ft}] \cos^2(\omega t) \quad (3.33c)$$

$$[a1_t] = c[a1_t] \cos(\omega t) \quad (3.33d)$$

$$[a1_f] = c[a1_f] \cos(\omega t) \quad (3.33e)$$

$$[a2_{ft}] = c^2[a2_{ft}] \cos^2(\omega t) \quad (3.33f)$$

$$[a2_f] = c^2[a2_f] \cos^2(\omega t) \quad (3.33g)$$

The nonlinear stiffness and aerodynamic influence matrices are defined as follows using the linearized definitions of Eqs. (2.36), (2.49), (2.51), (2.59), and (2.60):

$$[\Theta] = \begin{bmatrix} [\phi_w]_{,x} \{\bar{\Phi}_{2f}\}_j & 0 \\ 0 & [\phi_w]_{,y} \{\bar{\Phi}_{2f}\}_j \\ [\phi_w]_{,y} \{\bar{\Phi}_{2f}\}_j & [\phi_w]_{,x} \{\bar{\Phi}_{2f}\}_j \end{bmatrix} \quad (3.34)$$

$$\{\mathcal{N}_A\} = [A][P_u] \{\bar{\Phi}_{2m}\}_j \quad (3.35)$$

which represents the linearized midsurface force.

Noting that

$$\{\mathcal{N}_A\} = \begin{Bmatrix} \mathcal{N}_{Ax} \\ \mathcal{N}_{Ay} \\ \mathcal{N}_{Axy} \end{Bmatrix} \quad (3.36)$$

then the linearized $[N_A], [\mathcal{N}_A]$, can be defined as

$$\begin{bmatrix} \mathcal{N}_{Ax} & \mathcal{N}_{Axy} \\ \mathcal{N}_{Axy} & \mathcal{N}_{Ay} \end{bmatrix} = [\mathcal{N}_A] \quad (3.37)$$

Similarly, the linearized $[N_B], [\mathcal{N}_B]$, is defined as

$$\{\mathcal{N}_B\} = [B][P_w] \{\bar{\Phi}_{2f}\}_j \quad (3.38)$$

which represents the linearized midsurface force due to the bending-extension coupling.

Noting that

$$\{\mathcal{N}_B\} = \begin{Bmatrix} \mathcal{N}_{Bx} \\ \mathcal{N}_{By} \\ \mathcal{N}_{Bxy} \end{Bmatrix} \quad (3.39)$$

then the linearized form becomes

$$\begin{bmatrix} \mathcal{N}_{Bx} & \mathcal{N}_{Bxy} \\ \mathcal{N}_{Bxy} & \mathcal{N}_{By} \end{bmatrix} = [\mathcal{N}_B] \quad (3.40)$$

$$\underline{\text{linearized stiffness}} \quad (3.41)$$

$$[k_{1mf}] = \frac{1}{2} \int_S [P_u]^T [A] [\Theta] [C_\theta] dS \quad (3.41a)$$

$$[k_{2ff}] = \frac{1}{2} \int_S [C_\theta]^T [\Theta]^T [A] [\Theta] [C_\theta] dS \quad (3.41b)$$

$$[k_{1Bff}] = \frac{1}{2} \int_S \left([C_\theta]^T [\mathcal{N}_B] [C_\theta] + [C_\theta]^T [\Theta]^T [B] [P_w] + [P_w]^T [B] [\Theta] [C_\theta] \right) dS \quad (3.41c)$$

$$[k_{1fm}] = \frac{1}{2} \int_S [C_\theta]^T [\Theta]^T [A] [P_u] dS \quad (3.41d)$$

$$[k_{1ff}] = \frac{1}{2} \int_S [C_\theta]^T [\mathcal{N}_A] [C_\theta] dS \quad (3.41e)$$

linearized aerodynamic influence (3.42)

$$[\mathbf{g1}_t] = \frac{q(\gamma+1)}{2V^2} \int_S ([\phi_w] \{\bar{\Phi}_{1f}\}_j) \{\phi_w\} [\phi_w] dS \quad (3.42a)$$

$$[\mathbf{g2}_t] = \frac{q(\gamma+1)M}{6V^3} \int_S ([\phi_w] \{\bar{\Phi}_{1f}\}_j)^2 \{\phi_w\} [\phi_w] dS \quad (3.42b)$$

$$[\mathbf{g2}_{ft}] = \frac{q(\gamma+1)M}{2V^2} \int_S ([\phi_w]_{,x} \{\bar{\Phi}_{2f}\}_j) ([\phi] \{\bar{\Phi}_{1f}\}_j) \{\phi_w\} [\phi_w] dS \quad (3.42c)$$

$$[\mathbf{a1}_t] = \frac{q(\gamma+1)}{V} \int_S ([\phi_w] \{\bar{\Phi}_{1f}\}_j) \{\phi_w\} [\phi_w]_{,x} dS \quad (3.42d)$$

$$[\mathbf{a1}_f] = \frac{q(\gamma+1)}{2} \int_S ([\phi_w]_{,x} \{\bar{\Phi}_{2f}\}_j) \{\phi_w\} [\phi_w]_{,x} dS \quad (3.42e)$$

$$[\mathbf{a2}_{ft}] = \frac{q(\gamma+1)M}{2V} \int_S ([\phi_w]_{,x} \{\bar{\Phi}_{2f}\}_j) ([\phi] \{\bar{\Phi}_{1f}\}_j) \{\phi_w\} [\phi_w]_{,x} dS \quad (3.42f)$$

$$[\mathbf{a2}_f] = \frac{q(\gamma+1)M}{6} \int_S ([\phi_w]_{,x} \{\bar{\Phi}_{2f}\}_j)^2 \{\phi_w\} [\phi_w]_{,x} dS \quad (3.42g)$$

where $(\cdot)_{,x} = \frac{\partial(\cdot)}{\partial x}$.

3.2.3 Linearizing Method for System Equations

Assembling the element equations for either panel configuration for the constrained system and using the linearized equations results in the following linearized eigenvalue problem:

$$\bar{c} e^{\alpha t} \left(\Omega \begin{bmatrix} [\mathcal{M}] & [0] \\ [0] & [I] \end{bmatrix} + \begin{bmatrix} [\mathcal{G}] & [\mathcal{K}] \\ [-I] & [0] \end{bmatrix} \right) \begin{Bmatrix} \Phi_1 \\ \Phi_2 \end{Bmatrix} \cos(\omega t) = \{0\} \quad (3.43)$$

where the linearized matrices $[\mathcal{G}]$ and $[\mathcal{K}]$ are defined for either the two- or three-dimensional panel as

two-dimensional panel

$$[\mathcal{M}] = [M_f] \quad (3.44)$$

$$[\mathcal{G}] = [\mathcal{G}] + \frac{\sqrt{2}}{2} \left(\frac{c}{h}\right) [\mathbf{G1}_t] + \frac{3}{4} \left(\frac{c}{h}\right)^2 [\mathbf{G2}_t] + \frac{3}{4} \left(\frac{c}{h}\right)^2 [\mathbf{G2}_{ft}] \quad (3.45)$$

$$\begin{aligned} [\mathcal{K}] = & [K_{ff}] + \frac{\sqrt{2}}{2} \left(\frac{c}{h}\right) [\mathbf{K1}_{ff}] - \frac{3}{4} \left(\frac{c}{h}\right)^2 [\mathbf{K1}_{fm}] [K_{mm}]^{-1} [\mathbf{K1}_{mf}] + \frac{3}{4} \left(\frac{c}{h}\right)^2 [K_{2ff}] \\ & + [\mathcal{A}] + \frac{\sqrt{2}}{2} \left(\frac{c}{h}\right) [\mathbf{A1}_t] + \frac{\sqrt{2}}{2} \left(\frac{c}{h}\right) [\mathbf{A1}_f] + \frac{3}{4} \left(\frac{c}{h}\right)^2 [\mathbf{A2}_{ft}] + \frac{3}{4} \left(\frac{c}{h}\right)^2 [\mathbf{A2}_f] \end{aligned} \quad (3.46)$$

three-dimensional panel

$$[\mathcal{M}] = \begin{bmatrix} [M_f] & [0] \\ [0] & [M_m] \end{bmatrix} \quad (3.47)$$

$$[\mathcal{G}] = \begin{bmatrix} \left([G] + \frac{\sqrt{2}}{2}c[\mathbf{G}1_t] + \frac{3}{4}c^2[\mathbf{G}2_t] + \frac{3}{4}\left(\frac{c}{h}\right)^2[\mathbf{G}2_{ft}] \right) & [0] \\ [0] & [0] \end{bmatrix} \quad (3.48)$$

$$\begin{aligned} [\mathcal{K}] = & \begin{bmatrix} \left([\mathcal{A}] + \frac{\sqrt{2}}{2}(c)[\mathbf{A}1_t] + \frac{\sqrt{2}}{2}(c)[\mathbf{A}1_f] + \frac{3}{4}(c)^2[\mathbf{A}2_{ft}] + \frac{3}{4}(c)^2[\mathbf{A}2_f] \right) & [0] \\ [0] & [0] \end{bmatrix} \\ & + \begin{bmatrix} [K_{ff}] & [K_{Bfm}] \\ [K_{Bmf}] & [K_{mm}] \end{bmatrix} + \frac{\sqrt{2}}{2}(c) \begin{bmatrix} [\mathbf{K}1_{ff}] & [\mathbf{K}1_{fm}] \\ [\mathbf{K}1_{mf}] & [0] \end{bmatrix} \\ & + \frac{\sqrt{2}}{2}(c) \begin{bmatrix} [\mathbf{K}1_{Bff}] & [0] \\ [0] & [0] \end{bmatrix} + \frac{3}{4}(c)^2 \begin{bmatrix} [\mathbf{K}2_{ff}] & [0] \\ [0] & [0] \end{bmatrix} \end{aligned} \quad (3.49)$$

A detailed look at the nonlinear problem from the physical viewpoint indicates that what is required, is to find a deflected shape in order to compute the eigenvalues. Since from the physical problem, the eigenvectors are related to the deflected shape, all that is needed to approximate the solution is a shape that satisfies the geometric (essential) boundary conditions and is a variation of the exact shape. Taking direction from the classical methods, the first approximation is the normalized linear mode shape of interest. Further refinements are made by using the normalized nonlinear mode shape as an estimate of the deflected shape. This can be repeated until the estimated deflected shape and the computed normalized eigenvector differ by as small a value as required. This solution procedure can best be described as a linearized updated mode with a nonlinear time function approximation (LUM/NTF) method. The numerical differencing solution methods, which have been shown to converge in a stable manner, are based on the same iterative procedure of using refined estimates of previous solutions to start the current solution. Proceeding from this point, the remainder of this chapter is to outline and define the solution procedure.

3.3 Solution Procedure

If Eq. (3.17) is normalized, then it can be scaled to a given limit-cycle amplitude c . Having normalized and scaled Eq. (3.17), then Eq. (3.23) results, and u, v, w , and their derivatives for

each element can be easily computed. Thus, by dropping the nonlinear terms in Eq. (3.19) and solving the linear eigenvalue problem, the first estimate of the nodal quantities can be approximated. With the linear eigenvectors, the process just described, see Fig. 3.1, can be used to approximate the quantities necessary to assemble the nonlinear element matrices and the assembled constrained system matrices. The same process can be repeated until successive iterations yield the same eigenevalues, both real and imaginary, and the same eigenvectors within the limits of a convergence criterion [56]. Therefore, for a given panel configuration and dynamic pressure, the nonlinear system eigenvalues and eigenvectors can be computed.

As the dynamic pressure is increased monotonically from zero ($\lambda = 0$ corresponds to in-vacuo large-amplitude free vibration), the symmetric, real and positive-definite stiffness matrix is perturbed by the skewed aerodynamic-influence matrix so that two of the eigenvalues approach each other until they coalesce. A critical dynamic pressure, λ_{cr} , for the linear structure ($c/h = 0$) and a limit-cycle dynamic pressure, λ_ℓ , for the nonlinear structure are determined when the real part of one of the eigenvalues approaches positive values for a fixed dynamic pressure.

At each value of λ , an iterative solution of Eq. (3.19) must be performed. Each converged solution for a fixed λ generally requires three to ten iterations (at 85 cpu seconds per iteration for an 8×4 half symmetric plate with 3600 degrees of freedom). Thus, to determine the critical or limit-cycle λ may require as many as 100 iterations. Couple this with the large number of degrees-of-freedom to accurately model a fluttering composite panel; the entire success of achieving a solution depends on an efficient, vector-version, generalized unsymmetric eigensolver.

Fortunately, only a few of the lowest eigenpairs are required during the solution of each iteration. This feature makes it possible to develop an efficient eigensolver [57] for either large-amplitude vibration or the nonlinear panel flutter analysis. The solver described in ref. [57] was developed specifically for the unsymmetric eigenequation Eq. (3.19).

1. For a given λ , solve

$$-\Omega \begin{bmatrix} [\mathcal{M}] & [0] \\ [0] & [I] \end{bmatrix} \{\Phi\}_0 = \begin{bmatrix} [\mathcal{G}]_0 & [\mathcal{K}]_0 \\ [-I] & [0] \end{bmatrix} \{\Phi\}_0$$

0 = linear matrix

2. Iteration count $n = 1$, with the n -th approximation displacements

$$\{W\}_n = c\{\bar{\Phi}\}_{n-1}$$

3. Compute and solve

$$-\Omega \begin{bmatrix} [\mathcal{M}] & [0] \\ [0] & [I] \end{bmatrix} \{\Phi\}_n = \begin{bmatrix} [\mathcal{G}] & [\mathcal{K}] \\ [-I] & [0] \end{bmatrix} \{\Phi\}_n$$

4. Test for convergence. If fail, increment $n = n + 1$ and go to step 2.

5. Compute stresses and fatigue life

Fig. 3.1 Nonlinear Panel Flutter Solution Procedure.

Chapter 4

VERIFICATION OF FINITE ELEMENT METHOD

The primary objectives of this study are to develop a finite element formulation and solution procedure for the large-amplitude free vibration and large-amplitude, nonlinear panel flutter response for both two- and three-dimensional isotropic/composite panels. In addition, a full evaluation of the effects of the complete third-order piston aerodynamic theory to assess the influence of each of the higher-order terms was required. Unless specifically noted, all of the material properties used for this study are from Ref. [58] and are summarized in Table 4.1.

Thus, the purpose of this chapter is to perform a detailed comparison of the proposed method with alternate solution methods to assess the validity of the proposed approach. A detailed evaluation of the full problem, for a range of system parameters pertaining to the large-amplitude composite panel flutter problem using the full third-order piston aerodynamic theory is presented in Chapter 5.

An extensive effort has been made to correlate the present finite element method with as many alternate solutions as possible. Since the proposed finite element method is highly nonlinear, i.e. nonlinear in both geometrical and aerodynamic-loading terms, a thorough evaluation of the proposed method is conducted in order to validate the approach and procedure with as many known published solutions as possible. Also, since there are not any known solutions to compare these results with directly, a systematic comparison with existing alternate methods is attempted with as many cases as possible to validate many of the individual complexities. Because the computation of the limit-cycle dynamic pressure is a result of two nonlinear modes coalescing, the validation starts with the large-amplitude free-vibration (the wind-off condition, $\lambda = 0$) of two-dimensional panels. An excellent and current review of the nonlinear vibration of plates is given by Sathyamoorthy [59]. Building from this case, the linear aerodynamics are included and compared with existing panel flutter solutions. Next,

the same comparisons are made for isotropic and composite three-dimensional panels where alternate solutions exist. Since the solution methods for different boundary conditions, clamped or simply supported, vary in complexity, and in some cases approach, comparisons are also made for several boundary support conditions.

4.1 Two-Dimensional Isotropic Panels

A study to determine the number of finite elements necessary to achieve a converged nonlinear panel flutter solution was performed. It was found that there was approximately 2% difference between an eight-finite-element solution and a twelve-finite-element solution, whereas there was less than 0.1% difference between twelve- and sixteen-finite elements. Therefore, all of the two-dimensional results for this study are for twelve-finite-element solutions.

4.1.1 Large-Amplitude In-vacuo Vibration

A comparison between various classical analytical solutions and a twelve-element-finite element solution ($u(0) = u(a) = 0$) was performed for both simply supported and clamped supported in-plane immovable panels. The first comparison is for a simply supported panel [8]. The panel material properties are shown in Fig. 4.1 and the numerical results are shown in Table 4.2. Analytical solutions using two different approaches from Ref. [60] are also shown. All of these methods, assumed space mode (ASM), assumed time mode (ATM), and Ritz-Galerkin use a single space mode to separate the spatial and time dependence on the displacements in the governing equations. The finite element method also uses a single mode, but it is a nonlinear mode that is iterated in Eq. (3.5) until subsequent iterations both use and produce the same mode shape and eigenvalue. The comparison between the single mode analytical solutions and the finite element method is good and predicts the same type of response as that of reference [8] for the first and second modes.

The second comparison is with Yamaki and Mori's [61] three-mode Galerkin procedure for the nonlinear vibration of a clamped two-dimensional panel. The nondimensional first mode frequency for several amplitude ratios is presented in Table 4.3. For moderately large-amplitude vibrations ($c/h < 2.$), the multi-mode results agree with the finite element results extremely well up to an amplitude ratio of two. For the amplitude ratios greater than two, the finite element results exhibit a softer response than a three-mode Galerkin solution. For the larger

amplitudes, it is possible that more modes are necessary for a converged solution. To achieve a converged solution, for the panel flutter problem, Dowell [18] determined that as a minimum six modes were required.

4.1.2 Large-Amplitude Flutter with Linear Aerodynamics

A comparison is made with Dowell's six-mode numerical integration limit-cycle oscillation and Eslami's [32] six-mode method of multiple scales and harmonic balance results using the first-order piston aerodynamic theory. However, since the finite element formulation presented here differs slightly from the formulation presented in [18] and [32], the finite element in-plane stiffness matrices were scaled by $(1 - \nu^2)$ to correlate with Eq. (1.4) of Ref. [18]. The comparison with [18] is shown in Fig. 4.2 for several μ/M ratios, and the finite element numerical results are tabulated in Table 4.4. The comparison with Ref. [32] is shown in Table 4.5. The finite element results agree extremely well with the alternate methods of Refs. [18] and [32]. This agreement indicates that the (LUM/NTF) method for two-dimensional structures is a viable approach for solving these types of problems.

4.2 Three-Dimensional Rectangular Panels

A convergence study was conducted for the three-dimensional panels in a similar fashion as was done for the two-dimensional panels to assess the number or refinement of the finite element mesh to assure reasonable convergence. Due to complexity of the additional dimension and the large number of degrees-of-freedom per node for the conforming element, the convergence study also evaluated the appropriate mesh when symmetry was employed.

For a square isotropic simply supported panel a quarter-symmetric model for various meshes was analyzed, and the large-amplitude free vibration results compared with the results for a full model. The results presented in Table 4.6 show both the linear frequency, ω_o , and the nonlinear frequency ratio, ω_{n1}/ω_o , for an amplitude ratio of 1.0 for several meshes. Also noted in the table is the exact linear frequency for the panel [62]. These results clearly indicate that the quarter-symmetric model and the full model yield exactly the same results, and that a quarter symmetric 2×2 model or 4×4 full model are quite accurate for the linear case. However, for the nonlinear model, the improvement for a refined mesh is less than .02% for a 8×8 mesh when compared to the 12×12 mesh and less than .05% from a 6×6 to a 12×12 mesh.

Similarly, the nonlinear frequency ratio for five different alternate methods shows that the 6×6 full mesh is quite adequate to predict the appropriate response. Since the clamped panel is more difficult to evaluate because of the constraints on the assumed functions that satisfy the geometric boundary conditions as well as requiring more finite elements to simulate the zero-slope condition at the boundaries, a convergence study for this condition is also conducted. These results are presented in Table 4.7. For both the linear frequency and the nonlinear frequency ratio, the 8×8 full mesh or the 4×4 quarter mesh show very little improvement when a mesh refinement is made. For the nonlinear frequency ratio using an amplitude ratio of 1.0, the 8×8 finite element results compare quite well with alternate methods.

4.2.1 Large-Amplitude In-vacuo Vibration—Isotropic

A more detailed comparison for the simply supported, in-plane immovable ($u(0, y) = u(a, y) = v(x, 0) = v(x, b) = 0$), isotropic panel over a wider range of amplitude ratios is shown in Table 4.8 and compared to the results for three different alternate methods. The present finite element results are using a 6×6 quarter symmetric mesh. These results at all amplitude ratios compare quite well. A similar comparison for the clamped panel is made in Table 4.9. These results, for the same mesh, compare within 0.5%.

Using the same clamped panel configuration, the nonlinear frequency ratios for in-plane movable boundary conditions are compared to a single mode elliptical integral and perturbation solution in Table 4.10. These results compare within 8.7%. The larger difference can be attributed to the single mode assumption for the perturbation and elliptical integral solutions coupled with the solution approach of only requiring the midsurface strains at the boundaries to vanish in an average sense.

4.2.2 Flutter with Linear Aerodynamics—Isotropic

The linear panel flutter solutions for the critical dynamic pressure are presented in Table 4.11. The present finite element solution is compared to exact and approximate classical solution as well as three other finite element solutions for both simply and clamped supported panels. In addition, the linear critical frequencies are also compared and are found to agree extremely well. The better comparison is with the classical exact solution of Houbolt [12] for a simply supported panel. The present finite element method, however, does agree extremely well with all of the

other finite element methods for both simply and clamped supported panels for the critical dynamic pressure and frequency. These results were obtained using an 8×4 half-symmetric mesh; thus, this mesh will be used for the further evaluation of isotropic panel flutter analyses.

To establish additional confidence in the present solution method, an 8×4 half-symmetric mesh was used to compare with existing methods. Dowell's [18] well known numerical integration results along with Eslami's harmonic balance solution for a simply supported, in-plane immovable, square panel are presented in Table 4.12. Since both of these investigators display their limit-cycle results in the form of charts, the limit-cycle data shown in the table were read from their figures. The finite element results compare favorably with the maximum difference of only .2%. Also shown in Table 4.12 are the limit-cycle results for the clamped, in-plane immovable panel. Kuo et al. [21] and Eslami's [32] limit-cycle six-mode perturbation results were also evaluated from charts and compared within 1.8%.

4.2.3 Linear In-vacuo Vibration—Composite

Since an unsymmetrical response is usually associated with a general laminate, most of the results for a composite panel are performed using a full mesh. Similar to the isotropic case, a convergence study was conducted to evaluate the mesh refinement required to produce accurate results.

The linear frequency results shown in Table 4.13 compare the present finite element solution to those from a commercially available finite element code [68]. The material used in this study was selected to have a high orthotropic ratio of $E_{11}/E_{22} = 40$ and the more difficult clamped boundary conditions were employed to analyze an unsymmetrical 30° two-layer angle-ply laminate. These results indicate that the conforming element handles the composite plate characteristics quite well by only changing the linear frequency by 0.5% when refining from a 10×10 to 12×12 mesh. The commercial code's converging characteristics behave in a like manner. However by adding an additional layer to the laminated, making the panel symmetrical, requires the commercial code to undergo extensive refinement to approach a converged solution. These results are shown in Table 4.14 where it is seen that the present element conforming solution converges very quickly while the commercial code needs over twenty times more elements. Thus far, the convergence rate was determined to be better

for the present element, but the point of convergence remains to be addressed. The present finite element, the commercial code's finite element, and a 144 term Ritz-method solution are shown in Table 4.15. These results clearly indicate the excellent convergence characteristics for the conforming element with an 8x8 mesh for both symmetric and unsymmetrical angle-ply laminates.

4.2.4 Large-Amplitude In-vacuo Vibration—Composite

Based on the previous evaluation, the large-amplitude free vibration of composite three-dimensional panels was conducted using an 8x8 mesh. The results in Table 4.16 compare a two-layer 45 degree angle-ply laminate perturbation solution with the present finite element solution. For the properties noted in the table, this comparison indicates good agreement over an amplitude ratio of one plate thickness with less than 1% difference. Similarly, the present finite element solution for a four-layer cross-ply agrees with both a single mode numerical integration and single mode perturbation solutions. These results, over a range of amplitude ratios, are presented in Table 4.17 for a simply supported panel using the properties noted.

Clamped boundary condition finite element results are shown in Table 4.18. These results compare the present large-amplitude response with both single mode elliptic integral and perturbation solutions for a four-layer cross-ply laminate. The nonlinear clamped response in Table 4.18 is for the same panel geometry used to develop the results in Table 4.17. Thus, a comparison of the effect that changing boundary support conditions has on the panel's response is made by comparing Tables 4.17 and 4.18.

4.2.5 Flutter with Linear Aerodynamics—Composite

The final comparison to validate the present finite element method and solution procedure is for a single layer anisotropic square panel. This panel is clamped along one edge parallel to the free stream flow with the other three edges free. This comparison combines the flutter phenomena with the full anisotropic material effects along with a mixed set of boundary conditions. The present finite element results for the critical dynamic pressure for three lamination angles are presented in Table 4.19. Since reference [72] elected to use a 5x5 mesh, these results are also for a 5x5 mesh. The information presented in Table 4.19 is for a slightly different definition of the nondimensional dynamic pressure which is noted in the table; thus,

the values are smaller than those normally presented for a similar isotropic panel. For all three lamination angles that were evaluated, the present finite element method agreement is good.

Table 4.1 Material Properties

Material Number	Material	E_{11} , Msi	E_{22} , Msi	G_{12} , Msi	ν_{12}	Weight Density, lb/in ³
1	G _{rs} /Ep T300/5208	21.30	1.58	0.93	.38	.058
2	B/Ep Avco 5505/4	30.00	2.70	0.93	.21	.0725
3	B/AL B5.6/Al 6061-F	31.00	20.00	8.40	.27	.095
4	Steel Isotropic	30.00	30.00	11.54	.30	.283
5	Aluminum Isotropic	10.00	10.00	3.84	.30	.100

Table 4.2 Effects of Amplitude Ratios, c/h , on In-vacuo
Frequency Ratios, ω_{n1}/ω_o , for Simply Supported
In-plane Immovable 2-D Panel

Amplitude c/h	Mode n	Present FEM	Assumed Space Mode [8]	Assumed Time Mode [60]	Ritz- Galerkin [60]
0.0	1	1.0000	1.0000	1.0000	1.0000
	2	1.0000	1.0000	—	—
0.2	1	1.0436	1.0439	1.0296	1.0440
	2	1.0441	1.0439	—	—
0.4	1	1.1662	1.1644	1.1136	1.1662
	2	1.1662	1.1644	—	—
0.6	1	1.3455	1.3397	1.2410	1.3454
	2	1.3452	1.3397	—	—
0.8	1	1.5623	1.5506	1.4000	1.5620
	2	1.5621	1.5506	—	—
1.0	1	1.8024	1.7844	1.5811	1.8028
	2	1.8027	1.7844	—	—
1.2	1	2.0588	2.0335	1.7776	2.0591
	2	2.0590	2.0335	—	—

Table 4.3 Comparison of Amplitude Ratios, c/h , on In-vacuo
Frequency Ratios, ω_{n1}/ω_o for Clamped Supported
In-plane Immovable 2-D Panel

Amplitude c/h	Nondimensional Frequency ω_{n1}/ω_o	
	Galerkin Assumed Space Mode, Yamaki and Mori [61]	
	Present FEM	
0.0665	22.4	22.40
0.5307	24.0	24.00
0.9833	27.5	27.53
1.4571	32.5	32.55
2.0451	40.0	39.81
2.6602	50.0	48.06
3.0683	60.0	53.73

$$\omega_o = \sqrt{\frac{D}{\rho h a^4}}$$

Table 4.4 Effects of μ/M on λ_ℓ vs. Amplitude Ratio for

Simply Supported In-plane Immovable 2-D Panel

[in-plane stiffness modified by $(1 - \nu^2)$]

Amplitude c/h	μ/M			
	.01	.1	.2	.5
0.0	344.49	355.09	367.56	410.44
0.2	355.22	366.35	379.45	424.93
0.4	387.73	400.63	415.89	469.29
0.6	443.46	459.57	478.91	548.44
0.8	525.64	547.32	573.72	673.12
1.0	640.81	671.78	710.58	867.65

$$\lambda_\ell = \frac{2qa^3}{MD}$$

Table 4.5 Flutter Amplitude, c/h , Critical Dynamic Pressure, λ_ℓ , Flutter

Frequency, ω , for a Simply Supported In-plane Immovable

2-D Panel [in-plane stiffness modified by $(1 - \nu^2)$]

c/h	Present FEM		H. Eslami (6 mode solution), [32]	
	λ_{cr}	ω	λ_{cr}	ω
0.0	344.44	32.68	344.20	32.44
0.3751	382.47	34.56	381.98	34.46
0.4681	403.98	35.70	403.27	35.57
0.7486	501.67	40.59	499.49	40.28
0.8446	548.14	42.76	545.11	42.39
0.9435	604.38	45.28	600.28	44.86

$$\lambda_\ell = \frac{2qa^3}{MD}$$

Table 4.6 Finite Element Mesh Convergence Study for an In-plane
Immovable Simply Supported Isotropic 3-D Square Panel
($E = 30$ Msi, $\nu = .3$, $\rho = .00026$ lbs-sec/in⁴,
 $a = b = 12$ in, $h = .04$ in)

Finite Element Mesh	Plate Size	ω_{n1}/ω_o ($c/h = 1.0$)	ω_o , rad/sec 325.9716 [62]
2×2	1/4	1.4335	326.0377
3×3	1/4	1.4234	326.0027
4×4	1/4	1.4198	325.9992
6×6	1/4	1.4174	325.9970
4×4	Full	1.4335	326.0377
6×6	Full	1.4234	326.0027
8×8	Full	1.4198	325.9992
12×12	Full	1.4174	325.9970
Inc. FEM [63]	—	1.4109	—
Perturb. [64]	—	1.4024	—
Elliptic [65]	—	1.4097	—
Perturb. [66]	—	1.4327	—
Num. Int.[66]	—	1.4141	—

Table 4.7 Finite Element Mesh Convergence Study for an In-plane
Immovable Clamped Supported Isotropic 3-D Square
Panel ($E = 30$ Msi, $\nu = .3$, $\rho = .00026$ lbs-sec²/in⁴,
 $a = b = 12$ in, $h = .04$ in)

Finite Element	Plate Size	ω_{n1}/ω_o ($c/h = 1.0$)	ω_o , rad/sec
2×2	1/4	1.2137	595.4875
3×3	1/4	1.1866	594.2050
4×4	1/4	1.1762	594.3917
6×6	1/4	1.1702	594.3188
4×4	Full	1.2137	595.4875
6×6	Full	1.1866	594.2050
8×8	Full	1.1762	594.3917
12×12	Full	1.1702	594.3188
Inc. FEM [63]	—	1.1762	—
Perturb. [67]	—	1.1713	—
Elliptic [67]	—	1.1731	—

Table 4.8 Free Vibration c/h Ratio vs. ω_{n1}/ω_o Ratio for In-plane

Immovable Simply Supported Square Isotropic 3-D Square

Panel (6×6: Quarter Plate)

c/h	Present FEM	Inc. FEM Lau et al. [63]	Chu- Herrmann [64] Single Mode	Eisley [65] Single Mode
0.2	1.0200	1.0196	1.0195	1.0196
0.4	1.0771	1.0763	1.0757	1.0761
0.6	1.1664	1.1645	1.1625	1.1642
0.8	1.2839	1.2779	1.2734	1.2774
1.0	1.4174	1.4109	1.4023	1.4097

Table 4.9 Free Vibration c/h Ratio vs. ω_{n1}/ω_o Ratio for In-plane

Immovable Clamped Supported Square Isotropic 3-D Square

Panel (6×6: 1/4 Quarter Plate)

c/h	Present FEM	Inc. FEM Lau et al. [63]	Elliptic Int. [67] Single Mode	Perturbation [67] Single Mode
0.2	1.0075	1.0073	1.0075	1.0075
0.4	1.0293	1.0291	1.0030	1.0296
0.6	1.0644	1.0648	1.0066	1.0652
0.8	1.1115	1.1138	1.1139	1.1130
1.0	1.1702	1.1762	1.1731	1.1713

Table 4.10 Free Vibration c/h Ratio vs. ω_{n1}/ω_o Ratio for In-plane
Movable Clamped Supported Square Isotropic 3-D Square
Panel (6×6: 1/4 Quarter Plate)

c/h	Present FEM	Elliptic Int. [67] Single Mode	Perturbation [67] Single Mode
0.2	1.0039	1.0075	1.0075
0.4	1.0145	1.0030	1.0296
0.6	1.0287	1.0066	1.0652
0.8	1.0482	1.1139	1.1130
1.0	1.0707	1.1731	1.1713

Table 4.11 Linear Panel Flutter of 3-D Isotropic Square Panel

($E = 10$ Msi, $\nu = .3$, $\rho = .00026$ lbs-sec²/in⁴,
 $a = b = 12$ in, $h = 0.04$ in)

Solution Method	Simply Supported		Clamped Supported	
	Dynamic Pressure λ_{cr}	Eigenvalue k_{cr}	Dynamic Pressure λ_{cr}	Eigenvalue k_{cr}
FEM [41]	512.33	1846.55	852.73	4294.07
FEM [35]	511.79	1834.29	850.42	4282.03
FEM [68]	512.20	1844.00	853.40	4292.00
Exact/Approx [12]	512.65	1848.21	876.80	4077.00
Present FEM (8×8 Half-Plate)	512.37	1846.15	850.97	4286.49

$$k = \omega^2(\rho h a^4/D), \lambda_{cr} = \frac{2qa^3}{MD}$$

Table 4.12 Nonlinear Panel Flutter with Linear Aerodynamics, λ_L ,
for 3-D Isotropic Square Panel ($E = 10$ Msi, $\nu = .3$,
 $\rho = .00026$ lbs-sec²/in⁴, $a = b = 12$ in, $h = 0.04$ in)

c/h	Simply Supported		Clamped Supported	
	Dowell [18]/ Eslami [32] †	Present FEM (8×4 Half Plate)	Kuo [21]/ Eslami [32] †	Present FEM (8×4 Half Plate)
0.0	540.5	535.75	881.0	887.59
0.4	578.4	583.38	940.5	940.12
0.8	724.8	731.53	1081.1	1100.67

†Values read for charts, $\lambda = \frac{2qa^3}{MD}$

Table 4.13 Linear Free Vibration of Clamped Angle-Ply Laminated 3-D Square
Panel ($E_{11} = 30$ Msi, $E_{22} = .75$ Msi, $G_{12} = .375$ Msi, $\nu_{12} = .25$,
 $\rho = .00026$ lbs-sec²/in⁴, $[30/-30]$, $a = b = 12$ in, $h = .12$ in)
NOTE: A_{16} , A_{26} , D_{16} , $D_{26} = 0$, $B_{ij} \neq 0$

F-E Mesh	Present FEM ω_o , rad/sec	EAL [64] ω_o , rad/sec
10×10	727.9216	714.1854
12×12	724.4325	715.2916
36×36	—	717.9477
48×48	—	718.1226

Table 4.14 Linear Free Vibration of Clamped Angle-Ply Laminated 3-D Square

Panel ($E_{11} = 30$ Msi, $E_{22} = .75$ Msi, $G_{12} = .375$ Msi, $\nu_{12} = .25$,
 $\rho = .00026$ lbs-sec²/in⁴, $[30/-30/30]$, $a = b = 12$ in, $h = .12$ in)

NOTE: A_{16} , A_{26} , D_{16} , $D_{26} = 0$, $B_{ij} \neq 0$

F-E Mesh	Present FEM ω_o , rad/sec	EAL [69] ω_o , rad/sec
8×8	1611.1372	1481.2051
10×10	1609.9117	1521.4849
12×12	—	1545.5150
36×36	—	1600.4785
48×48	—	1603.8232

Table 4.15 Linear Free Vibration (ω_o rad/sec) of Simply Supported Angle-Ply

Laminated 3-D Square Panel ($E_{11} = 30$ Msi, $E_{22} = 12.245$ Msi,
 $G_{12} = 5.9308$ Msi, $\nu_{12} = .23$, $\rho = .00026$ lbs-sec²/in⁴, $a = b = 12$ in,
 $h_{ply} = 0.04$ in)

Method	Lamination Angle	
	$[30/-30/30]$	$[30/-30/30/-30]$
Ritz-Method, 144 Terms Leissa [70]	1315.8897	1767.7612
EAL [69]		
8×8	1303.9182	1769.4746
12×12	1308.5281	1774.3209
Present FEM		
8×8	1312.6709	1766.5197
10×10	1312.6021	1766.4549

Table 4.16 Free Vibration c/h Ratio vs. ω_{n1}/ω_o Ratio Simply Supported

In-plane Immovable Angle-Ply $[45/-45]$ Laminated 3-D Square

Panel ($E_{11} = 39.39$ Msi, $E_{22} = 4.788$ Msi, $G_{12} = 1.959$ Msi,

$\nu_{12} = .3$, $\rho = .00026$ lbs-sec²/in⁴, $a = b = 12$ in, $h = 0.04$ in)

c/h	Chandra [71] Single Mode Perturbation	Present FEM (8×8 Full Plate)
0.2	1.0251	1.0261
0.4	1.0970	1.1001
0.6	1.2073	1.2134
0.8	1.3467	1.3563
1.0	1.5071	1.5204

Table 4.17 Free Vibration c/h Ratio vs. ω_{n1}/ω_o Ratio Simply Supported

In-plane Immovable Cross-Ply $[0/90/90/0]$ Laminated 3-D

Square Panel ($E_{11} = 40$. Msi, $E_{22} = 1$. Msi, $G_{12} = .5$ Msi,

$\nu_{12} = .25$, $\rho = .00026$ lbs-sec²/in⁴, $a = b = 12$ in, $h = 0.04$ in)

c/h	Singh et al. [66] Single Mode Numerical Integration	Chandra [71] Single Mode Perturbation	Present FEM (8×8 Full Plate)
0.2	1.0535	1.0489	1.0505
0.4	1.2038	1.1836	1.1894
0.6	1.4172	1.3791	1.3924
0.8	1.6691	1.6135	1.6374
1.0	2.2355	2.1466	2.1958

Table 4.18 Free Vibration c/h Ratio vs. ω_{n1}/ω_o Ratio Clamped Supported

In-plane Immovable Cross-Ply [0/90/90/0] Laminated 3-D

Square Panel ($E_{11} = 40$. Msi, $E_{22} = 1$. Msi, $G_{12} = .5$ Msi,

$\nu_{12} = .25$, $\rho = .00026$ lbs-sec²/in⁴, $a = b = 12$ in, $h = 0.04$ in)

c/h	Elliptic Integral Single Mode [67]	Perturbation Single Mode [67]	Present FEM (8×8 Full Plate)
0.2	1.0127	1.0127	1.0135
0.4	1.0497	1.0499	1.0524
0.6	1.1083	1.1091	1.1142
0.8	1.1850	1.1871	1.1954
1.0	1.3792	1.3859	1.4023

Table 4.19 Linear Panel Flutter, λ_{cr} , for 3-D Anisotropic Cantilever

Square Panel ($E_{11}/E_{22} = 2.$, $G_{12}/E_{22} = 0.364$, $\nu_{12} = .24$,

$\rho = .00026$ lbs-sec²/in⁴, $a = b = 12$ in, $h = 0.04$ in)

Solution Method	Lamination Angle		
	$\theta = 15^\circ$	$\theta = 45^\circ$	$\theta = 90^\circ$
K.-J. Lin et al. [72]	2.470	3.920	3.455
Rossettos, Tong [73]	2.385	4.055	3.505
Present FEM (5×5 Full Plate)	2.386	4.060	3.507

$$\lambda_{cr} = \frac{2ga^3}{MD_c}, \text{ where } D_c = E_{22}h^3$$

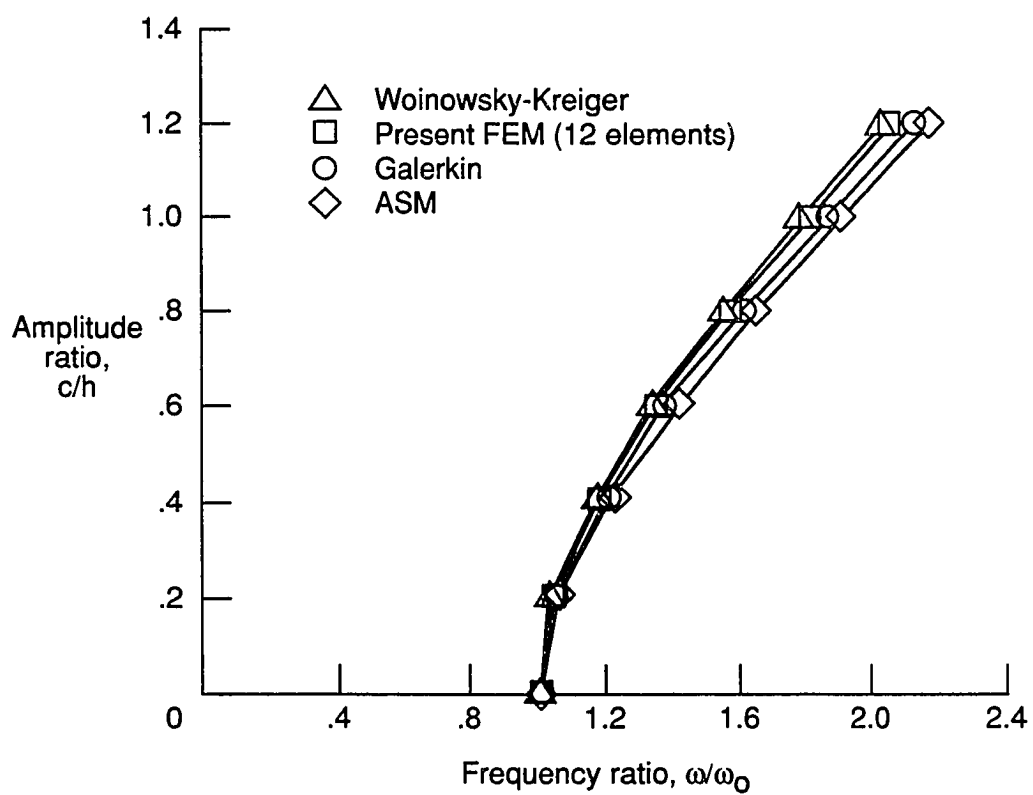


Fig. 4.1 Comparison of Large-Amplitude Vibration Solutions for a Simply-Supported Panel.

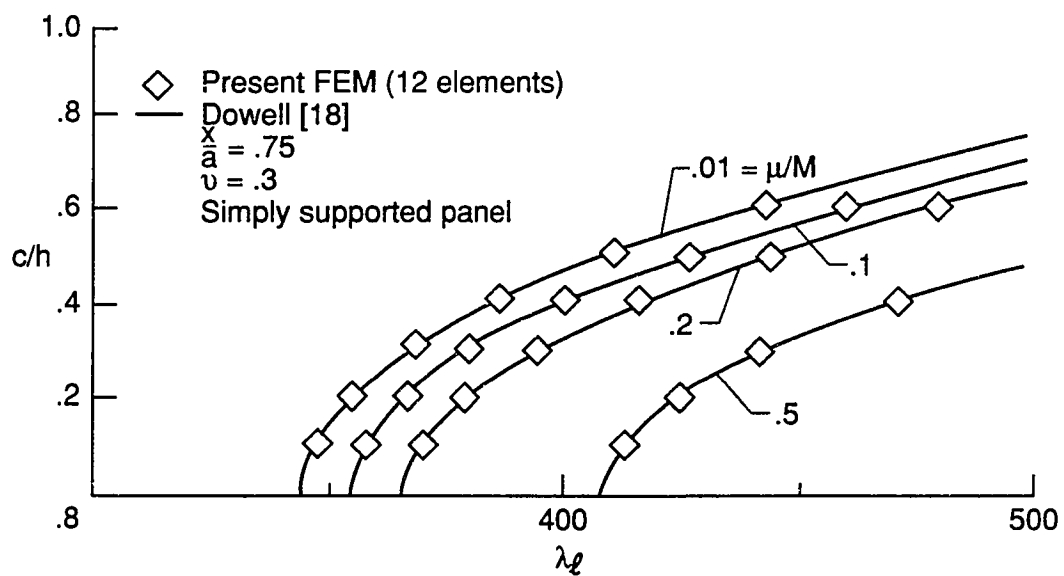


Fig. 4.2 Limit-Cycle Amplitude Ratios vs. Nondimensional Dynamic Pressure, λ_ℓ .

Chapter 5

NONLINEAR PANEL FLUTTER NUMERICAL RESULTS

To meet the primary objectives of this study, a finite element formulation and solution procedure (Chapters 2 and 3) for the large-amplitude, panel flutter response has been developed. For both two- and three-dimensional isotropic/composite panels the finite element method has been employed to provide a full evaluation of the effects of the complete third-order piston aerodynamic theory. Several cases are presented that assess the influence of each of the higher-order terms. In addition, an evaluation of the composite panel effects is offered to investigate the influence of material orthotropy, number of layers, and stacking sequence. All of the material properties used in this chapter are from Ref. [58] and are summarized in Table 4.1.

Thus, the purpose of this chapter is two-fold. The first is to perform a detailed evaluation of the proposed method for the two-dimensional panel. Second, a detailed evaluation of the full problem is made for a wide range of composite material parameters pertaining to the large-amplitude composite panel flutter problem using the full third-order piston aerodynamic theory. For both of these cases, an assessment of third-order piston aerodynamic theory is also provided.

5.1 Two-Dimensional Isotropic Panel

A study to determine the number of finite elements necessary to achieve converged results was performed and discussed in section 4.1. These results concluded that twelve elements were sufficient, thus for all of the two-dimensional results presented in this chapter are for twelve-finite-element solutions. Also, since orthotropic materials for two-dimensional structures have little significance, these results are for isotropic-type materials.

5.1.1 System Parameter Effects

The effects of the nonlinear structure and hypersonic third-order piston theory (for $c/h = \pm 0.6$) when compared to the linear structure and first-order piston theory ($c/h = 0$) for a simply

supported panel can be seen in Fig. 5.1, which depicts coalescence of the first and second linear modes at $\lambda_{cr} = 343.35$. Classical analytical methods establish coalescence at $\lambda_{cr} = 343.35$ [41]. Thus, linear finite-element results compare well with linear classical solutions. The complete panel behavior is characterized by plotting the complex eigenvalue $(\alpha + i\omega)$ variation with increasing dynamic pressure λ . These variations are shown in Fig. 5.1 for the first two modes. As λ increases from zero (in-vacuo), the $lm(\Omega_1) = \omega_1$ for the first mode increases and the $lm(\Omega_2) = \omega_2$ for the second mode decreases until the two modes coalesce. When damping is present, the instability sets in at a somewhat higher value of λ as indicated when $\alpha = 0$. This point (λ_{cr}) for the linear cases is a function of the system parameter $\frac{\mu}{M}$; however, for the nonlinear case it (λ_ℓ) is a function of $\frac{\mu}{M}$ and $\frac{Mh}{a}$. Other than the obvious increase in λ at coalescence, the nonlinear aerodynamics also produces another significant effect which is seen by the dependence of λ on the sign of the assumed mode shape. McIntosh [9] attributes this effect to the nonlinear $w_{,x}^2$ term in Eq. (2.8) producing an overpressure which in turn tends to push the panel into the cavity.

The comparison between the first-order and third-order aerodynamic theories is shown in Fig. 5.2. Again, the effect of the sign of the mode shape on the response is noted. As shown by the solid curve, the first-order aerodynamic theory and nonlinear structure shows no response change relative to the sign of the assumed mode; in fact, the first-order response for these particular system parameters falls between the $\pm c/h$ for the third-order theory. As cited in Ref. 9, the change in the frequency oscillation is quite small. The variation of frequency is indeed small, but the variation in λ is on the order of 10%. In Fig. 5.3 the panel deflection shapes at λ_ℓ for $c/h = \pm 1$ and -0.909 for the third-order piston theories are plotted—note that the maximum deflection occurs at $x/a = .75$.

Since λ_ℓ depends on the system parameters $\frac{\mu}{M}$ and $\frac{Mh}{a}$, effect of increasing these parameters on the change in eigenvalues for a variation in λ is shown in Fig. 5.2 for $c/h = .6$. Most noticeable is the change in the variation in λ_ℓ for the increase in system parameters. This change, for these parameters, results in a lower dynamic theory than what would be predicted using the linear aerodynamic theory, compare with Fig. 5.1. For $\frac{Mh}{a} = .1$, and $+c/h$, the response is more destabilizing than Fig. 5.1 for $\frac{\mu}{M} = .01$.

A comparison of the limit-cycle amplitude verses λ_ℓ for the first-order and third-order aerodynamic theory is shown in Fig. 5.4. For the parameters noted on the figure and a limit-cycle amplitude less than one-half of a plate thickness, the amplitude-dynamic pressure relationship can be reasonably estimated by the linear aerodynamic theory; however for the larger limit-cycle amplitudes of the order of a plate thickness, the nonlinear aerodynamic theory may be required. This is more clearly illustrated when the effects of $\frac{\mu}{M}$ and $\frac{Mh}{a}$ are considered. Figure 5.5 shows the influence of varying these parameters on the c/h vs λ_ℓ relation. Due to the strong influence of the nonlinear effects from both the geometry ("hardening") and aerodynamic ("softening"), these results suggest that the third-order aerodynamic theory should be employed for limit-cycle amplitudes that are greater than half-a-plate thickness.

5.1.2 Boundary Support Effects

In Fig. 5.6, the panel amplitude of the limit-cycle oscillation is given as a function of λ_ℓ for various edge restraints. The most interesting result is that the limit-cycle motions are different for hinged-clamped and clamped-hinged panels. This condition is difficult to analytically evaluate; however, it is easy to account for using finite-elements. This occurs because the constrained system matrices are different for these support conditions, which easily accounts for the different deflection shapes for the panels. It is also interesting to note that the slopes for the various boundary conditions behave according to the trailing edge support conditions.

5.1.3 Nonlinear Aerodynamic Effects

Another interesting aspect is the influence that the aerodynamic nonlinear terms have on the motion of the panel as it oscillates at a high dynamic pressure. Table 5.1 summarizes, for the parameters shown, a comparison between the first-order, second-order, and third-order piston theories and the effect of neglecting each of the nonlinear aerodynamic terms independently of the others. The term that has the most significant influence when deleted is the $w_{,x}^2$.

It should be pointed out that there are a couple of ways to group the nondimensional parameters. For example, Refs. 1 and 9 each elect to nondimensionalize the $w_{,t}$ term differently. Reference 9 chooses to make the coefficient a function of λ whereas Ref. 1 eliminates λ in favor

of a nondimensional damping parameter, g_a . The work presented here follows the parameter notion of Ref. 9 so that the in-vacuo free vibration of a panel can be assessed by setting $\lambda = 0$.

5.2 Three-Dimensional Rectangular Panel

An effort has been made to present finite element results for as many of the three-dimensional parameters as possible. Since for the two-dimensional panel, a range of $\frac{\mu}{M} = .01\text{--}0.1$ and $\frac{Mh}{a} = .05\text{--}0.1$ flow parameters was presented, the finite element results for the three-dimensional panel are provided for $\frac{\mu}{M} = .1$ and $\frac{Mh}{a} = .05$. An assessment of how these flow parameters influence the panel flutter phenomena was considered in detail for the two-dimensional panel. Limiting the flow parameters for the three-dimensional panels minimizes the total number of complete system parameters necessary to study the flutter of composite panels. In addition, unless specifically noted the results presented in this chapter are for a square, simply-supported 8×4 half-symmetric mesh.

5.2.1 Limit-Cycle Oscillations

Panel flutter designs are generally focused on fatigue life (or service life) considerations. That is, the repeated cyclic application of a self-excited loading to a stress level in excess of the material's endurance limit results in a finite number of these applications before a structural failure becomes emanate. Since the aerodynamic damping forces are nonlinear and amplitude-dependent, a stationary motion is achieved in which the panel gains energy during part of the cycle and dissipates energy during the remaining part of the cycle, so that during each cycle the net energy exchange is zero. Thus at a given flow velocity (dynamic pressure), the flow and the structure interact to produce a stable repeated oscillation at a specific amplitude and frequency. This stable repeated motion is known as a limit-cycle. At a given amplitude for a given dynamic pressure, the panel develops stresses associated with the limit-cycle, and the stresses are repeatedly applied at the limit-cycle frequency. Therefore, the structure is limited to a finite time in which it can sustain a given flow velocity.

This section presents the numerical results necessary to develop a description of the limit-cycle flutter of a composite panel. The orthotropic, simply supported, square panel ($a = 12$ in, $h = 0.04$ in) used for this first study is a single layer of boron aluminum, B/Al B5.6/Al—material 3 Table 4.1. Solving only the linear portion of Eq. (3.43) and varying the dynamic

pressure from zero monotonically results in a variation of the system frequencies. As shown in Fig. 5.7, the eigenvalues of the first mode and third mode increase while the second and fourth mode decrease until two of the eigenvalues coalesce. For this configuration, the first and second eigenvalues coalesce; however, with aerodynamic damping present, the real part of the system eigenvalue vanishes at a slightly higher dynamic pressure. When the real part of the eigenvalue vanishes the associated value of the dynamic pressure is, for the linear analysis, referred to as the critical dynamic pressure and defines the stability boundary. The nondimensional dynamic pressure shown in Fig. 5.7 is defined as

$$\lambda = \frac{2qa^3}{MD_c} \quad (5.1)$$

where

$$D_c = E_{11}h^3 \quad (5.2)$$

The nondimensional λ for this study has a different definition than that which is usually used for isotropic materials. This is necessary due to orthotropic material requiring four material properties to completely define their constitutive relationship, whereas isotropic materials need only two. This definition of the dynamic pressure will be employed when presenting or discussing three-dimensional panels whether isotropic or composite.

By including the nonlinear effects (geometric and aerodynamic) in Eq. (3.43) for a fixed displacement amplitude and repeating the same analysis process, the value of λ for which the real part of the eigenvalue vanishes is found to occur at a larger dynamic pressure. For both a $c/h = +1.0$ and $c/h = -1.0$ amplitude ratios, the dynamic pressure and eigenvalue variations are shown in Fig. 5.8. As was the case for the two-dimensional panel, the response is different for a positive or negative assumed displacement amplitude. When the real part of the eigenvalue vanishes for a fixed displacement amplitude, the corresponding dynamic pressure is the limit-cycle dynamic pressure. Associated with this dynamic pressure and amplitude is the frequency at which the panel will oscillate.

Figure 5.8 shows the panel response for a fixed amplitude ratio. If this approach is repeated for several amplitude ratios, then the response shown in Fig. 5.9 results. These results show that as the limit-cycle dynamic pressure is increased above the critical value, then the panel will oscillate at increasing amplitude levels. For this case, the corresponding nonlinear limit-cycle

frequency to critical frequency is shown in Fig. 5.10 for both assumed positive and negative amplitudes. These results indicate that the variation in frequency between positive and negative amplitude ratios up to about 75% of the panel thickness is negligible, and begins to become discernible at a displacement on the order of a panel thickness.

The typical panel limit-cycle deflection shape is shown in Fig. 5.11 for a full 8×12 finite element mesh. Figure 5.12 also shows these results plotted along the lines $y/b = 0.5$ and $x/a = .75$. The basic shape remains similar to those for two-dimensional panels. Similarly, the maximum panel deflection is noted to occur at .75 of the length. Also shown is the shape at this station in the lateral direction.

Knowing the displacements for an element one can then calculate the element stresses. Using the limit-cycle deflections, in Eqs. (2.19), (2.21), (2.29), and (2.30), the finite strains and curvatures are computed for each element. For this study, the element finite strains and curvatures are computed at the element centroids. Next the lamina reduced stiffnesses are computed using Eq. (2.6) and then transformed to the panel coordinate system using Eq. (2.5). With the transformed reduced stiffnesses and the finite strains and curvatures, Eq. (2.4) can then be applied for each element to compute element centroidal stresses. The flow-side panel surface and cavity-side panel surface longitudinal stresses are (also stresses in the principal material direction σ_1 for orthotropic panel) shown in Fig. 5.13. These stresses are maximum in the vicinity of the peak displacement. Stresses on these same surfaces in the lateral direction are shown in Fig. 5.14.

Thus, using the information provided by this analysis, for a given flow velocity, the panel's service life, estimated operating time, can easily be evaluated using fatigue data from a source such as Ref. [58]. The fatigue data from [58] assess the number of cycles to failure for a given peak stress. The peak deflection amplitude is known once the flow velocity is fixed. The peak stress is computed from the flutter shape, and the time of allowable operations is computed from the limit-cycle frequency. All of this translates to an allowable operational time at any given velocity. For variable velocity operations, a cumulative fatigue damage theory such as Palmgren-Miner cycle-ratio summation theory [74-75]; or if the order of the fatigue damage is important, Manson's cumulative theory [75] is available.

5.2.2 Laminated Panel Effects

In the previous section the limit-cycle response of a panel for an orthotropic laminate was investigated in detail. Since the stiffness of a laminate depends substantially on the number and orientation of each lamina in the laminate, an evaluation of a regular cross-ply laminated panel was performed. This evaluation computed the limit-cycle dynamic pressure for a range of limit-cycle amplitudes for several regular laminates. To effect this, a panel thickness was selected and the number of layers were increased from one to six as the limit-cycle amplitude was varied from zero to one plate thickness. As each new lamina was added to the laminate, the orientation was alternated between 0° and 90° . This results in a laminate that alternates between symmetric and unsymmetric; thus, for the unsymmetric laminate the bending-extension $[B]$ matrix is non-zero. However, the $[B]$ matrix is diagonal and only a 8×4 -mesh half-plate was modeled to exploit global symmetry. The variation of the limit-cycle amplitude for a six-layer cross-ply laminate is shown in Fig. 5.15. It is noted that the stiffer response is characterized by an orthotropic laminate, $[0]$, and the softest response is exhibited by a two layer, unsymmetric laminate, $[0/90]$. This is to be expected since the two layer cross-ply has an equal number of 0 's and 90 's, 50% of each. At three layers, the total percentage of 0 's increase to 67%, the maximum percentage for a cross-ply. Any further increase in layers will reduce the effective stiffness of the laminate up to approximately six layers at which point it is noted that the response is no longer sensitive to the addition of alternating layers.

The frequency ratio variation, shown in Fig. 5.16, follows the same trend. The higher frequency at a given dynamic pressure is associated with the softer laminate, and the lowest frequency corresponds to the stiffer laminate. This does not imply that the multi-layer laminate is the best design choice. Referring to Fig. 5.15 for a fixed dynamic pressure, the multi-layered laminate will oscillate at both a higher frequency and amplitude; thus, it will develop higher stresses and consume its service life at a faster rate.

To further investigate the effects of lamination angle, a single layered laminate was evaluated. The lamination angle was varied from 0° to 90° and the limit-cycle dynamic pressure, for a fixed limit-cycle amplitude of 0.6 of the panel thickness, was computed. The variation of the lamination angle and its effect on the dynamic pressure is shown in Fig. 5.17. These results show that again the orthotropic layer exhibits the most stable response. The difference between

the 0° and 90° laminate is approximately a 20% reduction (for material 3) in the limit-cycle dynamic pressure changing more noticeably between 30° to 60°.

5.2.3 Boundary Support and Aspect Ratio Effects

As was noted in the introduction, all of the classical solution methods are for either simply supported or clamped supported panels. With the finite element method, any combination of support conditions is easy to accommodate. The limit-cycle results presented in Fig. 5.18 show the varying response that changing the support conditions has on panel flutter. These results indicate that the clamped panel resists flutter much better than the simply supported panel. It is again interesting to note that the slopes for the various boundary support conditions behave according to the trailing edge support conditions.

The influence that the in-plane immovable boundary condition has on a simply supported, orthotropic panel is shown in Fig. 5.19. The critical dynamic pressure (velocity) is unaffected by this constraint. However, the movable boundary will allow the panel to change rapidly from a small limit-cycle amplitude to a large limit-cycle amplitude over a relative small change in flow velocity. Thus, restraining the in-plane motion of a panel will greatly extend its useful service life.

Since most of these results were for a square panel, the effect of different aspect ratios ($a/b = 0.5, 1.0, \text{ and } 2.0$) is shown in Fig. 5.20. The larger aspect ratios produce a more stable response, and the smaller the aspect ratio, the less stable the response. However, for an aspect ratio of $a/b = 0.5$, the loss in stability is not as great as the increase in stability for $a/b = 2.0$. Thus, for the same panel flow area, the most effective use of the material is to configure the geometry such that the flow-direction dimension is greater than the width.

5.2.4 Influence of Orthotropic Materials

The major portion of this study on three-dimension panel flutter has focused on a single composite material. The orthotropic material was boron aluminum, B/Al, B5.6/Al—material 3 Table 4.1. For the materials listed in Table 4.1, it is easy to see that there are a considerable number of cases and conditions to evaluate in order to fully characterize flutter of a composite panel. This section attempts to address an approach to assess the panel fluttered for different composite materials. By defining a composite material parameter, $(E_{11}E_{22}/G_{12}^2) \nu_{12}$, the

limit-cycle dynamic pressure can be scaled and plotted against this material parameter for several limit-cycle amplitudes. The results shown in Fig. 5.20 show a strong linear correlation of these parameters. Thus, given any new material properties, a reasonable estimate of the limit-cycle response can be assessed provided the analysis has been performed for at least two material systems. Further work is required in this area to provide the designer with a meaningful tool to accommodate flutter constraints into flow surface structural designs.

5.2.5 Nonlinear Aerodynamic Effects

To complete this study an assessment of the third-order piston aerodynamic theory is provided. The influence that the nonlinear aerodynamic terms have on the motion of the panel as it oscillates at a high dynamic pressure is investigated for an isotropic material, and two composite material stacking sequences. Tables 5.2–4 summarize, for the parameters shown, a comparison between the first-order, and third-order piston theories and the effects of neglecting each of the nonlinear aerodynamic terms independently of the others. Since there is very little difference between second- and third-order piston theory, the three-dimension panel results are limited to just a first- and third-order comparison. Table 5.2 is for an isotropic material, and Tables 5.3 and 5.4 are for a boron aluminum material, B/Al B5.6/Al—material 3 Table 4.1. Table 5.3 is for an orthotropic laminate and Table 5.4 is for a [0/90/0] laminate. For all of these results, the term that has the most significant influence when deleted is the $w_{,x}^2$. The effect of including the higher-order theory for these cases when compared to the first-order theory is approximately 4%. The most interesting conclusion from these results is that nearly all of the contribution from the nonlinear aerodynamics is contained in the $w_{,x}^2$ term and does not contain any appreciable contribution from the nonlinear aerodynamic damping. However, since the number of parameters necessary to fully describe the limit-cycle motion can combine in a large number of ways, and since the third-order theory is destabilizing, it is recommended that, as a minimum, the $w_{,x}^2$ term be retained in panel flutter analyses. Using the first-order piston theory and only the $w_{,x}^2$ term, the limit-cycle dynamic pressures for an orthotropic laminate were computed and compared. The results presented in Table 5.5 clearly show that the $w_{,x}^2$ term has the most effect.

Table 5.1 Effects on λ_ℓ by Neglecting Higher Order Terms in
Aerodynamic Piston Theory (Eq. 2.8)^a

c/h	Piston Theory			Neglect						
	1st-order	2nd-order	3rd-order	w_t^2	$w_t w_x$	w_x^2	w_x^3	w_t^3	$w_t^2 w_x$	$w_t w_x^2$
0.0	344.49	344.50	344.49	344.49	344.49	344.49	344.49	344.49	344.49	344.49
0.2	356.28	353.50	353.50	353.51	353.48	356.25	353.53	353.50	353.50	353.50
0.4	392.08	385.90	385.71	385.71	385.68	391.91	385.89	385.71	385.71	385.71
0.6	453.60	442.30	441.87	441.82	441.88	453.18	442.32	441.88	441.88	441.87
0.8	545.04	525.60	524.76	524.75	524.67	544.18	525.63	524.76	524.76	524.76
1.0	674.76	641.70	640.24	640.22	640.10	673.27	641.68	640.24	640.24	640.23

^aSimply Supported, 2-D $\frac{\mu}{M} = .05$, $\frac{Mh}{a} = .01$, $\lambda = \frac{2qa^3}{MD}$

Table 5.2 Effects on λ_ℓ by Neglecting Higher Order Terms in
Aerodynamic Piston Theory (Eq. 2.8)^a

c/h	Piston Theory		Neglect						
	1st-order	3rd-order	w_t^2	$w_t w_x$	w_x^2	w_x^3	w_t^3	$w_t^2 w_x$	$w_t w_x^2$
0.0	49.06	49.06	49.06	49.06	49.06	49.06	49.06	49.06	49.06
0.2	50.15	49.85	49.84	49.88	50.16	49.85	49.85	49.85	49.85
0.4	53.42	52.76	52.76	52.72	53.64	52.75	52.76	52.76	52.77
0.6	58.98	57.84	57.84	57.77	59.00	57.84	57.84	57.83	57.88
0.8	66.99	65.19	65.2	65.09	67.01	65.13	65.2	64.19	65.28
1.0	77.77	75.04	75.05	74.89	77.80	75.04	75.04	75.03	75.18

^aSimply Supported, $\frac{\mu}{M} = .05$, $\frac{Mh}{a} = .01$, $\lambda = \frac{2qa^3}{MD}$

3-D Isotropic Panel

Table 5.3 Effects on λ_t by Neglecting Higher Order Terms in
Aerodynamic Piston Theory (Eq. 2.8)^a

c/h	Piston Theory		Neglect						
	1st-order	3rd-order	w_t^2	$w_t w_x$	w_x^2	w_x^3	w_t^3	$w_t^2 w_x$	$w_t w_x^2$
0.0	41.78	41.78	41.78	41.78	41.78	41.78	41.78	41.78	41.78
0.2	42.86	42.62	42.62	42.56	42.91	42.62	42.62	42.62	42.62
0.4	46.03	45.60	45.49	45.38	46.11	45.49	45.49	45.49	45.51
0.6	51.50	50.51	50.56	50.35	51.62	50.53	50.53	50.53	50.55
0.8	59.50	57.85	57.96	57.62	59.63	57.88	54.89	57.87	57.91
1.0	70.46	67.71	68.03	67.42	70.59	67.79	64.05	67.76	67.81

^aSimply Supported, $\frac{\mu}{M} = .05$, $\frac{Mh}{a} = 0.1$, $\lambda = \frac{2qa^3}{MD}$

Single Layer Composite, Material 3-Table 4.1

Table 5.4 Effects on λ_t by Neglecting Higher Order Terms in
Aerodynamic Piston Theory (Eq. 2.8)^a

c/h	Piston Theory		Neglect						
	1st-order	3rd-order	w_t^2	$w_t w_x$	w_x^2	w_x^3	w_t^3	$w_t^2 w_x$	$w_t w_x^2$
0.0	41.38	41.38	41.38	41.38	41.38	41.38	41.38	41.38	41.38
0.2	42.34	42.10	42.11	42.04	42.39	42.10	42.10	42.10	42.11
0.4	45.25	44.73	44.74	44.61	45.34	44.73	44.73	44.73	44.75
0.6	49.97	49.05	49.07	48.88	50.09	49.05	49.05	49.05	49.09
0.8	56.95	55.47	55.53	55.22	57.10	55.47	55.48	55.46	55.55
1.0	66.38	64.05	64.18	63.68	66.53	64.05	64.05	64.03	64.17

^aSimply Supported, $\frac{\mu}{M} = .05$, $\frac{Mh}{a} = .01$, $\lambda = \frac{2qa^3}{MD}$

Composite, Material 3-Table 4.1, [0/90/0]

Table 5.5 Effects on λ_ℓ by Including $w_{,x}^2$ Higher Order Terms with
First-Order Aerodynamic Piston Theory (Eq. 2.8)^a

c/h	First-Order Piston Theory	Third-Order Piston Theory	First-Order Piston Theory Plus $w_{,x}^2$
0.0	41.78	41.78	41.78
0.2	42.86	42.62	42.57
0.4	46.03	45.60	45.40
0.6	51.50	50.51	50.41
0.8	59.50	57.85	57.75
1.0	70.46	67.71	67.71

^aSimply Supported, $\frac{\mu}{M} = .05$, $\frac{Mh}{a} = .01$, $\lambda = \frac{2ga^3}{MD}$

Single Layer Composite, Material 3-Table 4.1

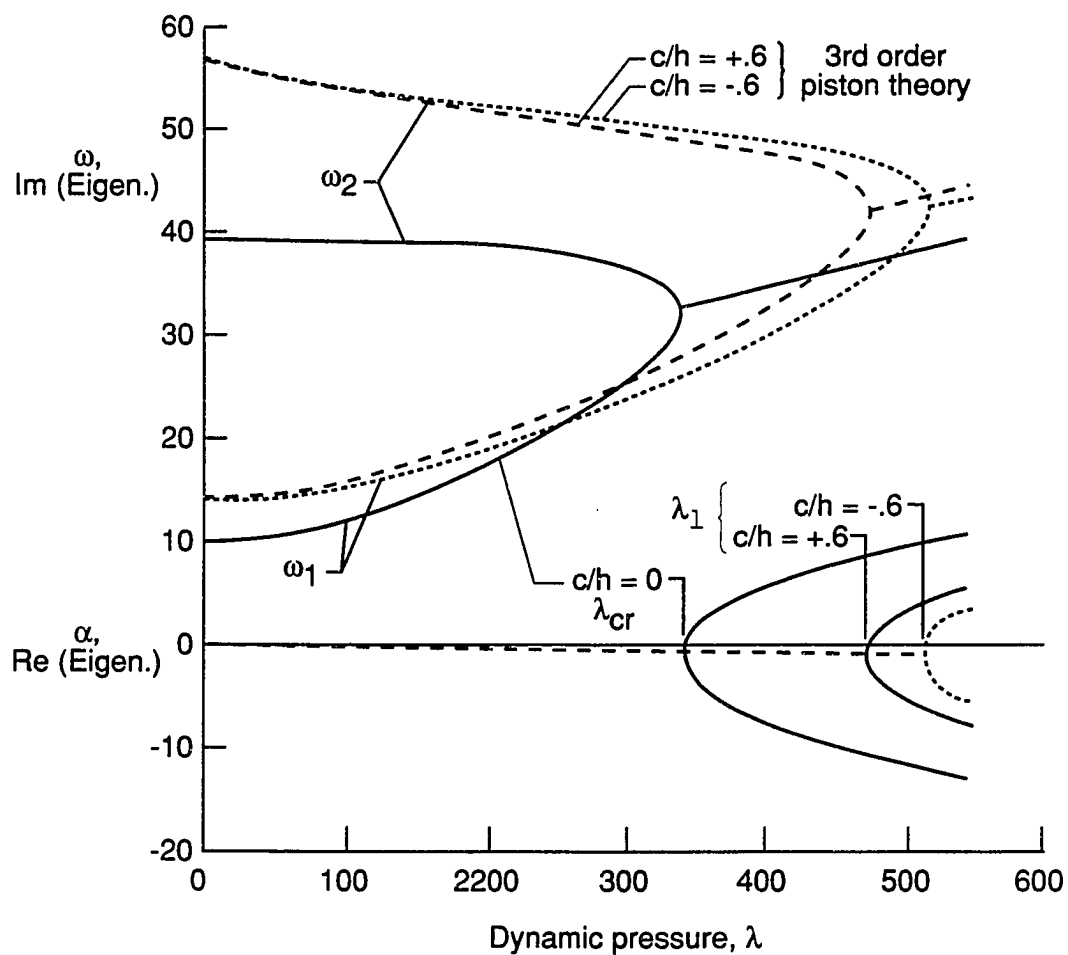


Fig. 5.1 Variation of Eigenvalue with Nondimensional Dynamic Pressure for a Simply-Supported Panel. ($\mu/M = .01$, $Mh/a = .05$).

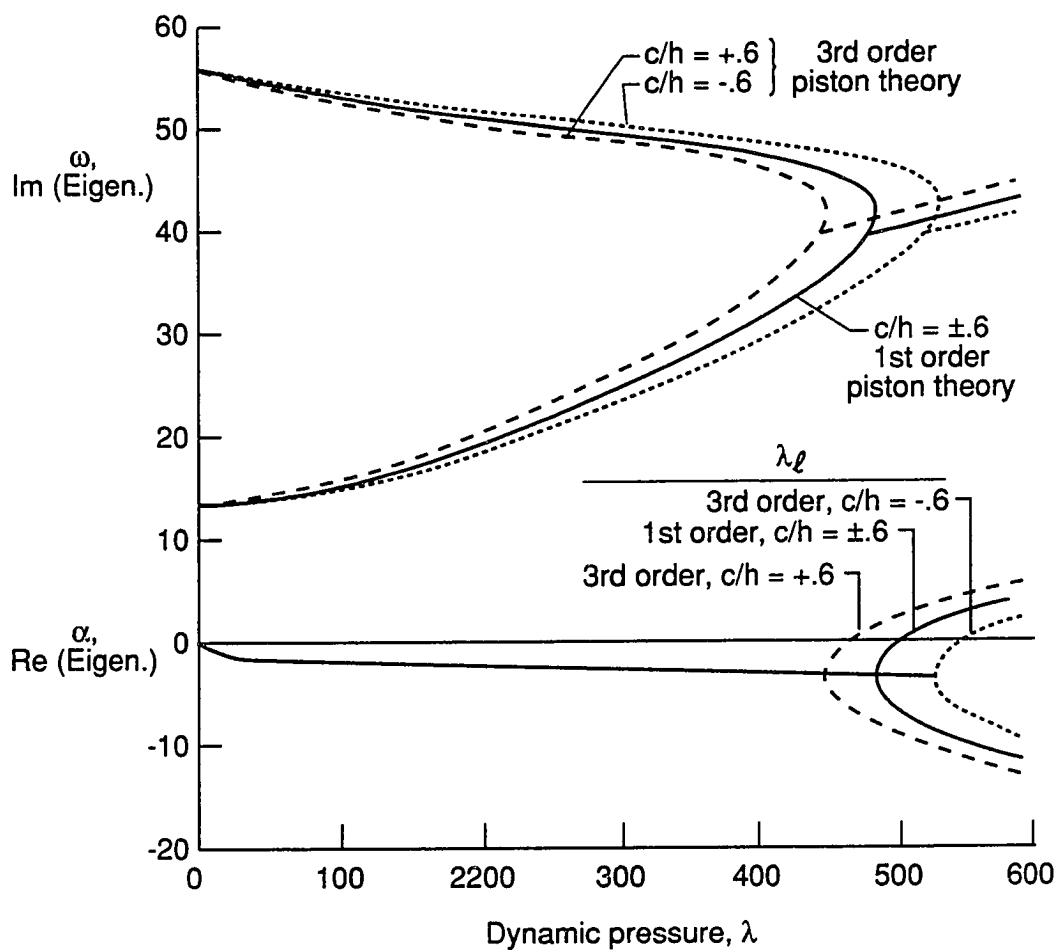


Fig. 5.2 Variation of Eigenvalue with Nondimensional Dynamic Pressure for a Simply-Supported Panel Using First- and Third-Order Piston Theory Aerodynamics. ($\mu/M = .1$, $Mh/a = .1$).

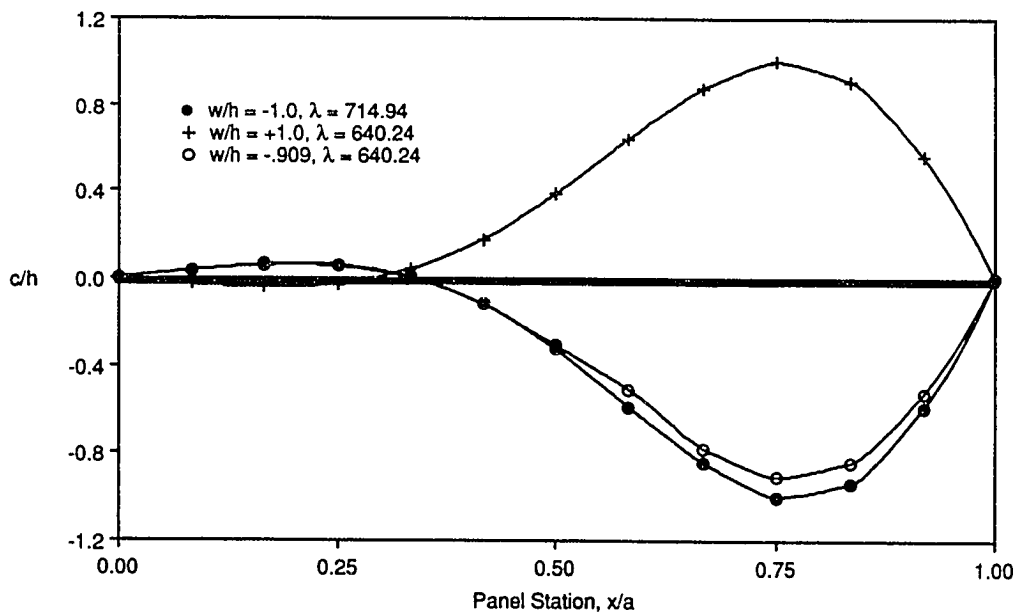


Fig. 5.3 Simply-Supported Panel Deflection Shapes for $c/h = +1.0$, $c/h = -1.0$, and $c/h = -.909$. ($\mu/M = .01$, $Mh/a = .05$).

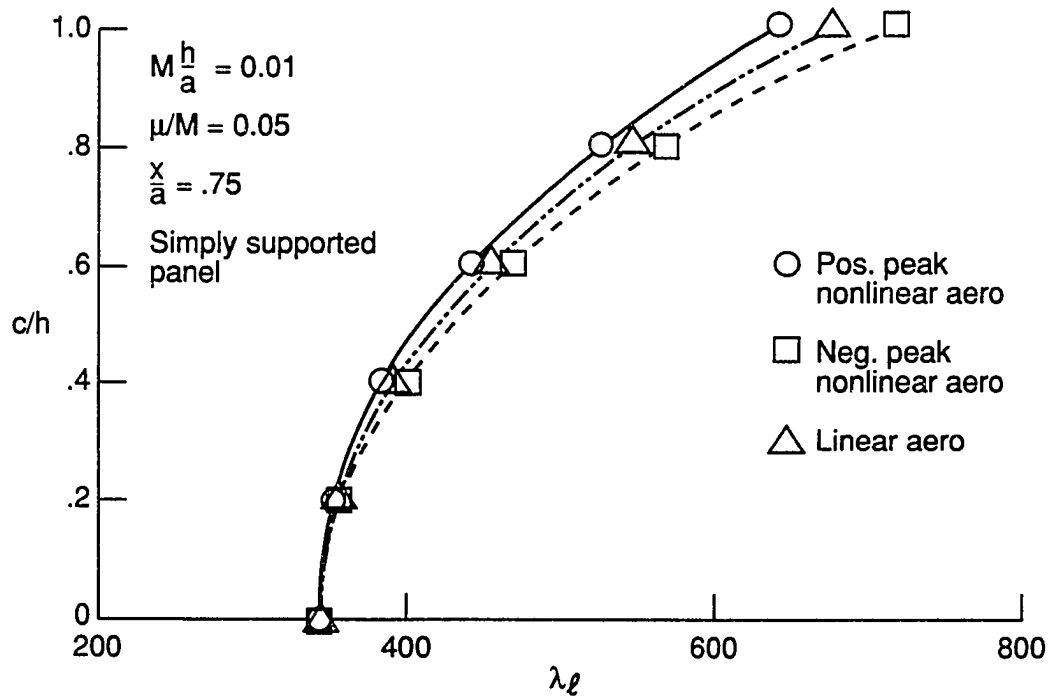


Fig. 5.4 Comparison of Nonlinear and Linear Piston Theory Aerodynamics on Large-Amplitude Panel Flutter. ($\mu/M = .01$, $Mh/a = .05$).

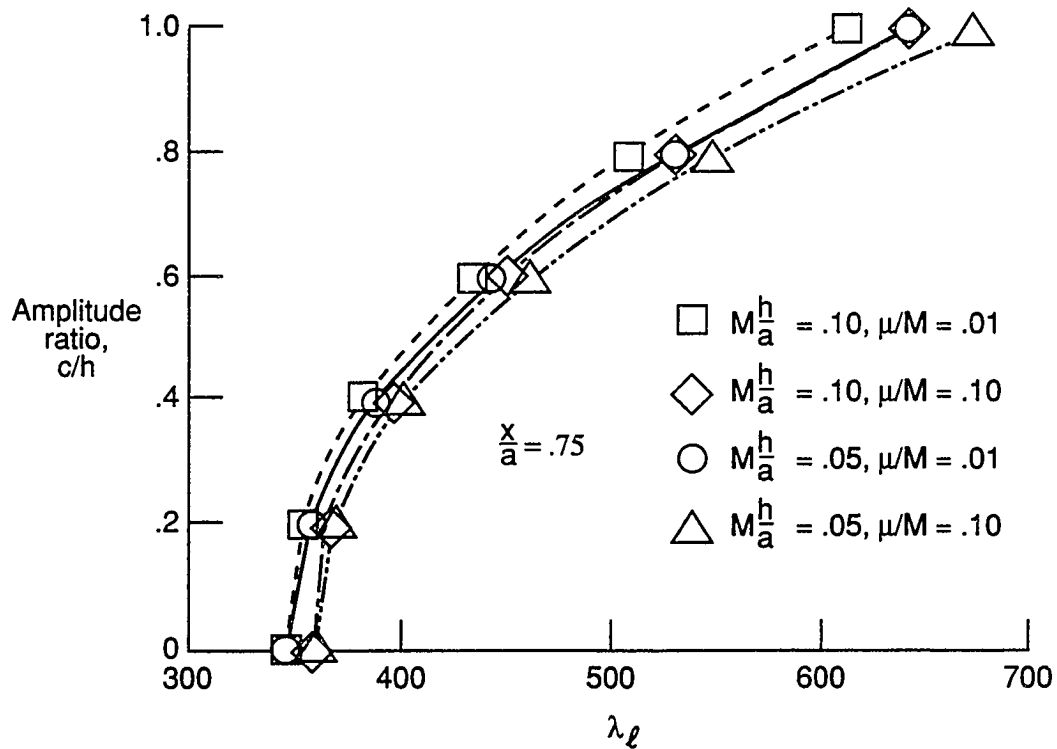


Fig. 5.5 Limit-Cycle Amplitude at $x/a = .75$ vs. Nondimensional Dynamic Pressure for a Simply-Supported Panel for Several Flow Parameters.

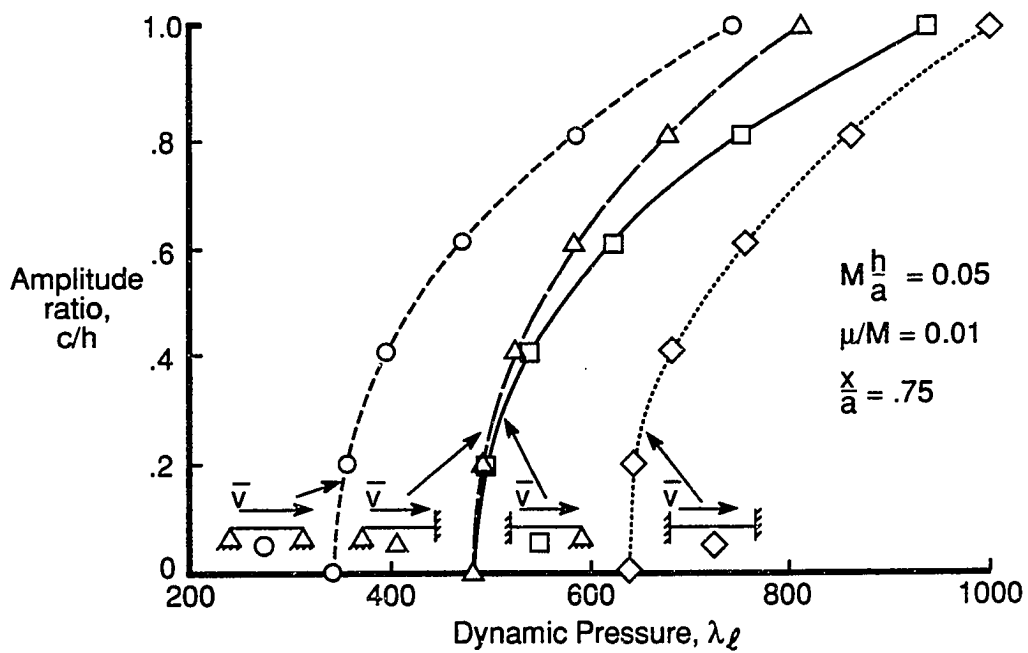


Fig. 5.6 Limit-Cycle Amplitude at $x/a = .75$ vs. Nondimensional Dynamic Pressure for Various Support Conditions.

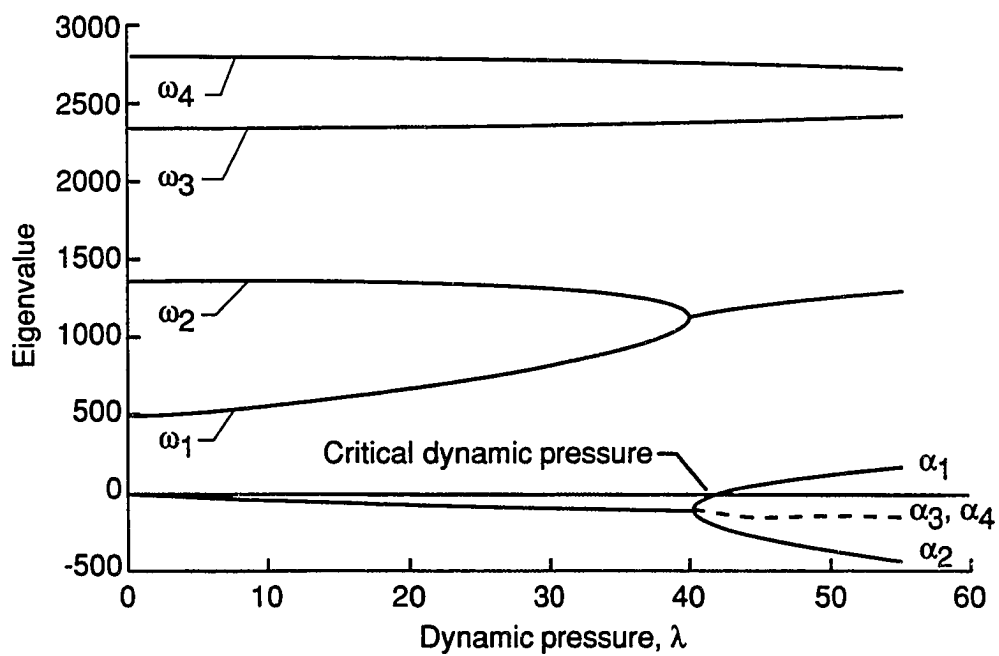


Fig. 5.7 Eigenvalue Variation for First Four Linear Modes of a Simply-Supported, Square Panel for Material 3. ($\mu/M = .10$, $Mh/a = .05$).

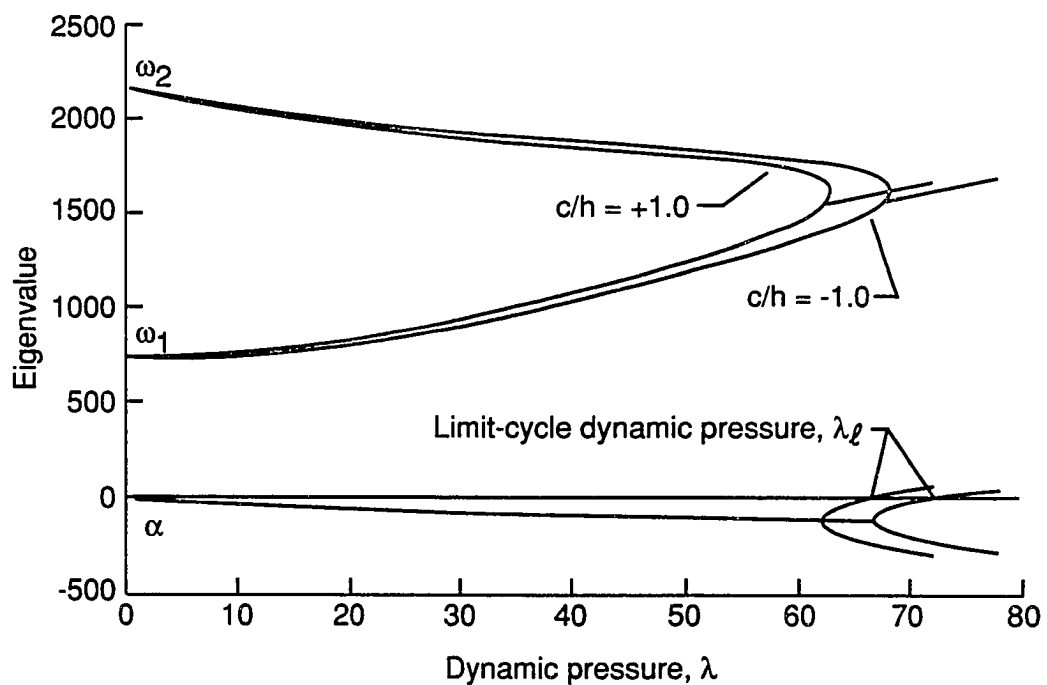


Fig. 5.8 Nonlinear Panel Flutter Eigenvalue Variation vs. Dynamic Pressure Using Third-Order Piston Theory Aerodynamics of a Simply-Supported, Square Panel for Material 3. ($\mu/M = .10$, $Mh/a = .05$).

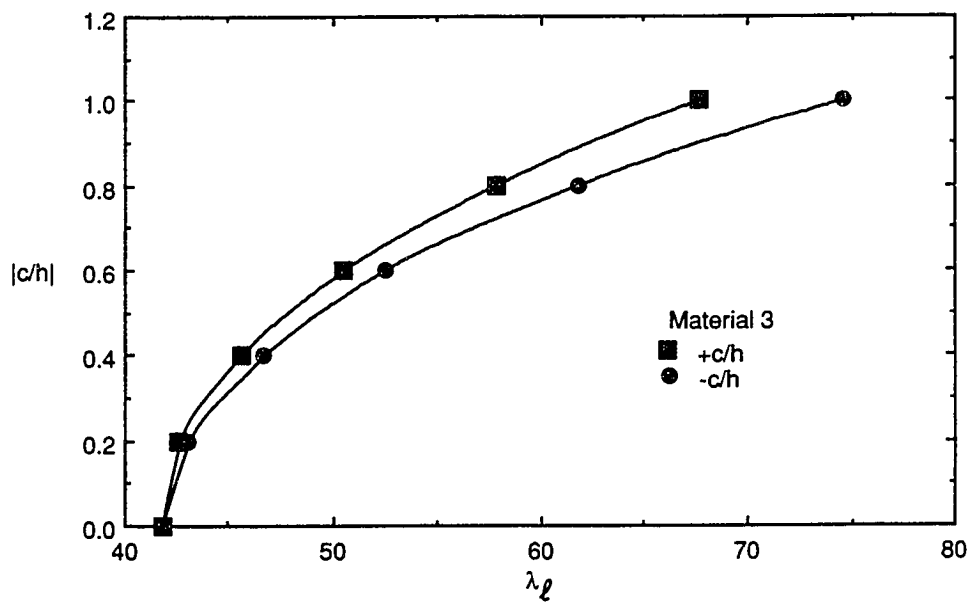


Fig. 5.9 Variation of Limit-Cycle Amplitude vs. Limit-Cycle Dynamic Pressure of a Simply-Supported, Square Panel for Material 3. ($\mu/M = .10$, $Mh/a = .05$).

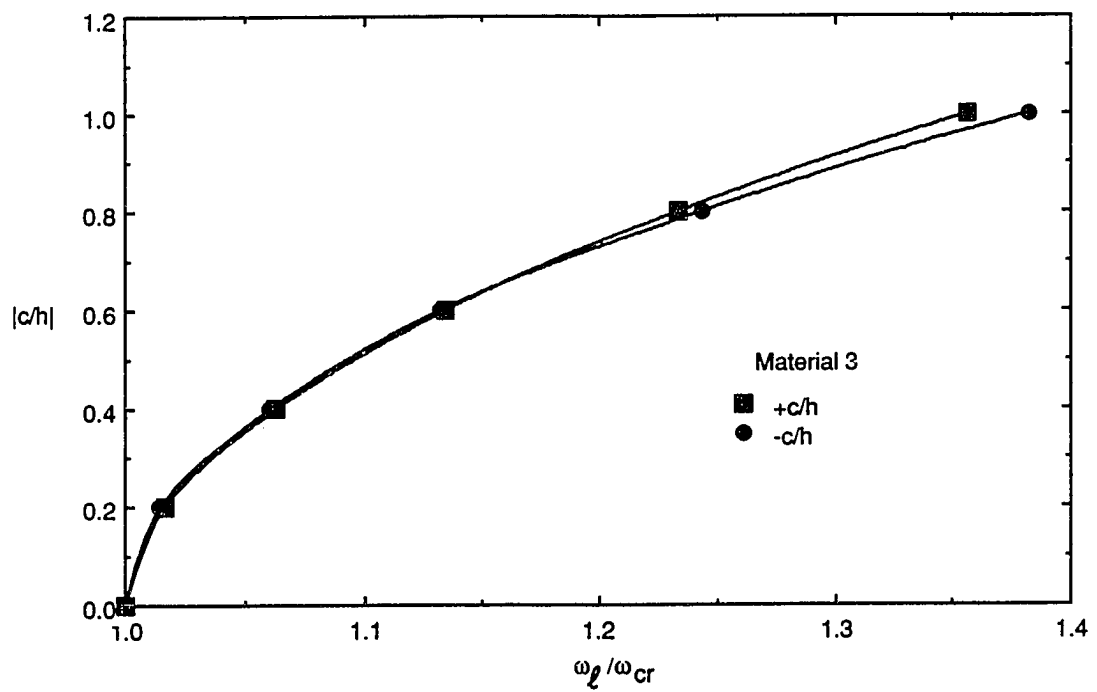


Fig. 5.10 Variation of Limit-Cycle Frequency Ratio vs. Limit-Cycle Amplitude of a Simply-Supported, Square Panel for Material 3. ($\mu/M = .10$, $Mh/a = .05$).

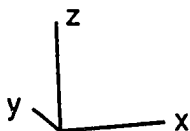
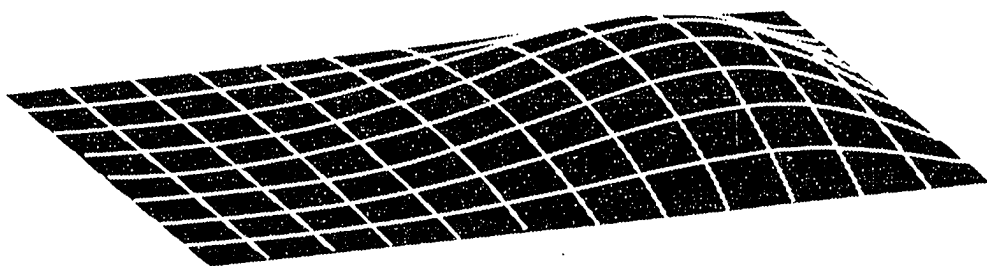


Fig. 5.11 Limit-Cycle Deflection Shape of a Simply-Supported, Single Layer Square Panel for Material 3. ($\mu/M = .10$, $Mh/a = .05$, $\lambda = 67.71$, $c/h = +1.0$, 12×8 Full Panel).

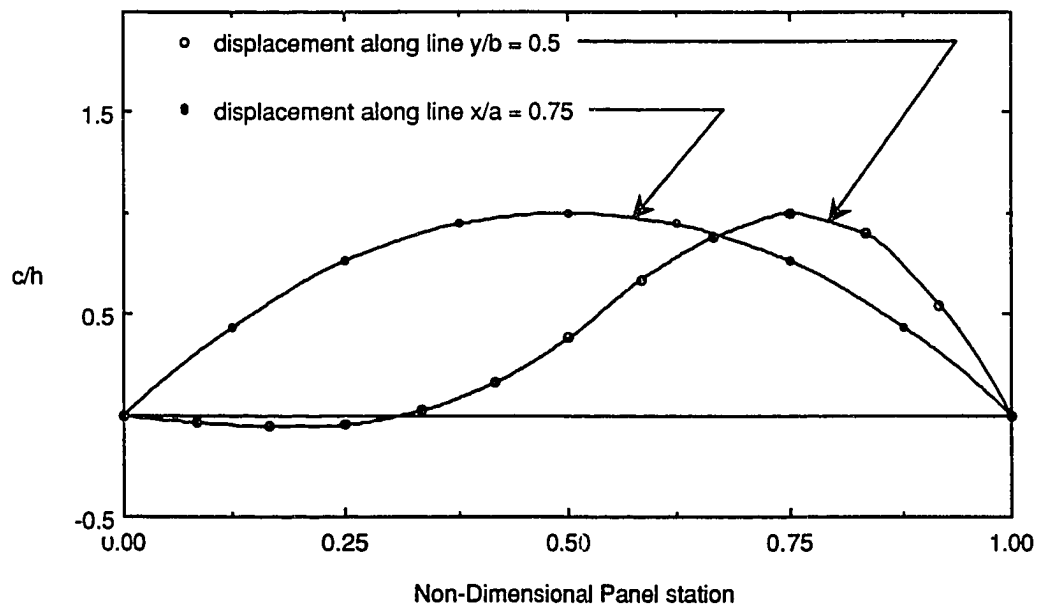


Fig. 5.12 Panel Limit-Cycle Deflection of a Simply-Supported, Single Layer Square Panel for Material 3. ($\mu/M = .10$, $Mh/a = .05$, $\lambda = 67.71$, $c/h = +1.0$, 12×8 Full Panel).

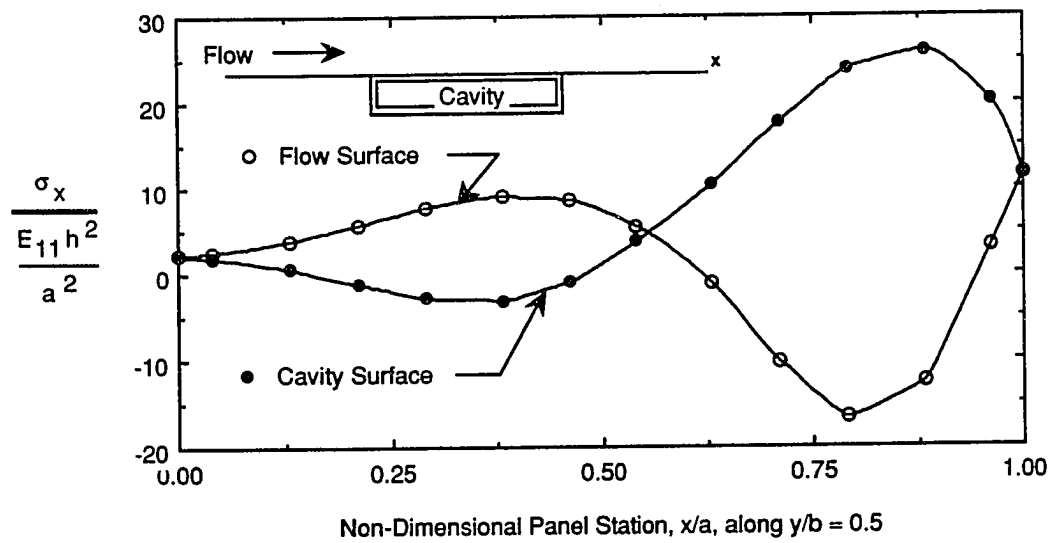


Fig. 5.13 Longitudinal Surface Stresses Along a Simply-Supported, Square Panel at $y/b = 0.5$ for Material 3. ($\mu/M = .10$, $Mh/a = .05$, $\lambda = 67.71$, $c/h = +1.0$, 12×8 Full Panel).

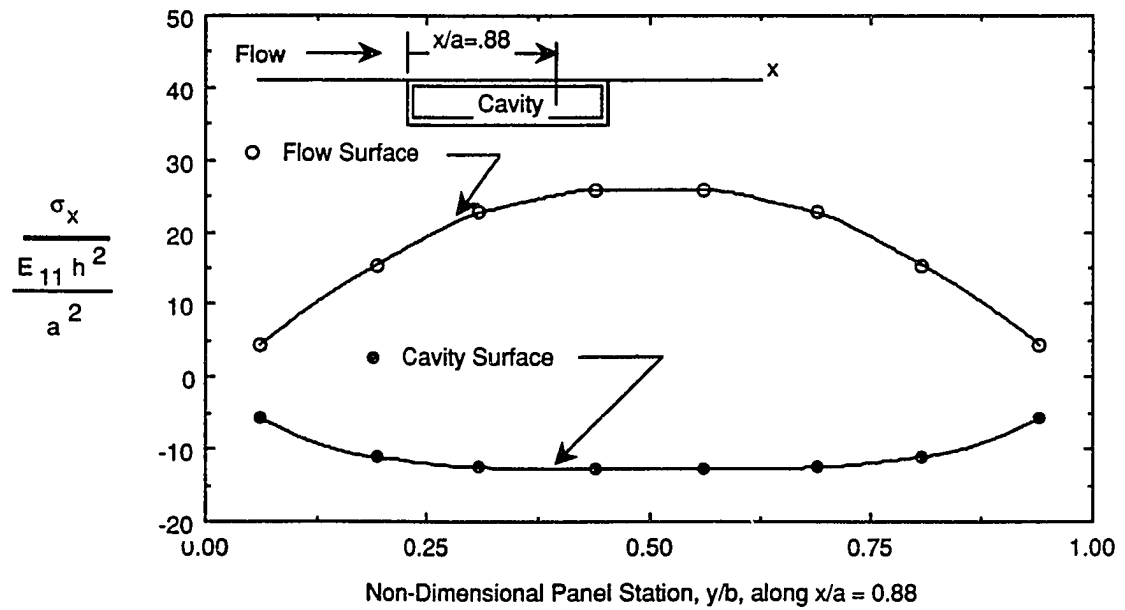


Fig. 5.14 Longitudinal Surface Stresses Along a Simply-Supported, Single Layer Square Panel at $x/a = .88$ for Material 3. ($\mu/M = .10$, $Mh/a = .05$, $\lambda = 67.71$, $c/h = +1.0$, 12×8 Full Panel).

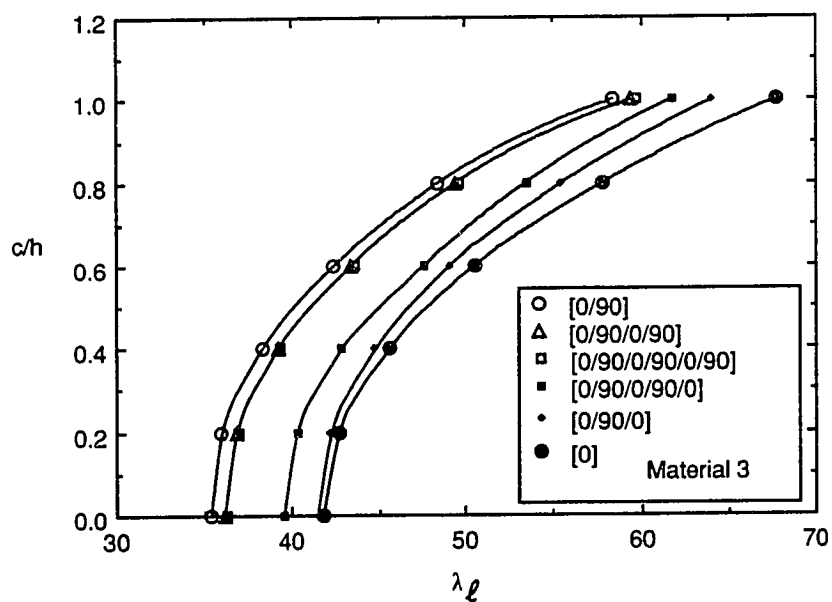


Fig. 5.15 Effects of Number of Plies on Limit-Cycle Amplitude and Dynamic Pressure for a Simply-Supported, Square Panel for Material 3. ($\mu/M = .10$, $Mh/a = .05$).

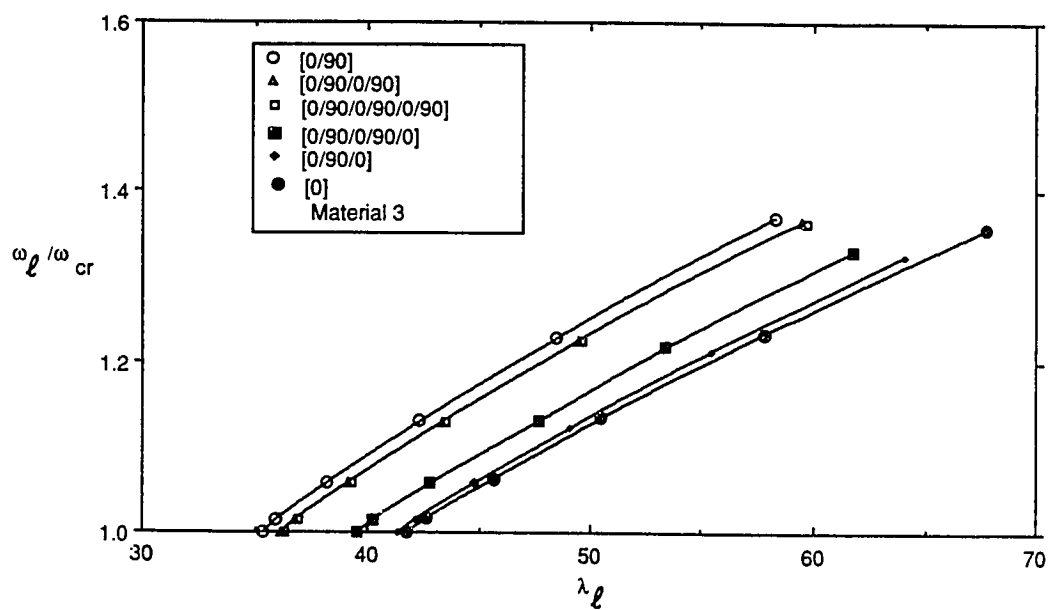


Fig. 5.16 Effects of Number of Plies on Limit-Cycle Frequency and Dynamic Pressure for a Simply-Supported, Square Panel for Material 3. ($\mu/M = .10$, $Mh/a = .05$).

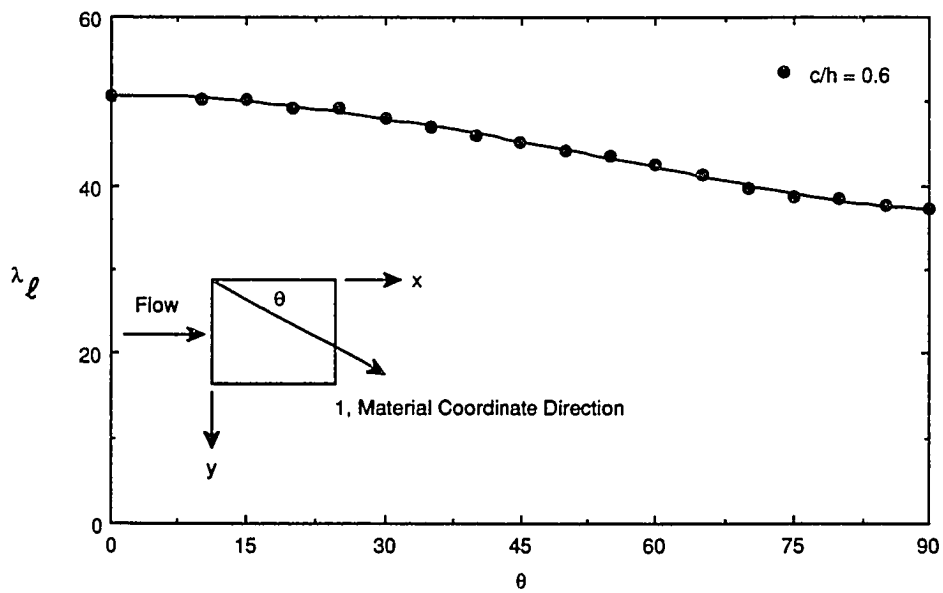


Fig. 5.17 Effects of Lamination Angle Variation on Limit-Cycle Dynamic Pressure for a Simply-Supported, Single Layer Square Panel for Material 3. ($\mu/M = .10$, $Mh/a = .05$, $c/h = 0.6$).

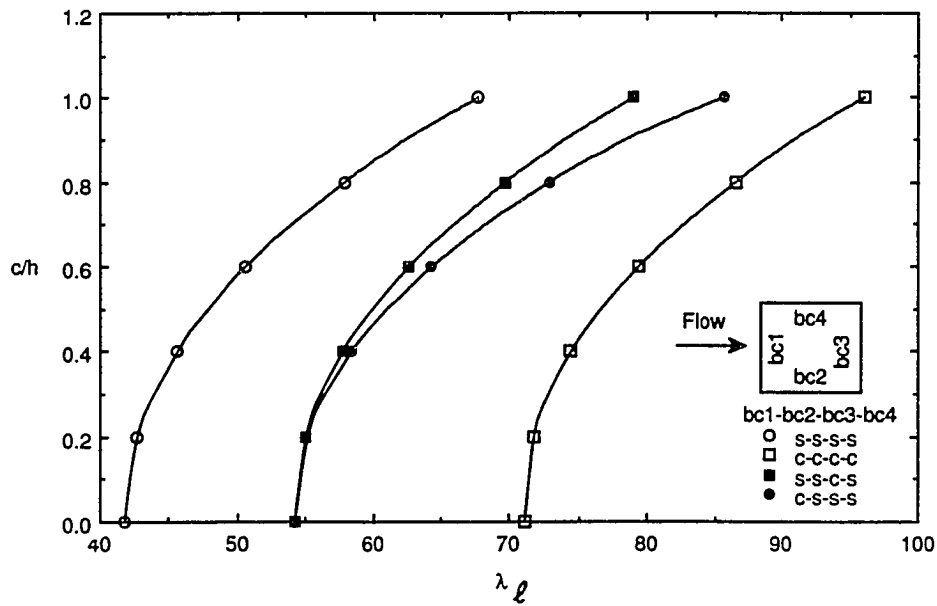


Fig. 5.18 Limit-Cycle Amplitude at $x/a = .75$ and $y/b = .50$ vs. Dynamic Pressure for Various Support Conditions for a Single Layer Square Panel of Material 3. ($\mu/M = .10$, $Mh/a = .05$).

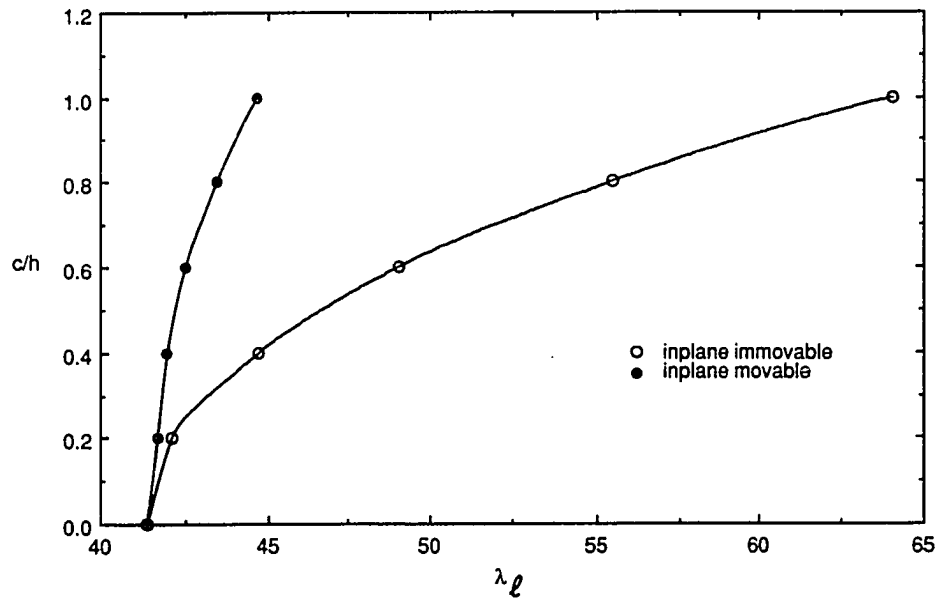


Fig. 5.19 Limit-Cycle Amplitude at $x/a = .75$ and $y/b = .50$ vs. Dynamic Pressure for a Simply-Supported, Single Layer Square Panel of Material 3 with In-Plane Movable and Immovable Support Conditions ($\mu/M = .10$, $Mh/a = .054$).

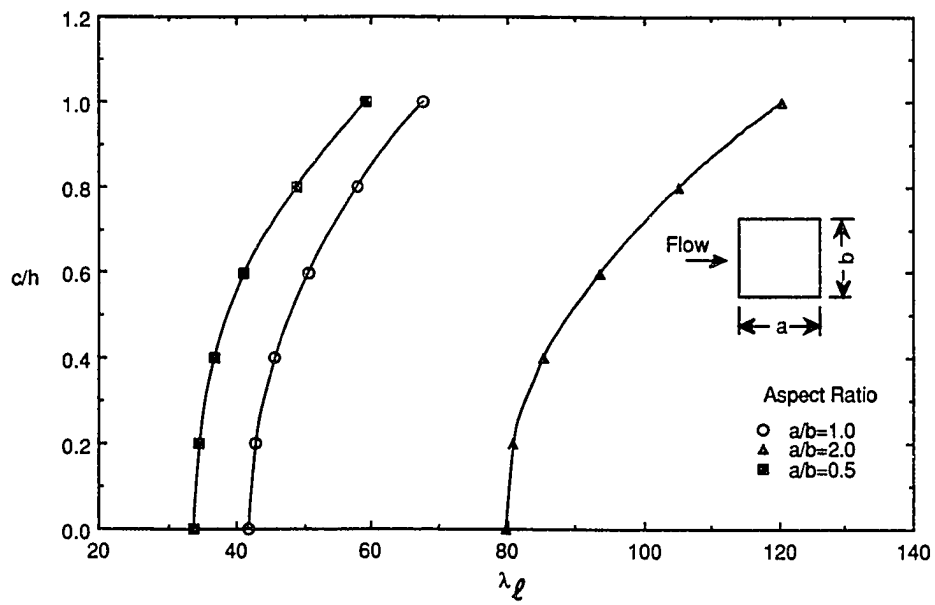


Fig. 5.20 Limit-Cycle Amplitude at $x/a = .75$ and $y/b = .50$ vs. Dynamic Pressure for a Simply-Supported, Single Layer Panel for Several Aspect Ratios for Material 3. ($\mu/M = .10$, $Mh/a = .05$).

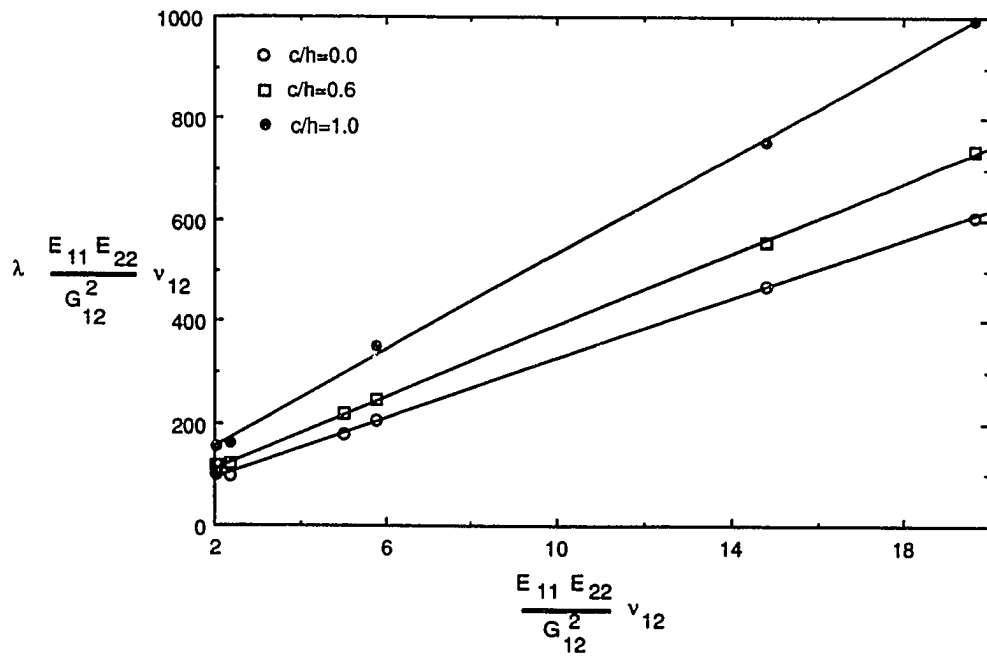


Fig. 5.21 Limit-Cycle Parameter vs. Orthotropic Material Parameter for Limit-Cycle Amplitudes and a Simply-Supported, Single Layer Square Panel of Material 3. ($\mu/M = .10$, $Mh/a = .05$).

Chapter 6

SUMMARY AND CONCLUSIONS

6.1 Concluding Remarks

This study, of the interaction between structures and aerodynamics, consisted of developing and evaluating a finite-element approach for determining the nonlinear flutter characteristics of two-dimensional isotropic and three-dimensional composite laminated panels using the third-order-piston aerodynamic transverse loading theory. The unsteady, hypersonic, aerodynamic theory and the von Karman large deflection theory were employed to formulate the aeroelastic problem. Nonlinear flutter analyses were performed to assess the influence of the higher-order aerodynamic theory on the structure's limit-cycle amplitude and the dynamic pressure of the flow velocity. The presented procedure has been used to solve the nonlinear panel flutter and large-amplitude free vibration finite element equations. This procedure utilizes a linearized updated mode approach with a nonlinear time function approximation (LUM/NTF) method. Nonlinear flutter analyses were performed for different boundary support-conditions and for various system parameters: plate thickness-to-length ratio, h/a ; aspect ratio a/b ; material orthotropic ratio, lamination angle, and number of layers; Mach number, M ; flow mass-density-to-panel-mass-density ratio, μ/M ; dynamic pressure, λ ; and maximum-deflection-to-thickness ratio, c/h . For large amplitude free vibration, alternative classical analytical solutions are available for comparison. Linear finite-element flutter for isotropic and composite panels and large amplitude isotropic panel flutter results were compared with existing classical solutions and excellent agreement between the proposed finite element method and alternate solution methods was found. The large amplitude panel flutter results using a frequency domain solution and the full third-order piston aerodynamic theory were presented to assess the influence of the nonlinear aerodynamic theory and for the cases investigated in this study for both two- and three-dimensional panel only the $w, \frac{\partial^2}{\partial x^2}$ term was found to be significant.

The overall goal of the present study was to develop an effective computational strategy for predicting the nonlinear flutter response of anisotropic panels in hypersonic flow. To this end, there were three global objectives. The first objective was to develop and validate a large-amplitude free vibration linearizing method. Second to assess the effects of the full nonlinear third-order piston theory aerodynamics, the objective was to develop and implement a solution method to solve the nonstandard, nonlinear eigenvalue problem. This objective also allows for the solution of large-amplitude, nonlinear damping free vibrating panels. The final objective was to combine the other two goals and extend the finite element formulation to include the anisotropic laminated plate theory to evaluate the large-amplitude fluttering composite panel in hypersonic flow. All of these objectives were achieved and thoroughly investigated using the proposed solution method. The proposed solution method develops the nonlinear stiffness and nonlinear aerodynamic influence matrices, linearizes the nonlinear matrices, transforms the problem formulation from the configuration space to the state space, then solves, in an iterative manner, the general eigenvalue problem. A computational solution procedure was developed. This procedure introduced a linearization technique for the nonlinear, displacement dependent stiffness, aerodynamic influence, and aerodynamic damping matrices.

The solution of the large-amplitude panel flutter problem, including anisotropic material behavior and unsteady displacement and velocity dependent aerodynamics, is the first finite element solution technique to include all of these effects. Numerical examples and discussion of results were to provide complete confidence in the numerical procedure and method and to also present flutter results for three-dimensional composite panels.

6.2 Future Work

The analysis presented in this study is not considered to be complete. Further work is recommended, and needed, to more adequately describe the aerodynamic loads. In the advent that more advanced aerodynamic theories become available the approach as outlined in this study will easily handle them. The degree of nonlinearity found in the implementation of the full third-order piston aerodynamic theory, displacement- and velocity-dependent loads, suggest that a more advanced nonlinear aerodynamic theory can most certainly be handled using the proposed method.

REFERENCES

1. Dungundji, J., "Theoretical Considerations of Panel Flutter at High Supersonic Mach Numbers," *AIAA J.*, Vol. 4, July 1966, pp. 1257-1266.
2. Dowell, E. H., "Panel Flutter: A Review of the Aeroelastic Stability of Plates and Shells," *AIAA J.*, Vol. 8, March 1970, pp. 385-399.
3. Reed, W. H., Hanson, P. W. and Alford, W. J., "Assessment of Flutter Model Testing Relating to the National Aero-Space Plane," NASP Contractor Report 1002, 1987.
4. Laurenson, R. M. and McPherson, J. I., "Design Procedures for Flutter-Free Surface Panels," NASA CR-2801, 1977.
5. Cunningham, H. J., "Flutter Analysis of Flat Rectangular Panels Based on Three-Dimensional Supersonic Potential Flow," *AIAA J.*, Vol. 1, No. 8, August 1963, pp. 1795-1801.
6. Ashley, H. and Zartarian, G., "Piston Theory—A New Aerodynamic Tool for the Aeroelastician," *Journal of the Aeronautical Science*, Vol. 23, No. 12, December 1956.
7. Dowell, E. H., *Aeroelasticity of Plates and Shells*, Noordhoff International Publishing, Lyden, The Netherlands, 1975.
8. Woinowsky-Krieger, S., "The Effects of Axial Force on the Vibration of Hinged Bars," *Journal of Applied Mechanics*, Vol. 17, 1950, pp. 35-36.
9. McIntosh, S. G., Jr., "Theoretical Considerations of Some Nonlinear Aspects of Hypersonic Panel Flutter," Final Report, September 1, 1965 to August 31, 1970, NASA Grant NGR 05-020-102, Department of Aeronautics and Astronautics, Stanford University, Stanford, CA., 1970.
10. Bolotin, V. V., *Nonconservative Problems of the Theory of Elastic Stability*, McMillan Co., New York, 1963, pp. 199-312.
11. Fung, Y. C., "On Two-Dimensional Panel Flutter," *Journal of the Aeronautical Sciences*, Vol. 25, March 1958, pp. 145-160.
12. Houbolt, J. C., "A Study of Several Aerothermoelastic Problems of Aircraft Structures," Mitteilung aus dem Institute fur Flugzeugstatik und Leuchbau, Nr. 5, E.T.H., Zurich, 1958.
13. Eisely, J. G., "The Flutter of a Two-Dimensional Buckled Plate with Clamped Edges in a Supersonic Flow," OSR-TN-56-296, July 1956.
14. Cunningham, H. J., "Flutter Analysis of Flat Rectangular Panels Based on Three-Dimensional Supersonic Unsteady Potential Flow," TRT-256, 1967 NASA.

15. Fralich, R. W., "Postbuckling Effects on the Flutter of Simply Supported Rectangular Panels at Supersonic Speed," NASA TN D-1615, March 1965.
16. Dowell, E. H., "Nonlinear Oscillation of a Fluttering Plate II," *AIAA J.*, Vol. 5, No. 10, October 1967, pp. 1856-1862.
17. Dowell, E. H., and Voss, H. M., "Experimental and Theoretical Panel Flutter Studies in Mach Number Range 1.0 to 5.0," *AIAA J.*, Vol. 3, No. 12, December 1965, pp. 2292-2304.
18. Dowell, E. H., "Nonlinear Oscillation of a Fluttering Plate I," *AIAA J.*, Vol. 4, No. 7, July 1966, pp. 1267-1275.
19. Ventres, C. S., "Nonlinear Flutter of Clamped Plates," Ph.D. Dissertation, Princeton University, 1970.
20. Kobayashi, S., "Flutter of Simply-Supported Rectangular Panels in a Supersonic Flow—Two-Dimensional Panel Flutter, I—Simply-Supported Panel, II—Clamped Panel," *Transaction of Japan Society of Aeronautical and Space Sciences*, Vol. 5, 1962, pp. 79-118.
21. Kuo, C. C., Morino, L., and Dungundji, J., "Perturbation and Harmonic Balance for Treating Nonlinear Panel Flutter," *AIAA J.*, Vol. 10, Nov. 1972, pp. 1470-1484.
22. Eastep, F. E., and McIntosh, S. C., "The Analysis of Nonlinear Panel Flutter and Response Under Random Excitation or Nonlinear Aerodynamic Loading," AIAA/ASME 11th Structural Dynamics, and Materials Conference, Denver, CO, April 22-24, 1970, pp. 36-47.
23. Eastep, F. E., "Nonlinear Oscillations of Elastic Panel in a Supersonic Nonviscous Airstream," SUDAAR No. 354, August 1968.
24. Morino, L., "A Perturbation Method for Treating Nonlinear Panel Flutter Problems," *AIAA J.*, Vol. 7, March 1969, pp. 405-410.
25. Morino, L. and Kuo, C. C., "Detailed Extensions of Perturbation Methods for Nonlinear Panel Flutter," ASRL TR 164-2, M.I.T., Cambridge, MA, March 1971.
26. Perlmutter, A. A., "On the Aeroelastic Stability of Orthotropic Panels in Supersonic Flow," *Journal of AeroSpace Science*, Vol. 29, November 1962, pp. 1332-1338.
27. Calligeros, J. M. and Dungundji, J., "Supersonic Flutter of Rectangular Orthotropic Panels with Arbitrary Orientation of the Orthotropicity," AFOSR5328, June 1963.
28. Ketter, D. J., "Flutter of Flat Rectangular, Orthotropic Panels," *AIAA J.*, Vol. 1, February 1966, pp. 116-124.
29. Shyprykevich, P. and Sawyer, J. W., "Orthotropic Panel Flutter at Arbitrary Yaw Angles—Experiment and Correlation with Theory," *AIAA J.*, Paper 73-192, January 1973.
30. Oyibo, G. A., "Flutter of Orthotropic Panels in Supersonic Flow Using Affine Transformation," *AIAA J.*, Vol. 21, February 1983, pp. 283-289.
31. Librescu, L., "Aeroelastic Stability of Orthotropic Heterogeneous Thin Panels in the Vicinity of Flutter Critical Boundary," *Journal de Mechanique*, 4, 1965, pp. 51-76.

32. Eslami, H., "Nonlinear Flutter and Forced Oscillations of Rectangular Symmetric Cross-Ply and Orthotropic Panels Using Harmonic Balance and Perturbation Method," Ph.D. Dissertation, Old Dominion University, Norfolk, VA, 1987.
33. Eslami, H. and Ibrahim, S. R., "Nonlinear Flutter of Specially Orthotropic Laminated Panels," Proceedings of 27th Structures, Structural Dynamics and Materials Conference, San Antonio, TX, 1986, pp. 393-302.
34. Olson, M. D., "Finite Element Approach to Panel Flutter," *AIAA J.*, Vol. 5, December 1967, pp. 2267-2270.
35. Olson, M. D., "Some Flutter Solutions Using Finite Element," *AIAA J.*, Vol. 8, April 1970, pp. 747-752.
36. Yang, T. Y. and Sung, S. H., "Finite Element in Three-Dimensional Supersonic Unsteady Potential Flow," *AIAA J.*, Vol. 15, December 1977, pp. 1677-1683.
37. Mei, C. and Rogers, J. L., Jr., "Application of Nastran to Large Deflection Supersonic Flutter of Panels," NASA TM X-3429, October 1976, pp. 67-97.
38. Mei, C., "A Finite Element Approach for Nonlinear Panel Flutter," *AIAA J.*, Vol. 15, August 1977, pp. 1107-1110.
39. Rao, K. S. and Rao, G. V., "Large Amplitude Supersonic Flutter of Panels with Ends Elastically Restrained Against Rotation," *Computer and Structures*, Vol. 11, 1980, pp. 197-201.
40. Mei, C. and Weidman, D. J., "Nonlinear Panel Flutter—A Finite Element Approach," Computational Methods for Fluid—Structure Interaction Problems, Ed. by Belytsechke, T. and Geers, T. L., AMP-Vol. 26, ASME, 1977, pp. 139-165.
41. Han, A. D. and Yang, T. Y., "Nonlinear Panel Flutter Using High Order Triangular Finite Elements," *AIAA J.*, Vol. 21, No. 10, October 1983, pp. 1453-1461.
42. Mei, C. and Wang, H. C., "Finite Element Analysis of Large Amplitude Supersonic Flutter of Panels," Proceedings International Conference on Finite Element Methods, Shanghai, China, Gordon and Breach Science Publishers, Inc., 1982, pp. 944-951.
43. Sarma, B. S. and Varadan, T. K., "Non-linear Panel Flutter by Finite Element Method," *AIAA J.*, Vol. 26, May 1988, pp. 566-574.
44. Gray, C. E., Jr., Mei, C., and Shore, C. P., "Finite Element Method for Large-Amplitude Two-Dimensional Panel Flutter at Hypersonic Speeds," *AIAA J.*, Vol. 29, February 1991, pp. 290-298.
45. Dowell, E. H., *A Modern Course in Aeroelasticity*, Noorhoff, Netherlands, 1978.
46. Bisplinghoff, R. L., Ashley, H., and Halfman, R. L., *Aeroelasticity*, Addison-Wesley, Massachusetts, 1957.
47. Dowell, E. H. and Ilgamov, M., *Studies in Nonlinear Aeroelasticity*, Springer-Verlag, London, 1988.

48. Mei, C., "Nonlinear Vibration of Beams by Matrix Displacement Method," *AIAA J.*, Vol. 10, October 1972, pp. 335-357.
49. Mei, C., "Finite Element Analysis of Nonlinear Vibration of Beam Columns," *AIAA J.*, Vol. 11, April 1973, pp. 115-117.
50. Mei, C., "Finite Element Displacement Method for Large Amplitude Free Flexural Vibrations," *Computers and Structures*, Vol. 3, April 1973, pp. 163-174.
51. Jones, R. D., *Mechanics of Composite Material*, McGraw-Hill, New York, 1975.
52. Wood, R. D. and Schrefler, B., "Geometrically Non-Linear Analysis—A Correlation of Finite Element Notations," *International Journal for Numerical Methods in Engineering*, Vol. 12, 1978, pp. 635-642.
53. Huebner, K. H. and Thornton, E. A., *The Finite Element Method for Engineers*, Second edition, John Wiley & Sons, New York, 1982.
54. Zienkiewicz, O. C., *The Finite Element Method*, Third edition, McGraw Hill, New York, 1977.
55. Reddy, J. N., *Energy and Variational Methods in Applied Mechanics*, John Wiley & Sons, New York, 1984.
56. Bergan, P. G. and Clough, R. W., "Convergence Criteria for Iterative Processes," *AIAA J.*, Vol. 10, August 1972, pp. 1107-1108.
57. Qin, J., Gray, C. E., Jr., and Mei, C., "A Vector Unsymmetric Solver for Nonlinear Panel Flutter Analysis on High-Performance Computers," Proceedings of 32nd Structures, Structural Dynamics and Materials Conference, Baltimore, MD, April 8-10, 1991, Paper no. 91-1169.
58. DOD/NASA Advanced Composite Design Guide, First Edition, 1983, Structures/Dynamics Division, Flight Dynamics Laboratories, Wright-Patterson Air Force Base, Ohio.
59. Sathyamoorthy, M., "Nonlinear Vibration Analysis of Plates: A Review and Survey of Current Developments," *Appl. Mech. Rev.*, Vol. 40, pp. 1553-1561.
60. Ray, J. D. and Bert, C. W., "Nonlinear Vibrations of Beams with Pinned Ends," Transactions of the American Society of Mechanical Engineers, *Journal of Engineering for Industry*, Vol. 91, November 1969, pp. 997-1044.
61. Yamaki, N., and Mori, A., "Nonlinear Vibrations of a Clamped Beam with Initial Deflections and Initial Axial Displacements, Part I: Theory," *Journal of Sound and Vibration*, Vol. 71, 1980, pp. 333-346.
62. Meirovitch, L., *Analytical Methods in Vibrations*, MacMillan, New York, 1967.
63. Lau, S. L., Cheung, Y. K., and Wu, S. Y., "Nonlinear Vibration of Thin Elastic Plates, Part I," *Journal of Applied Mechanics*, Vol. 51, December 1984, pp. 837-844.
64. Chu, H. N., and Herrmann, G., "Influence of Large Amplitudes on Free Flexural Vibration of Rectangular Elastic Plates," *Journal of Applied Mechanics*, Vol. 23, December 1956, pp. 532-540.

65. Eisley, J. G., "Nonlinear Vibration of Beams and Rectangular Plates," *Zeitschrift fur Angewand te Mathematik and Physik*, Vol. 15, 1964, pp. 167-175.
66. Singh, G., Raju, K. K., and Roa, G. V., "Nonlinear Vibrations of Simply Supported Rectangular Cross-Ply Plates," *Journal Sound and Vibration*, Vol. 142, No. 2, October 1990, pp. 213-227.
67. Gray, C. E., Jr., Decha-Umphai, K., and Mei, C., "Large Deflection, Large Amplitude Vibrations, and Random Response of Symmetrically Laminated Plates," *Journal of Aircraft*, Vol. 22, No. 11, November 1985, pp. 929-930.
68. Sanders, G., Bon, C., and Geradin, M., "Some Flutter Solutions Using Finite Element," *AIAA J.*, Vol. 8, April 1970, pp. 747-752.
69. Whetstone, W. D., *EISI-EAL Engineering Analysis Language Reference Manual—EISI-EAL*, System Level 320. Engineering Information Systems, Inc., August 1985.
70. Leissa, A. W., and Marita, Y., "Vibration Studies for Simply Supported Symmetrically Laminated Rectangular Plates," *Composite Structures*, Vol. 12, No. 2, July 1989.
71. Chandra, R. and Raju, B. B., "Large Deflection Vibration of Angle-Ply Laminated Plates," *Journal Sound and Vibrations*, Vol. 3, No. 2, November 1975, pp. 393-408.
72. Lin, K.-J., Lu, P.-J., and Tarn, J.-Q., "Flutter Analysis of Composite Panels Using High-Precision Finite Elements," *Computer and Structures*, Vol. 33, No. 2, August 1989, pp. 561-574.
73. Rossettos, J. N., and Tong, P., "Finite Element Analysis of Vibrations and Flutter of Cantilever Anisotropic Plates," *Journal of Applied Mechanics*, ASME Paper 74-WA/APM-15, 1974.
74. Juvinall, R. C., *Stress, Strain, and Strength*, McGraw-Hill, New York, 1967.
75. Shigley, J. E., *Mechanical Engineering Design*, McGraw-Hill, New York, 1967.

APPENDICES

APPENDIX A

DERIVATION OF THIRD-ORDER PISTON THEORY AERODYNAMICS

In Chapter 2, the final form of the aerodynamic theory used in this study is presented. The purpose of this appendix is to present a simplified derivation of the complete third-order expansion that is shown in Eq. (2.8). The assumptions that are used in deriving this analytical tool are:

- 1) The local motion of the panel behaves like a piston (law of plane sections holds).
- 2) During the panel's motion, the fluid process is ideal, isentropic, and has a constant specific heat.
- 3) The local panel velocity, $d\dot{w}$, is considerably less than the horizontal component of the free-stream velocity.
- 4) The fluid flow is parallel to the panel in the positive x -direction.

Piston theory aerodynamics is derived from the ideal wave propagation in a fluid disturbed by the motion of a moving surface, see Fig. A.1. For an ideal gas, the local motion of the panel, $d\dot{w}$, produces a sonic wave that propagates with sonic velocity, V_c , through the fluid. After the wave has passed, the properties of the fluid have changed an infinitesimal amount (dp , $d\rho_a$, dh); and the fluid is moving toward the wave front with velocity $d\dot{w}$.

The process as seen by a fixed observer moving with the wave front sees the fluid moving into the control surface at velocity, V_c , and exiting at velocity, $V_c - d\dot{w}$.

Expanding the continuity equation across the control surface and neglecting higher order differentials will yield a relationship for the sonic velocity of the fluid

$$V_c d\rho_a - \rho d\dot{w} = 0 \quad (\text{A.1})$$

Next, consider the momentum equation,

$$\sum F_z = \frac{\delta(mV_z)}{\delta t} \quad (\text{A.2})$$

where F_z is the z -component of the force and V_z is the z -component of the fluid velocity.

Summing the z -momentum equation over the control surface and solving for $d\dot{w}$ yields,

$$dp = \rho_a V_c d\dot{w} \quad (\text{A.3})$$

Solving (A.1) with (A.3) yields an expression for the sonic velocity

$$V_c^2 = \frac{dp}{d\rho_a} \quad (\text{A.4a})$$

or for an isentropic process,

$$V_c^2 = \left(\frac{\partial p}{\partial \rho_a} \right)_s \quad (\text{A.4b})$$

For constant specific heat ratio, γ , and isentropic, ideal gas, thermodynamics give

$$\left(\frac{\partial p}{\partial \rho_a} \right)_s = \frac{\gamma p}{\rho_a} \quad (\text{A.5})$$

Combining Eqs. (A.4) and (A.5) will give an expression for the sonic velocity in terms of the free stream flow properties.

$$V_c^2 = \frac{\gamma p}{\rho_a} \quad (\text{A.6})$$

Equation (A.5) can be integrated across the sonic wave as two separate states and solved using the notation that subscript o is to represent the free-stream properties. This leads to

$$\rho_a = \rho_{ao} \left(\frac{p}{p_o} \right)^{\frac{1}{\gamma}} \quad (\text{A.7})$$

From Eq. (A.6), the free-stream sonic velocity is

$$V_{co}^2 = \frac{\gamma p_o}{\rho_{ao}} \quad (\text{A.8})$$

or

$$\gamma = V_{co}^2 \frac{\rho_{ao}}{p} \quad (\text{A.9})$$

Using Eq. (A.3) with (A.6)–(A.9), integrating across the sonic wave from p to p_o and \dot{w} to 0 (the far field z -component of the free-stream flow is assumed to be zero), yields the “long established acoustic relationship”, [12]

$$p = p_o \left(1 + \frac{\gamma - 1}{2} \frac{\dot{w}}{V_{co}} \right)^{\frac{2\gamma}{\gamma - 1}} \quad (\text{A.10})$$

Equation (A.10) defines the pressure on the face of a moving surface with velocity \dot{w} in an isentropic, ideal fluid.

Next, since $\dot{w} \ll V_{co}$, Eq. (A.10) can be expanded using the binomial theorem

$$(1 + \chi)^\eta = 1 + \frac{\eta}{1!}\chi + \frac{\eta(\eta - 1)}{2!}\chi^2 + \frac{\eta(\eta - 1)(\eta - 2)}{3!}\chi^3 + \dots \quad (\text{A.11})$$

which is complete up to order three. Here the term $\eta\chi$ would be, using Eq. (A.10), the first order expansion.

Letting

$$\eta = \frac{2\gamma}{\gamma - 1} \quad (\text{A.12})$$

and

$$\chi = \left(\frac{\gamma - 1}{2} \frac{\dot{w}}{V_{co}} \right) \quad (\text{A.13})$$

and using Eq. (A.9) for γ , then recalling that the free-stream velocity has only a x -component when calculating the total derivative of \dot{w} along with using Eq. (A.11) into Eq. (A.10) results in the full third-order piston aerodynamic theory as shown in Eq. (2.8).

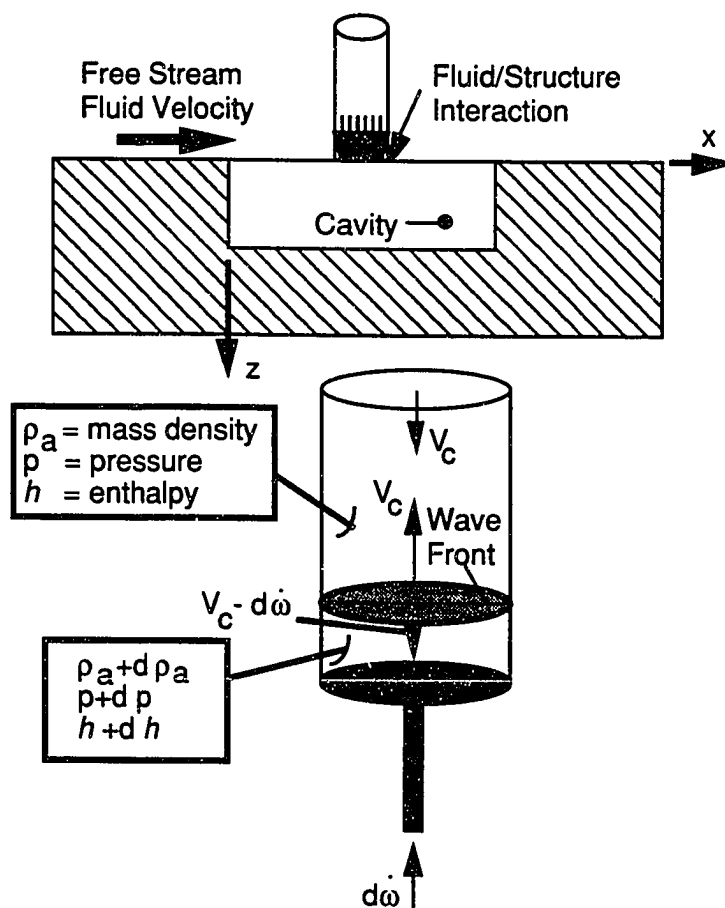


Fig. A.1 Piston Theory Aerodynamics.

APPENDIX B

DERIVATION OF THREE-DIMENSIONAL PLATE ELEMENT MATRIX

The rectangular composite plate element chosen for the nonlinear vibration and panel flutter analyses is a conforming element which has six displacements at each corner node, see Fig. B.1. The nodal displacements are: two in-plane, u and v , and the transverse deflection w and its derivatives $w_{,x}$, $w_{,y}$, and $w_{,xy}$ at each node for a total of 24 degrees-of-freedom per element. The element degrees-of-freedom are represented by the vector $\{\Delta\}$ as

$$\{\Delta\} = \begin{Bmatrix} \Delta w \\ \Delta u \\ \Delta v \end{Bmatrix} \quad (\text{B.1})$$

where the bending and membrane displacements, as shown in Fig. B.1 are

$$\{\Delta w\}^T = (w_1, w_2, w_3, w_4, w_{1x}, \dots, w_{1y}, \dots, w_{1xy}, \dots, w_{4xy}) \quad (\text{B.2})$$

$$\{\Delta u\}^T = (u_1, u_2, u_3, u_4) \quad (\text{B.3})$$

$$\{\Delta v\}^T = (v_1, v_2, v_3, v_4) \quad (\text{B.4})$$

The transverse and in-plane displacements within the rectangular plate element are assumed to be

$$w = (1 \ x \ y \ x^2 \ xy \ y^2 \ x^3 \ x^2y \ xy^2 \ y^3 \ x^3y \ x^2y^2 \ xy^3 \ x^3y^2 \ x^2y^3 \ x^3y^3) \{\eta_w\} \quad (\text{B.5})$$

$$u = (1 \ x \ y \ xy) \{\eta_u\} \quad (\text{B.6})$$

$$v = (1 \ x \ y \ xy) \{\eta_v\} \quad (\text{B.7})$$

where x and y are the element coordinates. The 24 generalized coordinates

$$\{\eta_w\} = (\eta_{w1}, \eta_{w2}, \dots, \eta_{w16}) \quad (\text{B.8})$$

$$\{\eta_u\} = (\eta_{u1}, \eta_{u2}, \eta_{u3}, \eta_{u4}) \quad (\text{B.9})$$

$$\{\eta_v\} = (\eta_{v1}, \eta_{v2}, \eta_{v3}, \eta_{v4}) \quad (\text{B.10})$$

are related to the element displacements

$$\{\Delta w\} = [D_b]\{\eta_w\} \quad (\text{B.11})$$

$$\{\Delta u\} = [D_{bu}]\{\eta_u\} \quad (\text{B.12})$$

$$\{\Delta v\} = [D_{bv}]\{\eta_v\} \quad (\text{B.13})$$

Solving Eqs. (B.11)–(B.13), and putting the results into Eqs. (B.5)–(B.7), yields,

$$w = [\phi_w]\{\Delta w\} \quad (\text{B.14})$$

$$u = [\phi_u]\{\Delta u\} \quad (\text{B.15})$$

$$v = [\phi_v]\{\Delta v\} \quad (\text{B.16})$$

which relates the field equations to the discrete nodal quantities using interpolation functions, $[\phi_w]$, $[\phi_u]$, and $[\phi_v]$.

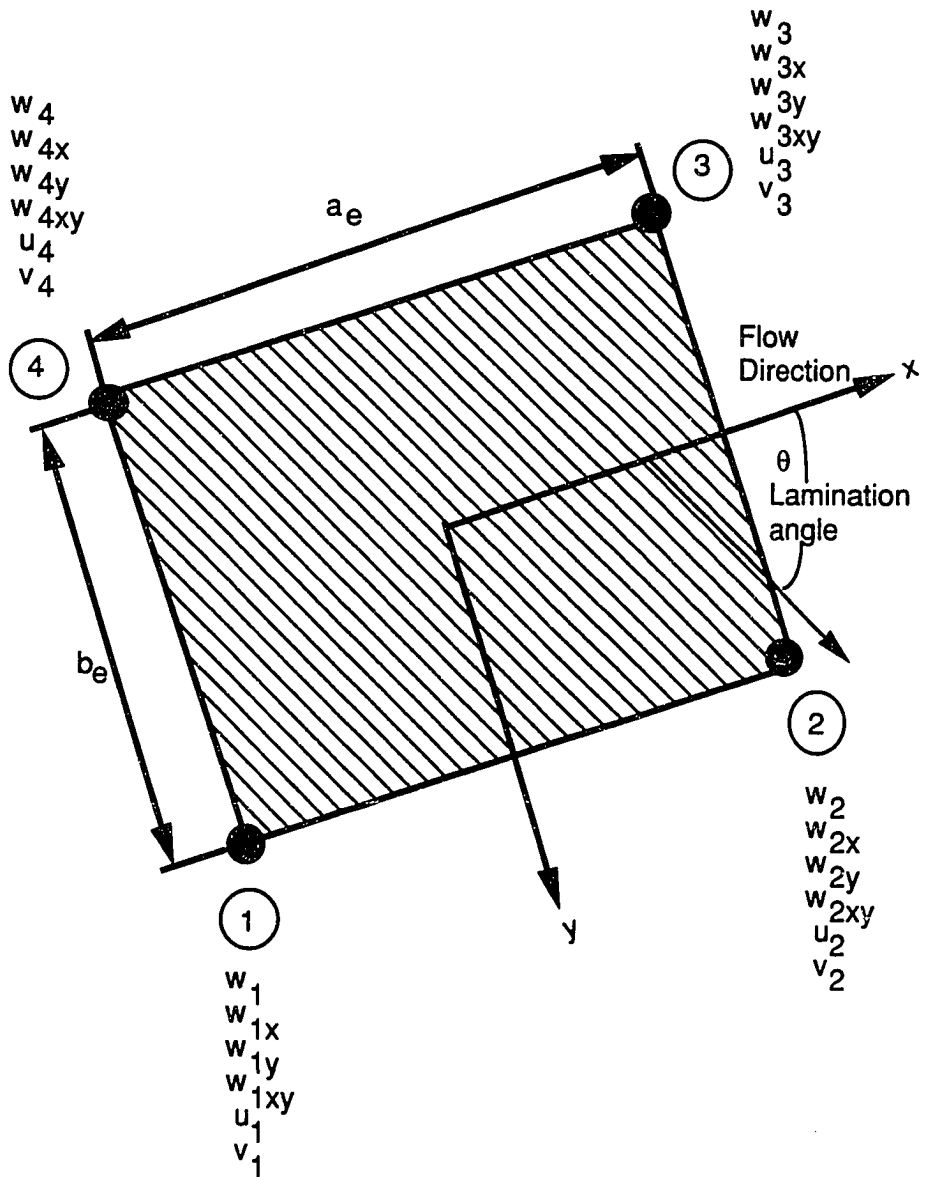


Fig. B.1 3-D Laminated Plate Finite Element.

APPENDIX C

TIME AND SPACE FUNCTIONS APPROXIMATIONS

For synchronous motion the nonlinear quadratic, $f2(t)$, and cubic, $f3(t)$, time functions need to be approximated over a limit-cycle oscillation. These functions, $f2(t)$ and $f3(t)$, are defined as follows:

$$\begin{aligned} f2(t) &= \left(\frac{1}{2} + \frac{1}{2} \cos(2\omega t) \right)^{\frac{1}{2}} \cos(\omega t) \\ f3(t) &= \frac{1}{4} (3 \cos(\omega t) + \cos(3\omega t)) \end{aligned} \tag{C.1}$$

where the linear frequency ($\omega = \omega_1, \omega_2, \omega_3, \dots$) illustrated in Fig. 5.7 is iterated for a particular mode shape as shown in Fig. 5.8. If the higher order harmonics in Eqs. (C.1) are neglected, then the linearized time functions, $F2(t)$ and $F3(t)$ can be estimated as follows:

$$\begin{aligned} F2(t) &= \frac{\sqrt{2}}{2} \cos(\omega t) \\ F3(t) &= \frac{3}{4} \cos(\omega t) \end{aligned} \tag{C.2}$$

Thus during the iterative procedure, Eq. (C.1) is approximated as follows:

$$\begin{aligned} f2(t) &\approx F2(t) \\ f3(t) &\approx F3(t) \end{aligned} \tag{C.3}$$

These approximations over a limit-cycle are shown in Fig. C.1 where the variations are reasonable approximations of the nonlinear time function.

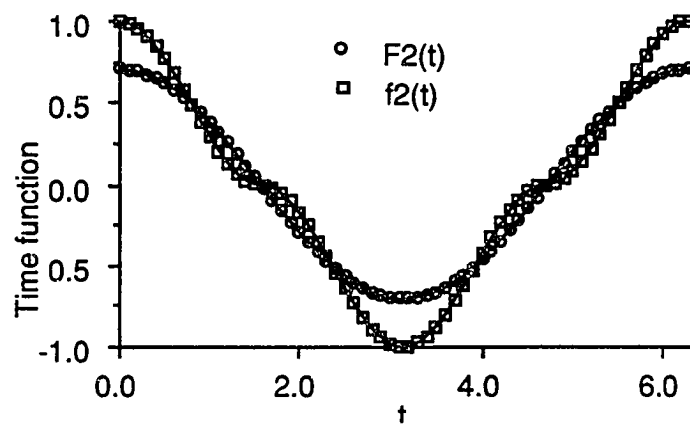
A comparison of the single space mode approximation can be assessed by performing a fourier analysis of the converged limit-cycle deflected shape for a two-dimensional panel. The converged deflected shape is shown in Fig. C.2(a) and Fig. 5.3. Decomposing the flutter shape into its linear mode shapes,

$$w(x, t) \approx \cos(\omega t) \sum_n a_n \sin(n\pi x/a) \tag{C.4}$$

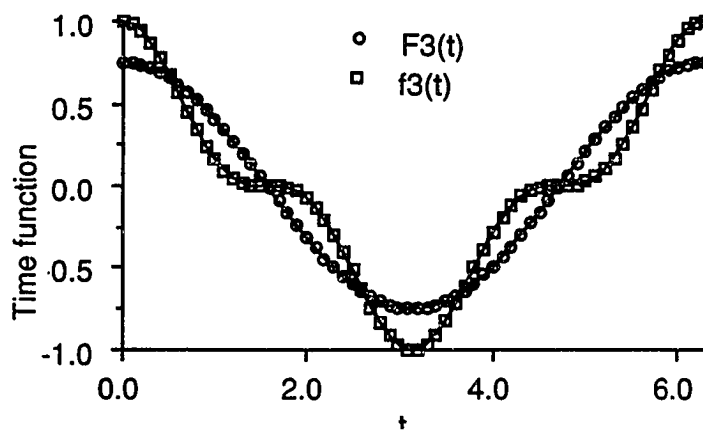
results in the coefficients, a_n , as shown in Table C.1 for the first eleven linear modes. As can be seen, the major modal participation for the two-dimensional panel is contained in the first five linear modes and are shown in Figs. C.2 (b)–(f). Thus, the proposed single mode linearizing method is equivalent to a multi-mode approach.

Table C.1 Linear Mode Shape
Participation Factors

n	a_n
1	+0.5382
2	−0.5172
3	+0.1602
4	−0.0333
5	+0.0125
6	−0.0033
7	+0.0016
8	−0.0007
9	+0.0005
10	−0.0002
11	+0.0002

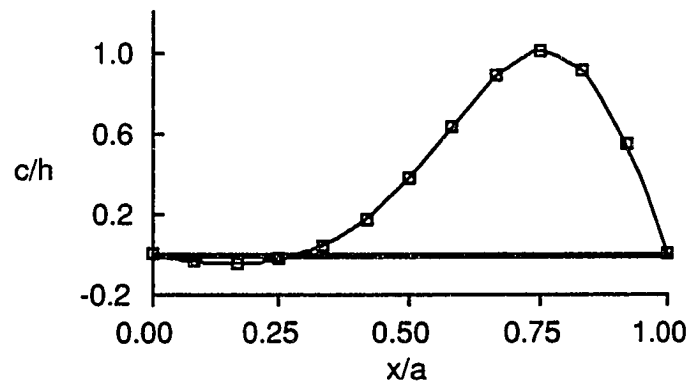


(a) Quadratic Time Function

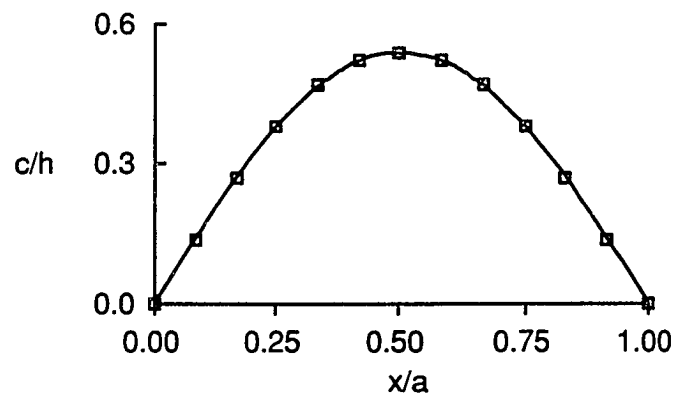


(b) Cubic Time Function

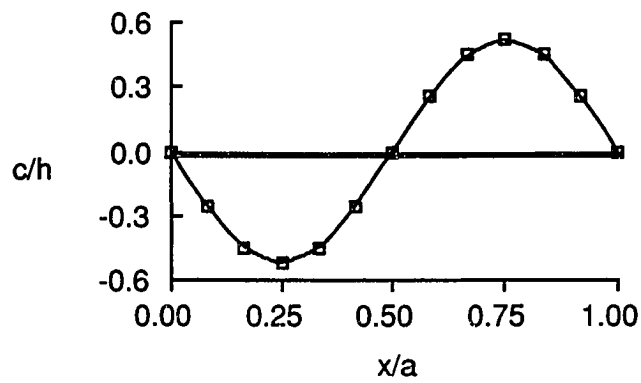
Fig. C.1 Time Function Approximation.



(a) Flutter Deflection Shape

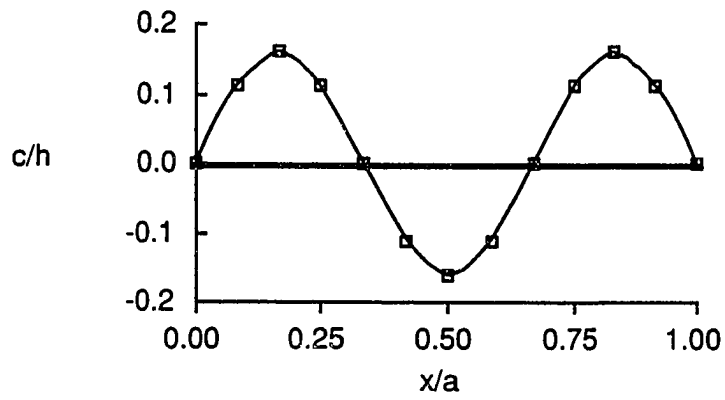


(b) Mode 1 Component

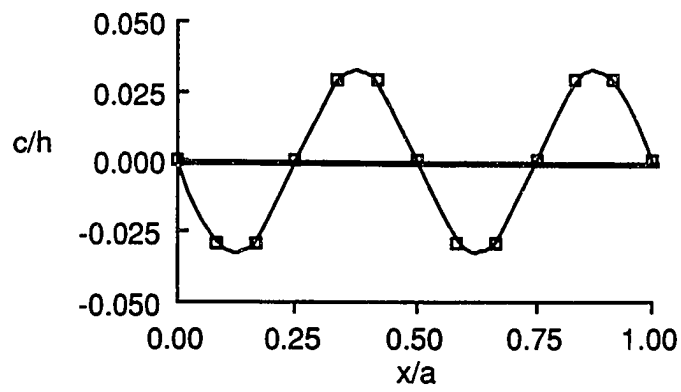


(c) Mode 2 Component

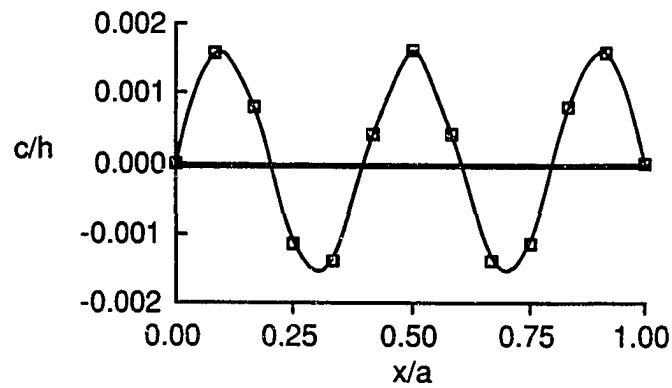
Fig. C.2 Panel Flutter Deformation Shape.



(d) Mode 3 Component



(e) Mode 4 Component



(f) Mode 5 Component

Fig. C.2 Cont. Panel Flutter Deformation Shape.